A NOVEL METHOD FOR THE FABRICATION OF POROUS POLY-ETHER-ETHER-KETONE USING SODIUM CHLORIDE AS A POROGEN

Abdur Rahman Siddiq

Thesis submitted

for the degree of Doctor of Philosophy

Department of Mechanical, Materials and Manufacturing Engineering

University of Nottingham

January 2016

Preface

The thesis is submitted to the University of Nottingham for the degree of Doctor of Philosophy. This research was carried out under the supervision of Dr. A. R. Kennedy and Dr. J. Segal in the Department of Mechanical, Materials and Manufacturing Engineering. This thesis is unpublished and original work by the author, Abdur Rahman Siddiq. The case study in Chapter 6 is intended for confidentiality.

Abstract

A novel technique to manufacture porous Poly-Ether-Ether-Ketone (PEEK) scaffolds via a tapped-packing route of fabrication incorporating rounded salt beads had been investigated. The conventional salt leaching technique has been improved via the tapping-route in manufacturing porous PEEK structure that possesses adequate structural and mechanical properties. Three types of PEEK, Vicote, LT3 and LT1 were used as main material and rounded salt as a porogen. PEEK powder and the rounded salt were mixed in 6:1 mass ratio by applying tapping to 22 mm cylindrical die. 5 g of PEEK/salt beads mixture was packed through 8000 taps. Alternative mixing techniques also involved wet (using sprayed water) and dry mixing routes prior to the compaction. To solidify the PEEK and to obtain free-salt PEEK scaffolds, then sintering, dissolving and drying were applied. The results show that only a combination of the tapping route and the LT1 PEEK could secure porous PEEK scaffolds with acceptable and required characteristics in associated with the pore size range (main pores of (560 $\pm$ 180) µm and windows of (204 $\pm$ 41) µm) and shape, good interconnectivity, and homogenous and high porosity > 80%. It was also successfully integrated into a viable spinal PEEK cage implant via injection moulding.

Publications

Publication included in thesis (Journal) :

Siddiq, A.R. and A.R. Kennedy, *Porous Poly-Ether-Ether-Ketone (PEEK) manufactured by a novel powder route using near-spherical salt bead porogens: Characterisation and mechanical properties.* Materials Science and Engineering: C, 2015. **47**: p. 180-188.

Publication not included in thesis (Journal) :

Jia, J., A.R. Siddiq, and A.R. Kennedy, *Porous titanium manufactured by a novel powder tapping method using spherical salt bead space holders: Characterisation and mechanical properties.* J Mech Behav Biomed Mater, 2015. **48**: p. 229-40.

Conference :

A.R. Siddiq, Fabrication of Macroporous Poly-Ether-Ether-Ketone (PEEK) Scaffolds Using Porogens. Cellular Materials Conference, Dresden, Germany, 2014.

Acknowledgment

I would like to express my deepest thanks to my two supervisors, Dr. Andrew Kennedy, and Dr. Joel Segal. My sincere appreciation is extended to Andrew for the continuous support of my Ph.D. study, for his patience and extensive knowledge. I could not have imagined being able to complete my research and writing of thesis without his mentor and guidance. He has given me invaluable experience to learn and to access some specific machines and technologies and to get involved in his work.

To industrial partner, Invibio Ltd, thank you for sponsoring our work and allowing me to contribute samples for further investigation producing solid-porous PEEK cage for a spinal implant.

Thank you to Dr. Nigel Neate, Tom Buss, Julie Thompson and technicians in the Wolfson Building for giving access and training related to this work. My appreciation is sent to my reviewers Dr. Adam Clare and Dr. Jonny Blaker for constructive criticism and feedback and comments so that this thesis can be reviewed completely. To Kanika and Romanus, thank you for your continued friendship and support for the last 4 years. To my besties, Alfa, Andhika, Edi, and Ova, thank you all for still keeping in touch and support while I am far away from home. In the academic world I wish to thank the Directorate General of Resources for Science, Technology and Higher Education (DG-RSTHE), the Ministry of Research, Technology and Higher Education of the Republic of Indonesia, for the generous sponsorship (October 2011 – March 2015) and also appreciation to the rector of UIN Sultan Syarif Kasim Riau for permitting me to study at University of Nottingham.

I cannot thank you enough to my parent, for the life lesson, unlimited support, motivation and encouragement and many things in my life. Both of you have been my inspiration to do great things. When I was still a little child, my father told many stories of his life, encouraged me to see the world and to get great experience in life. Mom and Dad, I am proud to be your son. To my brothers, Bang Mah, Didin and Imad, you all also have inspired me to be as I am today. We have been through sad, tough and happy moments together in the family and I will keep all good memories with me. To the memory of my mother whom I always remember, I would like to dedicate this to her and hope that she would have been proud.

Aku tidak tahu apa yang akan terjadi di masa depan,
Tapi aku tahu bahwa ini adalah sesuatu yang bisa membuatku tersenyum kelak.

I do not know what is going to happen in future,
but I surely know this is something that makes me smile one day.
(Nottingham, 16/06/2016)

Table of Contents

List of Figures

List of Tables

Nomenclature

BV/TV	Bone volume/Total volume
CFR PEEK	Carbon Fibre Reinforced PEEK
D_{10}	The size of particle below which 10% of the sample lies.
D_{50}	The size in microns at which 50% of the sample is smaller and 50% is larger, as the mass median diameter or the median of the volume distribution.
D_{90}	The size of particle below which 90% of the sample lies.
DA	Degree of Anisotropy
DEM	Discrete Element Method
EDX	Energy Dispersive X-ray
LVDTs	Linear Variable Differential Transducers
MicroCT	Micro Computed Topography
NaCl	Sodium Chloride (salt)
n_0, n_1, n_2, n_3;	The number of voxel corners, the number of voxel edges, the number of voxel faces and the number of voxels as counted parameters in Euler characteristic, respectively.
PEEK	Poly-Ether-Ether-Ketone
SE	Secondary Electron, mode position when using SEM
SEM	Scanning Electron Microscopy
STD	Standard Deviation
χ(X)	(Chi) Euler characteristic number
$\beta_0, \beta_1, \beta_2$	The number of separate particles of the structure, the number of handles (connectivity) and the number of cavities enclosed within the structure, respectively.

Chapter 1: Introduction

1.1 Problems and motivation for the study

1.1.1 The progress of PEEK studies in the area of spinal cages

Since 1998, Poly-Ether-Ether-Ketone (PEEK) has been commercially offered as a biomaterial for implants as a candidate to replace metals [1, 2] owing to PEEK's advantageous properties such as transparency to X-rays, leading to no artefacts blocking inspection of the bone growth when CT scanning [2, 5], easy surface modification and great flexibility in design and shape [2]. Furthermore, the elastic moduli of PEEK cages are close to that of bone, which helps to decrease the stress shielding [5].

The development and use of PEEK are in progress for implants in spine surgery, especially for cages used in vertebral fusion [1-5]. A PEEK cage as an implant device in vertebral fusion surgery could be in the form of an interbody lumbar fusion cage [2, 3, 6]. The PEEK cage, which is inserted between the vertebrae, replaces the damaged disc and is commonly made from solid PEEK with a hollow core in the center [3, 7, 8] and the standard sizes of cage vary from 11 to 15 mm in height [8].

Cho (2002) used a PEEK cage for the correction of cervical kyphosis [9] and in another study, his team found that PEEK cages for interbody fusion increased graft fusion rate and caused fewer surgical complications [10]. PEEK cages were found to be safe and efficient for anterior cervical fusion [11] and for degenerative lumbar spine disorders. PEEK cages provided good clinical results and fusion rates [12, 13], but Spruit (2005) found that PEEK cages

without porosity did not have a beneficial effect on the construct stability and led to the risk of failed fusion as a result of reduced segmental stability [14].

Thus, there is a desire to produce porous PEEK implants in order to enhance osteointegration for improved mechanical stability and longevity [15] and also for better interaction with the surrounding tissue and for bone ingrowth [1, 15-17]. However, to date, only a limited number of studies have focused on porous PEEK scaffolds such as those by Evans (2015), Wang (2013), Tan (2005) and Abu Bakar et al (2003) and their studies were limited to structures with low porosities of 24% - 70% [18-20] and were found to have poor inter-pore connectivity [21].

1.1.2 The development of techniques to fabricate porous PEEK scaffolds

One of the key issues in producing porous scaffolds is the limitation in technology to address specific requirements for architectural features and mechanical strength of the porous part [23]. The architectural features vary from the size of the pores, pore shape uniformity, porosity and interconnectivity between pores in the open network [22, 23]. In terms of mechanical strength, the porous scaffolds are expected to be strong enough to allow surgical handling during implantation and capable of supporting the structure under the service load during cell ingrowth and migration [23-28]. Since retaining high porosity with good mechanical properties has become one problem [23], finding a suitable technique to provide a balance between mechanical properties and porous architecture sufficient to allow cell growth

has attracted many researchers to introduce more manufacturing routes. However, in the area of PEEK, which is relatively new, these investigations are still limited but cover methods such as selective laser sintering [29, 30], injection moulding [18, 31]. The laser sintering has limited to the resolution due to the laser beam diameter to produce micron-scale pores of the scaffold, whilst the injection moulding has difficulty in producing a good connectivity for the scaffolds. On the other hand, other techniques [32, 33] incorporating extrusion and nanofiber-reinforced foam have some drawbacks such as non-flexible scaffold designs, non-uniform porosity and fragile structure issues. Comparing with those technologies, a common and simple approach to porous polymer scaffold fabrication is particulate leaching, or salt leaching when using salt as porogen [34-36]. The route is simple and potentially cost-effective but limitations include difficulty in salt removal and poor connectivity in the resulting porous structures [37].

Current developments and studies are attempting to improve this technique and combine it with injection moulding [38] [39]. They incorporated 150 – 300 μm of the salt size merely obtained from sieve shaker to control the pore size and the connectivity. However, problems still persist with a lack of control of the pore morphology and the residual NaCl content, especially when using salt particles with a cubic shape, in addition to creating structures in which the pores are only interconnected through small (<20 μm) windows. It has been investigated that spherical pore shapes evidently offer better pore interconnectivity [35]. Coupled with vibration, according to techniques developed by Jinnapat and Kennedy (2010), [40] spherical salt beads and enhanced packing can also increase salt removal rates from the scaffolds.

1.2 The aims and objectives

1.2.1 Aims of the study

This study aims to address the challenges in improving the salt leaching fabrication technique, to make porous PEEK structures with adequate structural and mechanical properties, with the potential to be integrated into a viable spinal PEEK cage implant.

1.2.2 Objectives of the study

The objectives of study are to address the aims and are achieved through a series of investigations described as follows;

1. To develop a new technique to manufacture porous PEEK scaffolds with structures that are consistent with those which will permit bone ingrowth. Three routes of fabrication, based on PEEK powder and a salt (NaCl) porogen, will be investigated, the optimum route being selected based on meeting the structural requirements and achieving good repeatability of the process and structure obtained.
2. To investigate in more detail the important processing factors which control the structural features and reproducibility for the processing method chosen.
3. To examine the potential for integrating a porous part into a solid PEEK structure using injection moulding using appropriate inserts and pre-treatments thereof.

4. To determine the mechanical properties of porous PEEK scaffolds and the integrated porous-solid PEEK parts produced by injection moulding.
5. To provide samples and transfer the accumulated “know-how” to industrial partners (Invibio Ltd) so that they might produce a prototype porous-solid PEEK spinal cage.

1.3 The structure of thesis

This thesis consists of seven chapters to cover (1) Introduction; (2) Literature review; (3) Materials and methods; (4) The comparison of porous PEEK scaffolds made by wet, dry and tapping routes; (5) Process development for the tapping route; (6) Integrating porous PEEK structures into injection moulded parts; and (7) Conclusions and future work.

Chapter 2: Literature Review

This section is aimed to review devices for spinal implants or spinal cages, particularly the use of Poly-Ether-Ether-Ketone (PEEK), critical aspects of porous structure for implants and the fabrication techniques used to produce porous parts using PEEK. The literature review also identifies the knowledge gap and some background theories related to the proposed fabrication technique using NaCl beads as a porogen.

2.1 Devices for spinal implants

2.1.1 Spinal implant materials

An implant is an object or instrument fabricated with the purpose of substituting, supporting or enhancing a structure of bones. The implant is placed into the human bones through surgery allowing cells to grow [41]. In medical practice, there are a number of different types of implant devices used by the surgeon to replace parts of the human bones. Examples including pins, rods, screws and plates, are commonly used to stabilise fractures while a healing process occurs [7, 42, 43]. The devices have been developed to address different purposes in; controlling the amount of motion between adjacent vertebrae; removing and replacing the suffering disc with an artificial disc or to the correct the acquired spinal deformities [44, 45] and providing rigid internal vertebral cages have been developed in order to act as a replacement for whole or multiple vertebral bodies [7]. A vertebral cage, also referred as a spinal cage, shown in Figure 2.1 allows the bone to grow through a columnar fenestration

in the device. The functionality of cages alone is a spacer, restoring disc space and at the same time preventing the unstable motion segment. Biologically, these cages enable two adjacent vertebrae to develop bony fusion by building a bridge in between them [7].

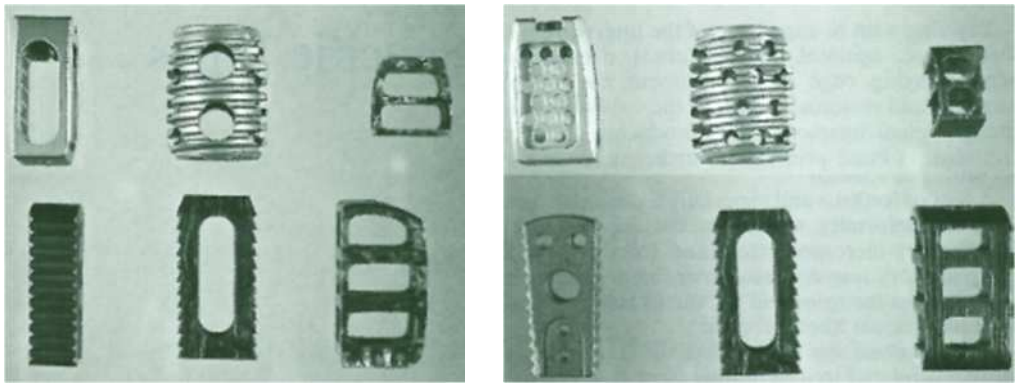

(a) (b)

Figure 2.1: 6 stand-alone spinal cages (a) viewed from above and (b) from the lateral side. The cages in the upper row made out of titanium and the lower row are from carbon fibre reinforced polymer [7].

In many cases, a spinal device may be composed of two or more materials. When one material is inappropriate, the entire device may not fit the host tissue either from adverse biological reactions or material failure [46]. Therefore, the selection of materials must be made with an understanding of these complex interactions. Spinal devices with or without porosity may be made from titanium, stainless steel, or non-metallic, but only limited metallic-based materials are allowed as implant materials [47]. For examples, stainless steel and titanium, they are easy to be machined and can be applied in different work conditions, but in many cases, metal implants can cause erosion of bone and loosening the implant, leading to the generation of particulate debris that might stimulate adverse biological responses [41]. They may also subside into adjacent bone and be susceptible to corrosion and be difficult to monitor using medical imaging technologies [48]. The drawbacks of cages made from

titanium and carbon fibre reinforced polymer materials are, firstly, related to the stiffness of the device [41] which might promote stress shielding (reduction in bone density as a result of the introduction of the implant that reduces the stress to the bone) and inhibit bone growth, and secondly the radiopacity of the device, which hinders diagnostic assessment of the bone growth [49]. Meanwhile, ceramics tend to be brittle, to have unpredictable degradation profiles in vivo and to have limited mechanical strength [16]. The limitations of metal and ceramic materials have brought researchers to engineer polymers as potential porous materials and, in particular, Poly Ether-Ether Ketone (PEEK) has been recommended by Kurtz (2012) as a potential spinal device material [1].

2.1.2 Poly Ether-Ether Ketone (PEEK) as implant material

PEEK is a linear homopolymer possessing a single monomer. This chain may contain 100 monomer units with 80,000 – 120,000 g/mol of molecular weight on average [50]. Its basic formula is $(–C_6H_4–O–C_6H_4–O–C_6H_4–CO–)_n$ as shown in Figure 2.2. The glass transition temperature is 143^{o}C.

Poly-Ether-Ether-Ketone (PEEK) is derived from the reaction of a potassium salt of hydroquinone with difluorobenzophenone in the solvent diphenylsulfone at high temperatures between 280 – 340^{o}C. This polymer is categorised as semi-crystalline and has a melting point at 335^{o}C (although some literature suggests 343^{o}) [51, 52].

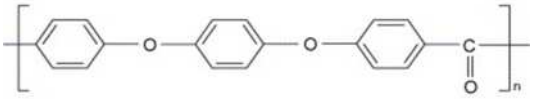

Figure 2.2: PEEK chemical structure

In particular, PEEK has some advantages such as its stability at high temperatures (exceeding 300^{o}C), resistance to chemical and radiation damage, compatibility with many reinforcing agents (glass and carbon fibres), and greater strength than many metals [1]. As it has been examined that the flexural modulus of the PEEK is around 4 GPa (Table 2.1 and Invibio Ltd). These properties have attracted many industries to invest in this polymer. Furthermore, aside its stability and biocompatibility, the radiolucency and the mechanical properties of PEEK make it a suitable biomaterial for spinal implants [50].

According to Invibio Ltd, the manufacturer of PEEK-OPTIMA® (the biomedical formulation of the PEEK material), this polymer can be processed by conventional techniques including injection moulding, extrusion or machining, allowing medical device manufacturers broad design and manufacturing flexibility. From the fabrication perspective, this particular type of polymer has great versatility in processing; melting, moulding and extrusion processing using the conventional equipment.

PEEK has very low water absorption with a water solubility of 0.5% w/w (Table 2.1, [52]), it is long-term water resistant to 260^{o}C, and withstands a wide pH range, 60% sulphuric acid to 40% sodium hydroxide, at elevated temperature. Indeed, PEEK can only be completely dissolved using fairly unusual solvents, such as diaryl sulfones [53]. Its outstanding performance

includes resistance to both abrasion and dynamic fatigue. Furthermore, low flammability, excellent resistance to gamma radiation, and good resistance to environmental stress cracking are other specific features of PEEK, [54] [52, 55]. PEEK has been classified as safe for medical implantation, withstanding long term human bone, blood and tissue contact [42] and has strength at 138 MPa, 3.45 GPa of compressive modulus and 4.1 GPa of flexural modulus [52] ; and it has become an option for long-term medical implants [1]. A summary of some of the key properties of PEEK are shown in Table 2.1 [52].

Table 2.1: Properties of PEEK [52]

Property	Units	PEEK
Density*	g/cc	1.30
Water absorption 24 h	%	0.5
Glass transition temperature	^{o}C	145
Melting point	^{o}C	334
Elongation	%	20 – 40
Flexural modulus	GPa	4.1
Compressive modulus	GPa	3.45
Compressive strength	MPa	138
Processing temperature	^{o}C	345 – 390

2.1.3 PEEK spinal cage

Since 1989, PEEK has been evaluated in a clinical study of the spinal cage and due to the radiolucency of the PEEK cage; the inter-body fusion could be identified in 100% of the cage levels [56] and resulted in extensive growth of trabecular bone into the cages and the absence of an inflammatory reaction [57]. These cages were fabricated by injection moulding of CFR-PEEK OPTIMA with a composition of 70% of PEEK and 30% of chopped carbon fibre [49]. The studies also focused on the use of PEEK for both cervical and lumbar spinal cages [58-62] and using PEEK cages to provide good clinical

results and fusion rate [12, 13]. The polymeric biomaterial PEEK has been considered to be a useful biomaterial for inter-body fusion cages due to the polymer's increased radiolucency and decreased stiffness [1]. Figure 2.3 shows an example of inter-body fusion cages made from PEEK implanted in the lumbar spine. The use of PEEK in spinal surgery is relatively recent [49] and further modification of spinal PEEK cages is still needed to support osseo-integration [63] since only incorporating non-porous PEEK material. Reportedly, the use of PEEK in spinal cage by Toth et al (2006) showed no device degradation or wear debris, indicating the polymeric biomaterial PEEK may be a useful biomaterial for spinal cages

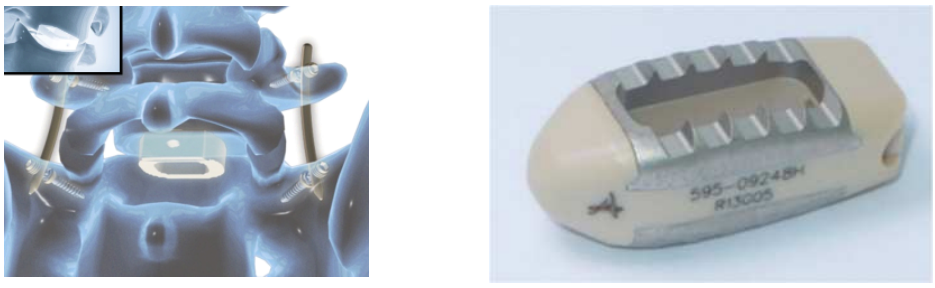

(a) (b)

Figure 2.3: (a) Spinal interbody fusion - examples of devices made from PEEK-OPTIMA from UK PEEK manufacturer Invibio implanted in the lumbar spine; (b) a PEEK-titanium lumbar cage.

2.1.4 Porous PEEK for spinal implants

Potential new implant designs for solid implants, porous scaffolds and various combinations have been investigated [64] and porosity has been employed in implant applications through various routes (such as laser sintering, injection moulding and salt leaching) to provide porous structural materials, cell support scaffolds and osteo-conductive filler materials [1, 16]. The osteo-conductive

refers to a property of a biomaterial that encourages bone repair. Regardless of where the implants will be used, materials with porosity allow them to better interact with the surrounding tissue and incorporating porosity into an implant may enable better integration of the implant with the body, prevent device movement which would cause abrasive damage to adjacent tissue, and allow cell infiltration and direct tissue repair [1, 16].

Studies associated with the use of polymers as porous scaffold materials have been developed in many areas of interest, referring to materials [41, 65], structures [35, 36, 66-68] and mechanical properties [69-72]. According to the cited studies in Figure 2.4, scaffolds with porosity had been obtained ranging from 40 – 93% porosity and also with a range of pore sizes (15 – 600 µm). However, only a few studies investigate porous PEEK scaffolds. For instance, studies on PEEK by laser sintering [20, 29] were able to produce a PEEK scaffold with high porosity (>80%), but their technology only allowed to fabricate a limited size of parts, i.e a strut length of 1.5 mm and 600 µm pore size with filament size of 0.10 mm using around 25 µm of PEEK particle size. In addition to that, it was also reported the trapped powder inside the pores of the made scaffold caused the structure less interconnected than that of the structure from the original design.

In a recent development, some other studies on spinal PEEK devices have tried to engineer the device with porosity, for instance, Jarman Smith (2012), and Landy (2013). However, their studies at that time still had limitation in providing open structures and high porosity and they only had closed structures with <50% porosity and limited pore diameters of < 100 µm [16] [32]. A different structure of scaffolds using PEEK was investigated by Edwards et al

(2012), the woven PEEK scaffolds. They used PEEK monofilament (10.2 g/km) and multifilament (7.5 tex/ 15 filament) yarns to create woven structures by repeating the same woven patterns of warp and weft threads. It was reported that the pore sizes of < 280 μm were in the scaffolds at 93% of porosity, but with poor cell adhesion due to the pattern creating curvature angles [73].

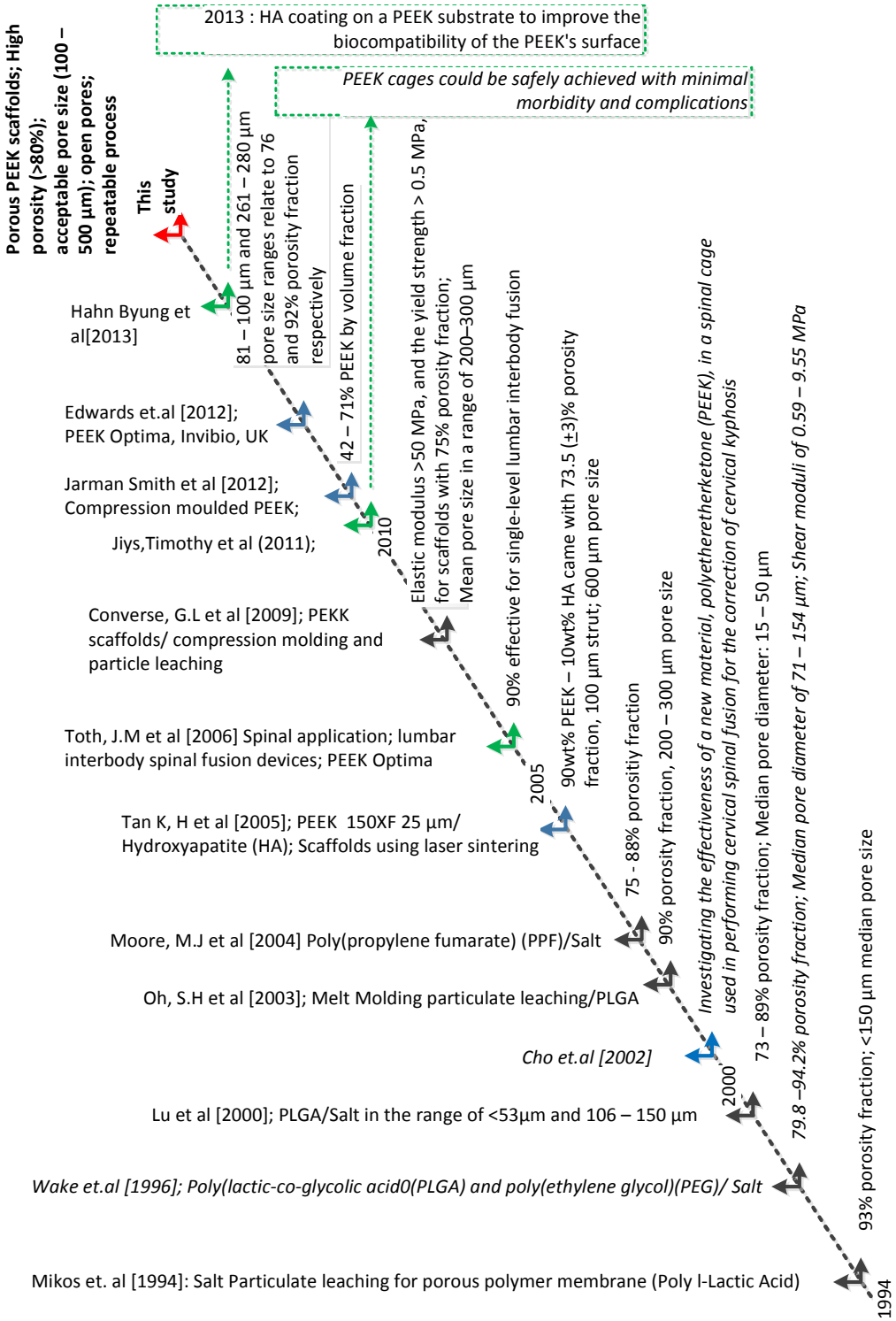

Figure 2.4: Studies on porous scaffolds using PEEK and other polymers. The black arrows represent studies employing salt leaching; the blue arrows represent studies using PEEK without porosity; the green arrows represent studies using PEEK as implants.

2.2 Critical aspects of the porous structure of implants

2.2.1 Scaffold design requirements

A scaffold, known as a cellular solid or solid matrix consisting of some interconnected networks of solid struts forming the edges and faces of cells [74], is required to provide the appropriate environment for the regeneration of tissues and organs [23] and to provide the structural support for cell attachment and subsequent tissue development [75]. Specifically, the scaffold design should provide high porosity and a suitable pore size [76, 77] and good mechanical strength to support the tissue structure [25-28] in order to be able to satisfy form and function needs [78].

2.2.2 Pore size, porosity and pore interconnectivity

The pore size distribution, porosity and pore interconnectivity can describe the physical characteristics of a scaffold [37, 79, 80]. It is reported that human trabecular bone has macro pore diameters of 300 – 600 μm and interconnected diameters in excess of 100 μm [81]. To allow cell migration, there is a certain range of sizes that is appropriate and a minimum pore size of 100 – 150 μm was suggested by many researchers [28, 42, 82-84] and as large as 700 μm to enable cell attachment [1]. This fact supports that the pore size plays an important role for bone integration [76, 85-88]. Furthermore, some other studies examining bone growth reported various evidence of pore effects [89-92]. For example, a pore size of about 325 μm enables optimal bone growth [85]. Tsuruga et al (1997) confirmed 300 – 400 μm was the optimum pore size for bone growth [84], whilst Bobyn et al (1980) concluded that optimum

fixation was for a 50 – 400 μm pore size [86]. Pore morphology influences the rate of fibro-vascular ingrowth into a scaffold in terms of the pore size. The growing cells, after sometime of post implantation, might occupy surface of scaffolds [93]. This indicates providing porous scaffolds could stimulate cells to grow.

In the use of PEEK, only a few studies have tried to produce porous scaffolds, such as Jarman-Smith (2012) comparing small pores of 70 μm and big pores of 636 μm from porous PEEK applying salt leaching [16], Tan et. al (2005) with 600 μm pore diameter [20], Conrad et al (2013) with 200 – 300 μm pore diameter [94] and Landy et al (2013) with 100 μm pore diameter. The cited studies were only able to produce limited pore size ranges, random pore shapes and low porosity.

Ideally, the scaffold must have an open-pore geometry, with a highly porous surface to enable cell distribution, cell proliferation and migration [22] and also improved efficacy in enhancing the cellular response to the material [16]. It has been reported that a high porosity (> 60%) and high interconnectivity allow bone in-growth and tissue differentiation [63, 95]. Interconnectivity is important. When the pores are not connected, cell migration will be hindered even if the overall porosity is high [80]. In relation to the use of PEEK, Jarman-Smith, Landy, Conrad and Tan reported obtaining 45 – 75% [16], 50% [32], 75% [94] and 80% [20] porosities, respectively. Controlling the pore size and enhancing interconnectivity has been major problems in these studies. In this study, a rational porosity of about 80% has been set as an initial target to achieve for the PEEK porous scaffold.

Micro-CT analysis is a common technique to measure the pore size and porosity [96, 97]. A characteristic of the structure volume fraction (BV/TV, the ratio of the segmented bone volume to the total volume of the region of interest) is generated and the porosity then can be measured. The measurement also gives information about pore size and its distribution [98]. The CT measurement also generates the anisotropy of the specimens to produce a degree of orientation showing the majority orientation of the pores in a porous structure [99], which refers to length of longest divided by shortest axis (vector) fitted in a measured object shape based on volume orientation [102].

A local volume orientation is defined for any point within a trabecula as the orientation of the longest intercept through the point TM (see Figure 2.5). The local volume orientation is in 2D space a semi-circular orientation, in 3D space a hemispherical orientation, and it is assumed that the main orientation of the volume orientation distribution must be known.

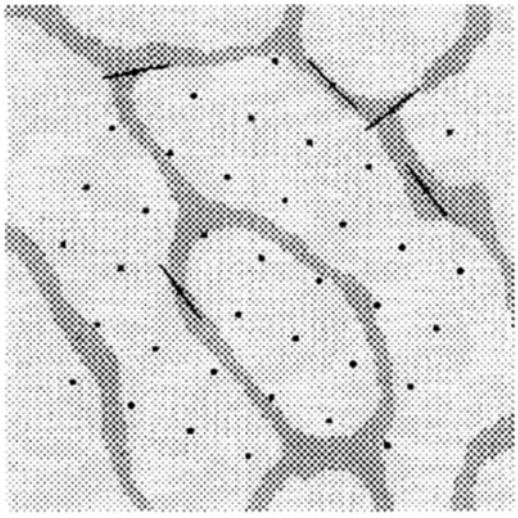

Figure 2.5: Volume orientation (VO) measurement. A randomly translated point grid is placed on the structure. For each point hitting the phase of interest (bone) the orientation of the longest intercept through the point is determined, and this orientation is the local volume orientation for the point. In the figure, five local volume orientations are sampled and depicted by the compass needles [102].

The degree of anisotropy can be obtained via microCT scanning result and also ImageJ software (imaging processing). Furthermore, CT also used by Kinney (1998) and Paukalova (2010) and other researchers, to investigate the connectivity density of vertebrae bone which is in the region of 2 – 15/mm^3 [100-103]. The connectivity density is one of parameter measured by microCT that informs a measure of the degree of connectivity of trabeculae normalized by total volume (TV) and it has been suggested that stiffness decreases when connectivity density increases and the higher the value, the more connections are present in the object [102, 103].

The connectivity density is based on the Euler characteristics reporting the number of particles of a structure plus the number of enclosed cavities minus the connectivity [102]. Pre knowledge is required that one should know volumetric pixel or voxel, which means the three-dimensional (3D) equivalent of a pixel and the tiniest distinguishable element of a 3D object. Thus a 1-voxel will be surrounded by 26 neighbouring voxels (Figure 2.6).

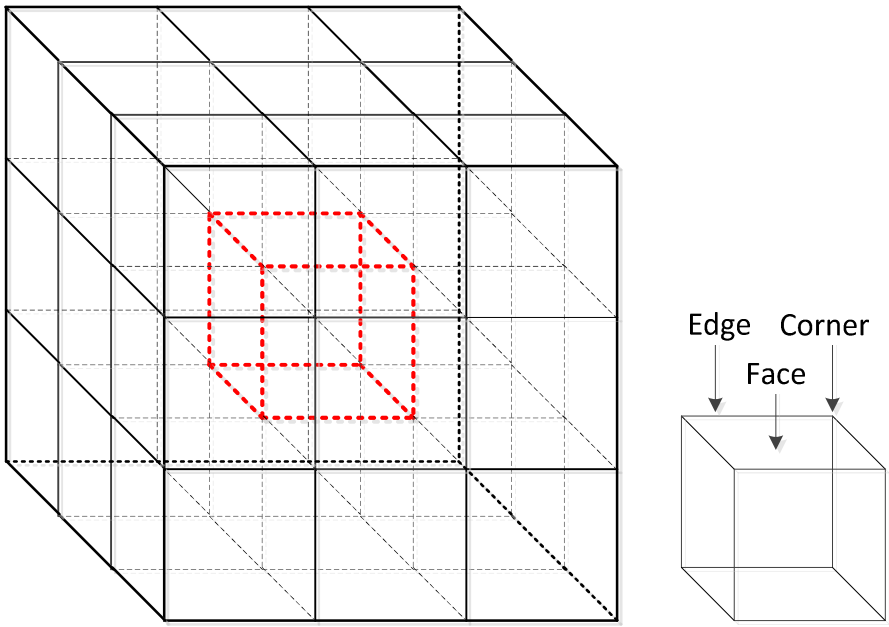

Figure 2.6: An illustration of neighbouring voxel (the 26 black cubes) and a surrounded voxel (one red cube). A voxel contains faces, edges and corners.

The Euler characteristics is defined as

$$\chi(X) = n_0 - n_1 + n_2 - n_3;$$

with n_0 (the number of voxel corners), n_1 (the number of voxel edges), n_2 (the number of voxel faces) and n_3 (the number of voxels) as counted parameters.

Combined with Euler-Poincare formula with Betti numbers, the expression is also expressed as $\chi(X) = \beta_0 - \beta_1 + \beta_2$ with β_0 reports the number of separate particles of the structure, $\beta_1$reports the number of handles (connectivity) and β_2 reports the number of cavities enclosed within the structure. By the assumption that bone does not complete encapsulate marrow space, then this equation may be reformulated as

$\beta_1 = 1 - \chi(X)$ or as a normalised connectivity density $\frac{\beta_1}{TV}$.

2.2.3 Mechanical properties of porous scaffolds

Porous scaffolds are expected to have adequate mechanical strength to perform its supporting function to enable cells to adhere and to proliferate [24]. The strength required depends on the target application. In many cases, the in-service load may not need to be supported by the porous implant and is instead supported by solid material surrounding it. It should, in any case, have sufficient strength to be handled and implanted without fragmentation and the generation of debris. Whilst the structure of bone is mechanically efficient using a lightweight material, there is no requirement that the porous support has to resemble bone, simply that it provides the cell morphology and interconnectivity required for cell migration and proliferation. The strength of bone could be a sensible target for the desired properties, but because bone may be from different parts of the body, then they may have different strengths [105]. As an illustration, the lumbar spine has cancellous parts in their five vertebrae; the so-called L1 – L5. Some researchers reported that the tensile strength of cancellous bone was 2 MPa [106], 2.06 MPa [107], and 5 – 10 MPa [108] and the elastic modulus 0.39 GPa [106, 109], 0.96 – 2.17 GPa [110], 0.2 – 0.5 GPa [111] and 0.05 – 0.1 GPa [108, 112]. Whilst the compressive strength of the lumbar may vary from 0.3 – 2.3 MPa according to Dreischarf [113], and 8 MPa [112] to 36 MPa [16] for the cancellous bone. For comparison, it was reported that the yield strength is 90 - 107 MPa and the 3.6 - 4.1 GPa Young Modulus is for PEEK [42, 72, 114, 115], while porous PEEK scaffolds have been reported to have a modulus of elastic of 42 – 86 MPa and a compressive strength of 12 – 30 MPa [16, 94]. Although it has been suggested that the mechanical properties should be as close as possible to the replaced

tissue to prevent stress shielding [80], it is still difficult to set an ideal target for the scaffold as there will be a large variation in the mechanical properties of "bone".

2.2.4 Biocompatibility of the device material

Biocompatibility refers to the ability of a material to perform with an appropriate host response in a specific application [41]. However, many materials are only biocompatible under one or more defined conditions not under all conditions and not capable of long-term success as an implant in the body. Some complications relate to metal implants, failure to heal the bone, bone resorption, and some cases of loosening of implants, bending of implants, and breakage or disintegration of implants, indicate metals do not always interact with body tissue in a synergistic way [41]. Compared to the substituted materials, polymer-based materials offer wide versatility in properties and processing [41].

In the use of PEEK, it was reported that PEEK cages resulted in good clinical outcomes [116, 117] and was proved as a suitable biomaterial for spinal implants [3, 50, 118-120]. More examples of careful and relevant studies associated with the use of PEEK reported that patients with PEEK cages had significantly better fusion rates and clinical outcome scores than those with poly-L-lactide-co-D,L-lactide cages [13]. Girasole (2013) also found that titanium cages achieved similar fusion rates to PEEK ones [121].

2.3 Fabrication techniques for porous PEEK scaffolds

One of the early uses of PEEK was in solid form as a solid posterior lumbar interbody fusion by machining to build the part [3, 56]. More recent studies have been trying to include porosity in the PEEK cages, by selective laser sintering [29, 30] and injection moulding [18, 31] to melt-extrusion [19]. Technologies of rapid prototyping and selective laser sintering are only capable of creating porosity in PEEK in limited circumstances (i.e certain heating temperatures, resulting in limited sizes of pore and strut, at low production rates) [29, 30]. Achieving high porosity is one of the current problems faced by researchers in providing adequate porous PEEK scaffolds. Existing techniques are only able to produce porous PEEK scaffolds with < 50% of porosity. For instance, Werner et al (2005) tried to produce porous PEEK using supercritical CO_2 and only obtained low porosity of 40% with a small pore size range of 45 – 175 µm [33] and Landy et al (2013) used a porogen and extrusion to produce porous PEEK and was only able to obtain 50% porosity and a 100 µm pore size [32]. Wang (2013) used a micro-porogen (NaCl) and was only able to produce low porosity (Figure 2.7a) [31]. Thus, the existing techniques only allow the production of, in some cases no pores [31], low porosity [18, 32] and limited pore sizes [18, 30, 31, 122].

Werner et al (2005) tried to produce carbon Nanofibers-reinforced PEEK foam by an injection moulding process and a chemical blowing agent, but the porosity formed is still closed cell (Figure 2.7b), due to of poor melt stability. With that technology, the pore diameters were limited up to 175 µm [33] although injection molding has successfully produced porous PEEK (Figure 2.8a and b). To overcome this limitation, some other authors tried to combine

the salt leaching technique with other techniques to achieve interconnected porosity [38, 39] although still with a lack of control of the morphology and the residual NaCl content (Figure 2.9a and b).

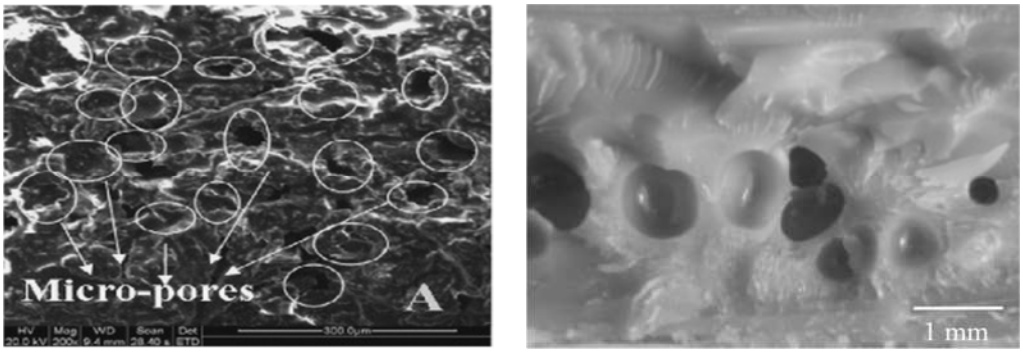

(a) (b)

Figure 2.7: PEEK foams from (a) incorporating micro-porogen (NaCl) [18]; (b) pure PEEK by injection moulding [33].

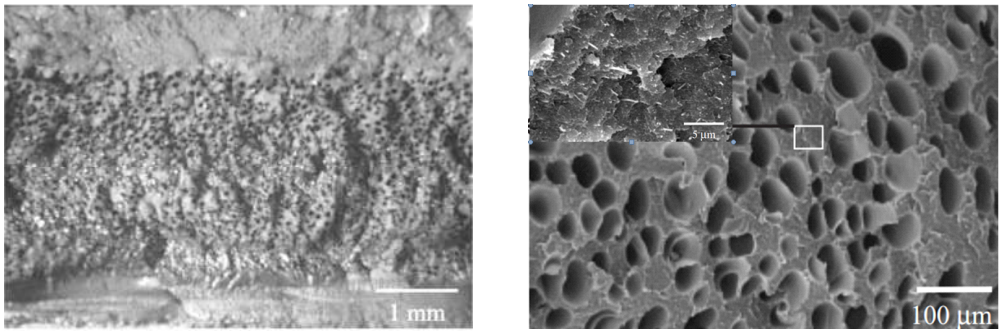

(a) (b)

Figure 2.8: (a) 10% Carbo Nano Fibers – PEEK foams by injection moulding and (b) SEM images of the fracture surface of the PEEK foams showing the scaffold structure [33].

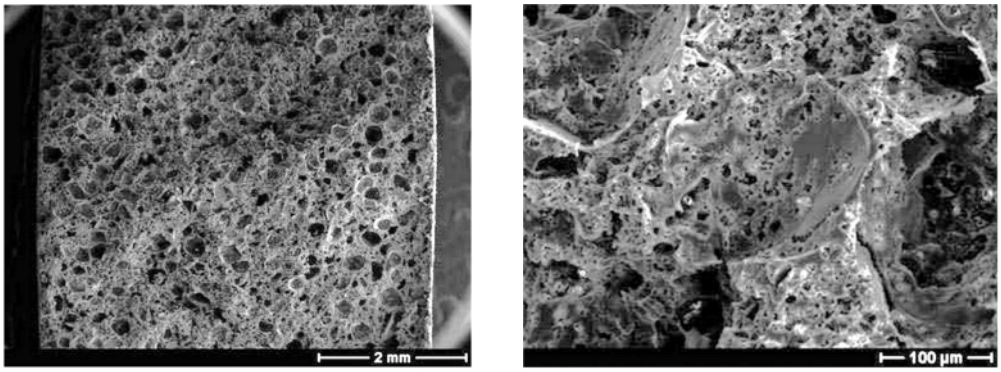

(a) (b)

Figure 2.9: (a) Cross-section of the scaffold using injection moulding with salt leaching; (b) the pores left behind by NaCl particles providing the interconnected network [38].

The conventional salt leaching technique is very simple but is limited in the variety of pore shape, as the pore shapes are dictated by the salt particles and are typically angular [37, 38] (see Figure 2.10). Even so, any porous scaffold fabrication technique adopted should be easy to conduct and address the minimum requirements for the scaffolds i.e high porosity, good pore interconnectivity and good mechanical properties [25-28, 76, 77]. These criteria may direct researchers to the particulate leaching technique for which the technique does not need complex technology and is easy to carry out. An interesting fact of the particulate leaching technique showed that a former study by Mikos et al [36] could control porosity and for salt weight fractions of 0.7-0.9, the structures were homogeneous with interconnected pores [34]. Another complementary finding by Zhang (2005) observed that spherical pore scaffolds exhibited better pore interconnectivity than ones with cubic pores [35]. Although the studies by Mikos and Zhang were not using PEEK, their findings could be a barometer of future research using PEEK as a porous material via a modified salt leaching technique.

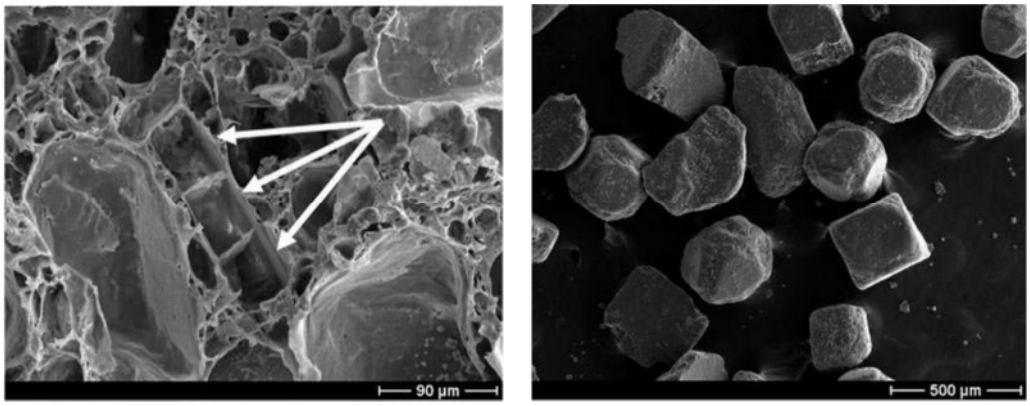

(a) (b)

Figure 2.10: (a) The pores left by direct leaching of the NaCl particles and (b) typical sieved NaCl particles [38].

Since PEEK is relatively new to porous scaffold studies and conventional particulate leaching has been applied in only a limited number of studies to produce porous PEEK scaffolds, with variable degrees of success, there is a drive to modify the existing technique in order to be able to produce adequate porous PEEK scaffolds. Some reported works related to porous PEEK incorporating NaCl as porogen as follows;

- Jarman-Smith et al (2012) tried to combine a moulding process with particulate leaching using salt (70 wt% and 100 -1000 µm size range) as a porogen. The made scaffolds had been reported to have 50% porosity with a small pore size of 70 µm and not perfectly porous [16] indicating a residual salt problem (Figure 2.11a).
- Wang et al (2013) tried to produce porous PEEK by mould-leaching and vacuum melting under high temperature using NaCl (30 wt%) as a porogen. The moulding-leaching process involved a pressing mould, followed by sintering at 360 °C for 2 h and via leaching out the porogen in an 80 °C deionized water bath. Whilst the vacuum melting is filling

process of the porous structure with lithium-base grease at 150 °C for 2 h under vacuum condition of 0.01–0.2 bar. However, the technique only produced low porosity of 24% [18] (Figure 2.12a).

- Evans et al (2015) tried injection moulding incorporating NaCl (200 – 312 µm in size range) to produce a layer of porous PEEK scaffold with high interconnectivity, but was only able to obtain porosity less than 70% [19] (Figure 2.12b).

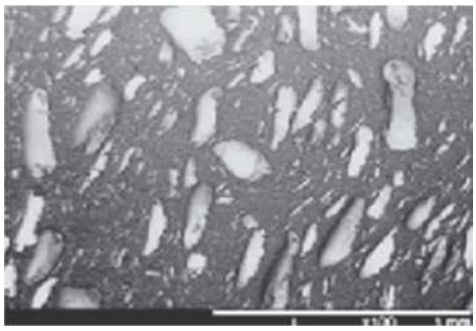

Figure 2.11: The surface of porous PEEK from injection moulding/particulate leaching [16].

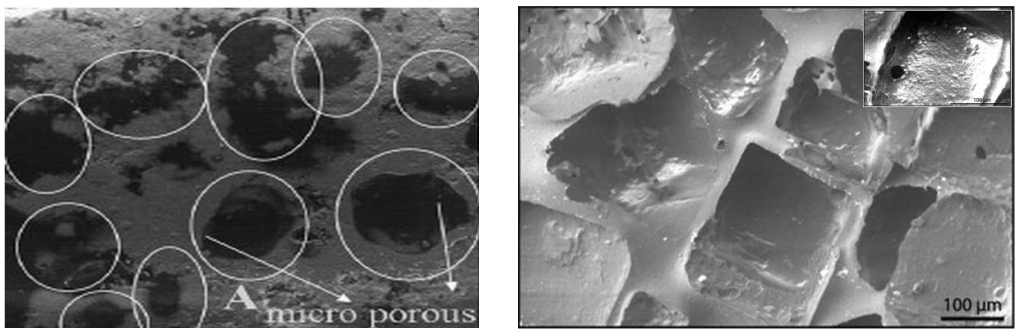

(a) (b)

Figure 2.12: (a) PEEK structure at 24% porosity [18] and (b) a pore layer –section of injection-moulded PEEK with < 70% porosity [19].

2.4 The use of spherical NaCl as a porogen

The manufacture of spherical salt beads and their use as dissolvable templates for the production of scaffolds was initiated by Jinnapat and Kennedy (2010)

[40]. The salt beads were made by disintegrating a flour-salt-water paste in oil (Figure 2.13a) and the manufacture of the porous Al scaffolds was affected by vibration-assisted packing [40].

Salt the beads were tapped to increase the packing fraction and then an Al alloy powder of 116μm size was poured on top of the salt bed and further tapped until it completely percolated into the gaps between the salt beads. The tapped composite was then cold compacted and sintered before salt removal in warm water. The structures of the resulting parts are shown in Figure 2.13b. Their findings demonstrated a repeatable fabrication technique with spherical salt beads in the size range of 0.5 – 3.0 mm [40] producing Al scaffolds with 79% porosity and good interconnectivity. The advantages of the technique, according to Jinnapat and Kennedy (2010) are salt separation from the scaffolds is relatively fast and by vibration, the gaps between the salt beads are sufficiently well filled for a continuous network of Al to act as a scaffold frame. Vibration or tapping thus appears to be an attractive process to produce porous structures with good inter-connection. However, this technique has not been applied to different materials such as polymers.

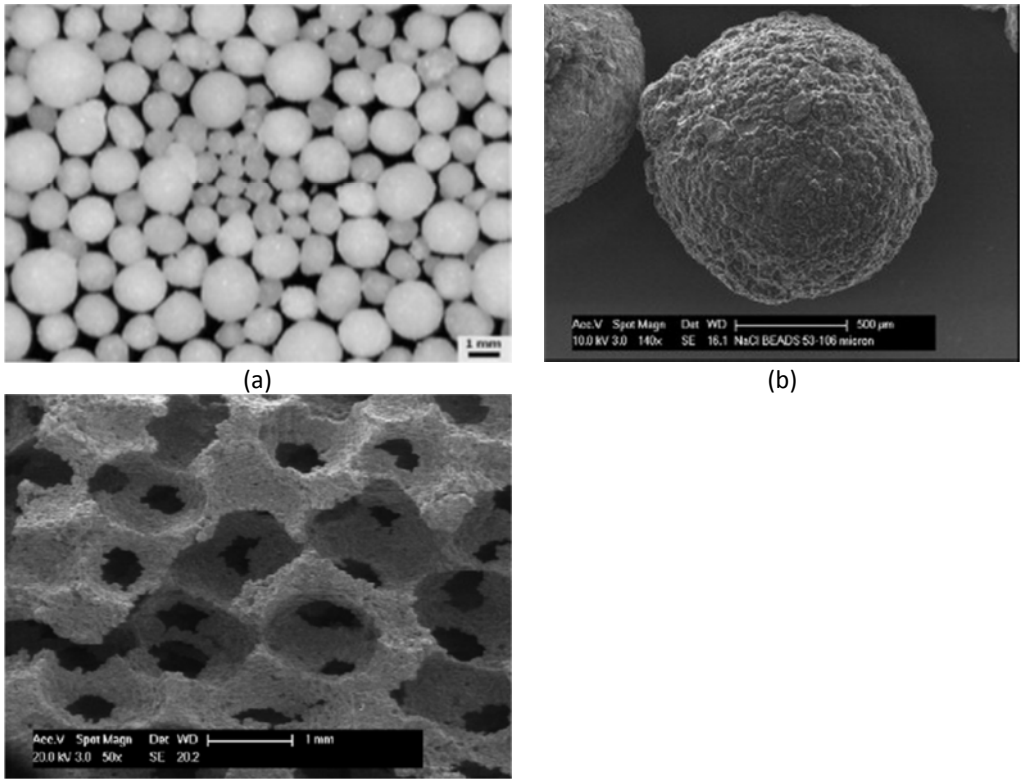

(a) (b)

(c)

Figure 2.13: (a) Typical structure of a spherical salt beads, (b) an example of salt beads and (c) the morphology of the Al scaffolds produced in [40] showing porous network after salt removal.

2.5 Vibrated packing studies

Sphere packing and effect of vibration or tapped packing has been studied by different researchers such as [123], [124], [125] and [126]. They investigated key parameters to provide optimum packing such as flow phenomenon [123, 127], coordination number and packing density [124, 126, 128, 129] and radial porosity [125, 130]. The coordination number refers to the number of contact points of a particle with its adjacent particles, whilst the radial porosity represents a structural characteristic of confined fixed packed beds due to the container wall effect and could inform an average porosity as a function of the radial direction. There would be different flow phenomenon due to the imposed vibration resulting in small and big surface waves [123] and an increasing

frequency of vibration may cause the packing density to increase to reach the maximum and then decreases. Furthermore, a smaller coordination number is found on a looser packing [124]. An analytical equation had been used to predict the radial porosity in the near and far wall regions [125], and Discrete Element Method, DEM, was applied to estimate the densification of the packing structure of equal spheres under mechanical vibration that of obtaining maximum packing densities of 0.64 [126]. A DEM approach is a numerical method for computing the motion and effect of a large number of small particles. In terms of the packing structure, it was also confirmed that the wall or floor of a container affects the packing structure of spherical particles and the packing structure [131-135], or local voidage surrounding the wall is different from that at the center of a container [136], or the packing of particles being denser at the centre (as shown in Figure 2.14) [132].

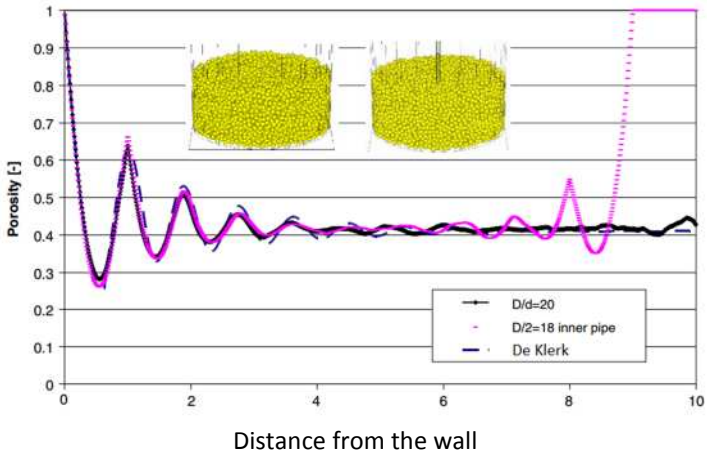

Figure 2.14: the radial porosity distribution for pipe (D) to particle diameter (d) ratio of 20 [132]. Porosity is referred as y-axis and distance the distance from the wall as x-axis.

More advanced modelling studies via the Discrete Element Method (DEM) also have been conducted by Zhang (2001), Remond (2010) and Jain (2012) to predict the flow of particles during vibration [137-139]. It is also said that the

wall effect will be less observable after few spheres away from the wall [125] depending the bulk density of the particles. Vibration or tapping of different particles will cause the smaller particles to sift toward the bottom and lead the large particles to the top [139-141]. Jain et al (2012) stated that if the particle is adjacent to the same-sized other particles, segregation is unlikely to occur and segregation is likely to occur when the particle is surrounded by different particle sizes [139], and when small and large particles are in the cylinder, when tapped, the large particles accumulate at the top [142, 143]. The convection flow in a vertically vibrated system of bi-modal particle sizes had been studied by [127, 139, 144] and showed that the convection at the wall and in the centre flows downward and upward, respectively [139] and vertical vibrations can result in symmetric and asymmetric convection rolls [144]. This is shown in Figure 2.15.

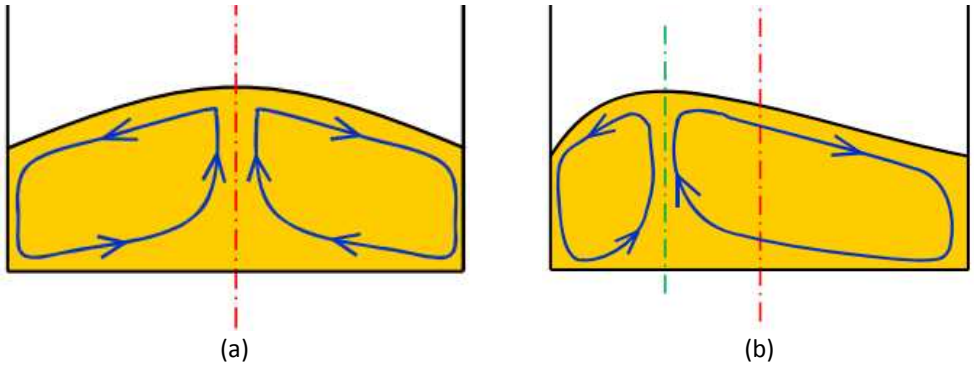

Figure 2.15: Examples of symmetric and asymmetric of convection flows observed in the vibrated granular bed. The arrows show the directions of granular flow [144].

2.6 Knowledge gap

The critical reasons for PEEK development are the capability for imaging bony in-growth visualisation and a porous version could make the accepted biomaterial osseoconductive (encouraging bony in-growth) [1]. The challenge

is to produce porous PEEK via a novel method where previous attempts have been limited to the technology and the resultant geometries have had limited their ability to fulfil the key end-user requirements [20].

Based on the cited studies in previous sections, it was shown that the salt leaching technique has great potential to produce porous scaffolds, but further improvements are still needed to address issues of a more controlled pore size range, improved interconnectivity and increasing the porosity without clogging the pores.

The use of spherical salt beads and vibration, demonstrated by Jinnapat and Kennedy (2010) produces promising-looking structures but has not been applied to polymers. Yet, some shortcomings of this process are still observed such as structural inhomogeneity from incomplete cell walls, fragile struts due to the incomplete filling of the gaps between the salt particles during the tapping stage and excessive solid material on either the top or bottom surfaces [104]. Since no researchers have reported the manufacture of porous PEEK scaffold via salt-leaching and vibration, this has the potential and form the basis of a novel approach to producing scaffolds with good porosity and connectivity.

Chapter 3: Materials and Methods

This chapter introduces the materials used in this research, rounded salt beads based on the work of [40] used as a porogen and three types of Poly-Ether-Ether Ketone (PEEK) powder used as the scaffold material including Vicote 701 PEEK, PEEK -OPTIMA® LT1 and PEEK -OPTIMA® LT3. These three types of PEEK have been potentially used by the manufacturer to produce implant parts. They had different behaviour through the proposed route of fabrication due to their particle size ranges. Hence, these three PEEK powder types were then engaged to seek the best material for a suitable fabrication technique. It also details the procedure for scaffold fabrication, using the established technique of porogen leaching, involving the steps of; material preparation; blending; compaction; sintering; dissolution and drying. Finally, the characterisation methods used to determine key morphological parameters for the materials and the porous PEEK are explained, as are methods for mechanical testing.

3.1 Materials and equipment

3.1.1 Rounded (NaCl) salt beads

Sodium chloride (NaCl or salt) powder with 99.5% purity, supplied by Fisher Scientific, was processed into rounded beads, using a method outlined in [40] and [145]. In brief, this method produces porous salt beads via the mechanical disintegration, in oil, of a paste containing fine (53 – 106 µm) salt powder,

flour and water. Before use the beads are cleaned, to remove the oil, and the flour is burnt out at 500°C for 24 hours.

Beads of three diameter ranges; 1.0 - 1.4 mm, 1.4 – 2.0 mm, and 2.0 – 2.5 mm were selected by sieving and stored in separate, sealed in plastic bags to keep them dry. The density of the salt beads (ρ_{sb}) of 1.0 – 1.4 mm was 1.65 ± 0.05 g cc^{-1} for the (23% porous) NaCl beads and 1.61 ± 0.10 g cc^{-1} and 1.57 ± 0.09 g cc^{-1} for the 1.4 – 2.0 mm and 2.0 – 2.4 mm salt beads, respectively, as measured in [40]. The morphologies of the salt beads were observed using optical microscopy and scanning electron microscopy (see section 4.1.1). The 23% porous of the salt beads was based on the density of salt at 2.15 g/cc(ρ_s). Thus, the porosity of the salt beads was calculated by 1 - (ρ_{sb})/ (ρ_s) in respect to each salt bead size ranges. Whereas the porosity of the 1.0 – 1.4 mm would be $1 - \frac{1.65}{2.15}$ or 0.23.

3.1.2 PEEK powder

Initially, three types of PEEK powder were compared; Vicote 701 PEEK, PEEK -OPTIMA® LT1 and PEEK -OPTIMA® LT3, all supplied by Invibio Ltd. The detailed characteristics of these materials are provided in Appendix 1. The distribution of PEEK particle size for each type was measured using a Malvern Mastersizer 2000 which uses a light scattering method for measuring the particle size. 0.5 g samples were analysed and measured three times to obtain an average, giving a frequency curve and a set of values for D_{10}, D_{50}, and D_{90} (the sizes of particle below which 10, 50, and 90% of the volume respectively lies) to describe the size distribution of the particles. The

morphologies of the PEEK powder were observed by scanning electron microscopy (see section 4.1.1).

The apparent and packing densities for these powders were determined by measuring the volume taken up by a known mass of powder (approximately 40g of beads, 10g of PEEK). The apparent density refers to the mass per unit volume of loose material when the material is poured through a specific funnel into a cylinder of known volume and was calculated as the mass of material divided by the volume of the material in the cylinder. While the packing density in this thesis was associated with the tap density determined after defined compaction of the powder. This was performed by loading the powders into a 100 ml transparent graduated cylinder (of 3 cm diameter), lightly tapping the vessel, to level the powder off, and recording the fill volume from which the apparent density was calculated. The tapped density was measured by automated tapping using a Quantachrome Autotap machine (Figure 3.1), tapping up to 4000 times. The volume of the tapped powder was recorded at 10, 1000, 2000, 3000 and 4000 tap intervals. The specifications of the machine as follows; the tap height at 5 mm, tapping rate at 260 per minute without loading more than 900 g on the top (with the existing die set, the tapping rate was 215 per minute).

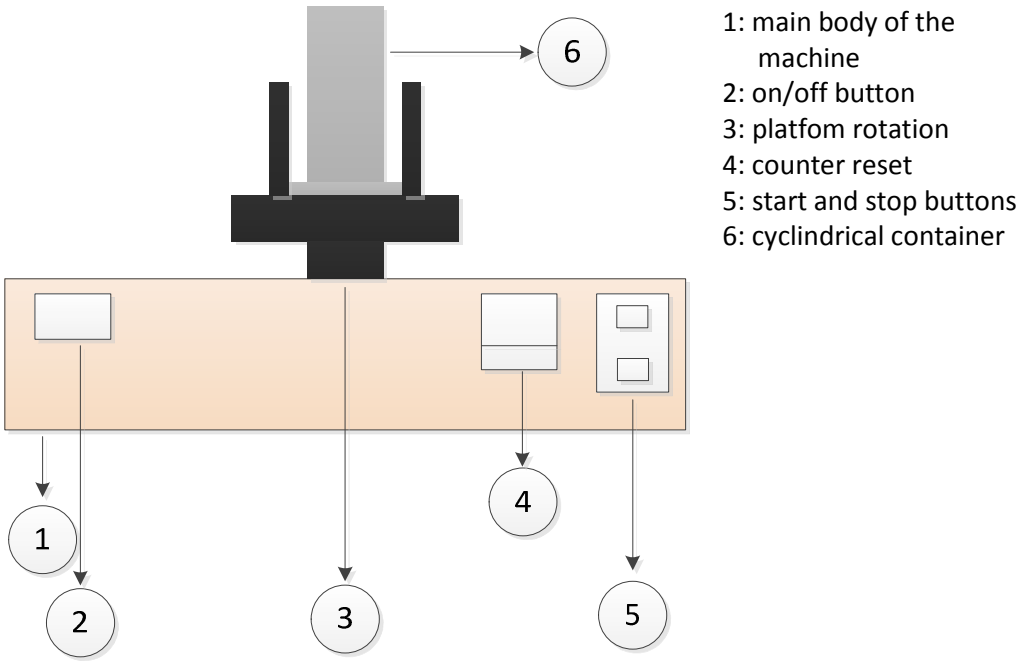

Figure 3.1: The schematic of Quantachrome Autotap machine.

3.2 Fabrication of porous PEEK scaffold

Figure 3.2 shows a schematic of the manufacturing steps required to produce porous PEEK specimens. Boxes with a dashed line contain brief descriptions of each step, and the circled numbers next to boxes show, step-by-step, the experimental procedure in fabricating the porous PEEK specimens. The detailed explanation is included in the following sections.

3.2.1 Material preparation

An initial target porosity of 80% was set (see 2.2.2), giving a volume ratio of PEEK/salt beads of 20/80. From the densities of the beads and PEEK powder, this gives rise to an approximate 1/6 mass ratio of PEEK/salt beads, which was set as the norm for the majority of the experimental trials. Appropriate quantities of 0.7 g of the PEEK powder and 4.2 g of the as-made rounded salt

beads were weighed out into a weighing dish using the same digital milligram scale, A&D-GF200, used in section 3.2.2. Prior to all weighing and subsequent blending processes, to prevent moisture uptake from humidity, the PEEK powder was dried in a drying cabinet at 90^{o}C for 15 minutes.

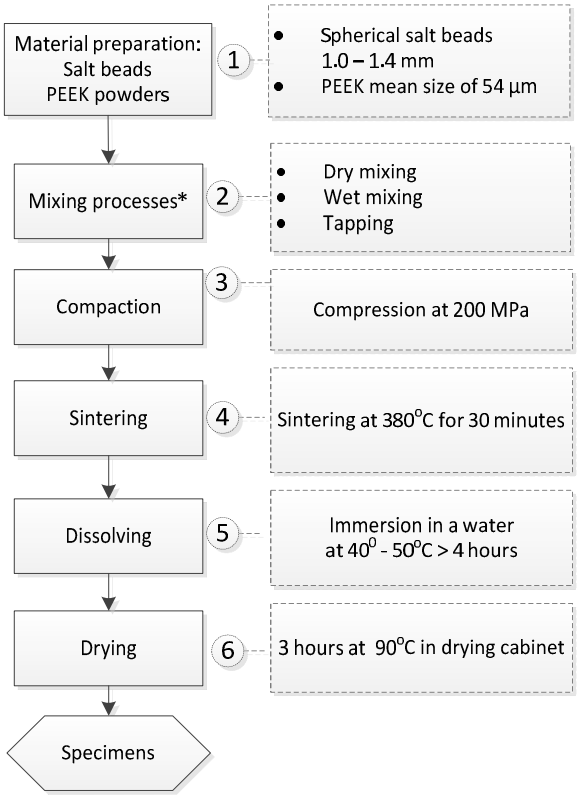

Figure 3.2: Schematic of the experimental method for fabricating specimen of porous PEEK

3.2.2 Blending

In this study, three methods of blending the PEEK and salt beads were explored using wet, dry and tapping methods.

3.2.2.1 Wet mixing

The wet mixture was aimed to force PEEK to attach to the slat bead surface in order to be able to create thin layers of PEEK onto the salt bead surface. The PEEK layers were expected to create continuous PEEK network along with the pores from the salt bead shapes after the mixture of PEEK and salt beads was compacted, sintered, dissolved and dried. In this method, to develop a batch of wet-mixed powders, 7 g of PEEK powder and 42 g of salt beads were weighed out separately and then the beads were first poured into the 500 ml beaker. A spraying bottle filled with water was already prepared prior to the mixing process. The salt beads in the beaker were then sprayed with roughly 0.6-0.7cc of water (5 sprays), producing a fine mist 100 mm away from the beads to aid their even coating with water, followed by adding 0.5 g of PEEK powder and subsequent stirring. This spraying-pouring-stirring cycle was performed in the beaker about 15 times, in total consuming 9-10 cc of water, and was conducted for 10 minutes until the PEEK coating appeared even. After this; the wet mixture was transferred to a flat tray for drying at 90^{o}C for 3 hours in a drying cabinet to evaporate the water. The dried mixture was then weighed into 4.9 g batches for subsequent compaction. The resulting mixture is shown in Figure 3.3.

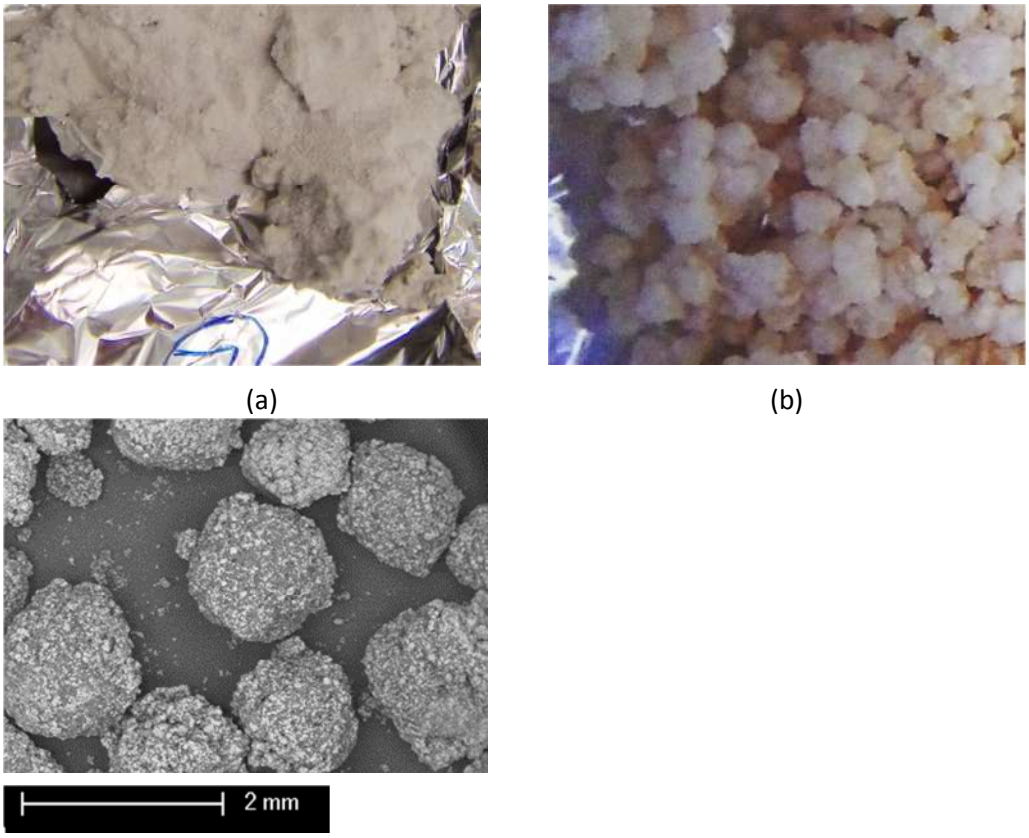

(a) (b)

(c)

Figure 3.3: The salt beads after the wet mixture process with (a) too much water sprayed, (b) The salt beads with the right amount of water sprayed and (c) The PEEK covered salt beads viewed under SEM

3.2.2.2 Dry mixing

In a dry mixing container, 42 g of salt beads were mixed with 7 g of PEEK powder and placed in a Turbula mixer (Figure 3.4), for 15 min. 4.9 g of the mixed powders were then weighed out for subsequent compaction.

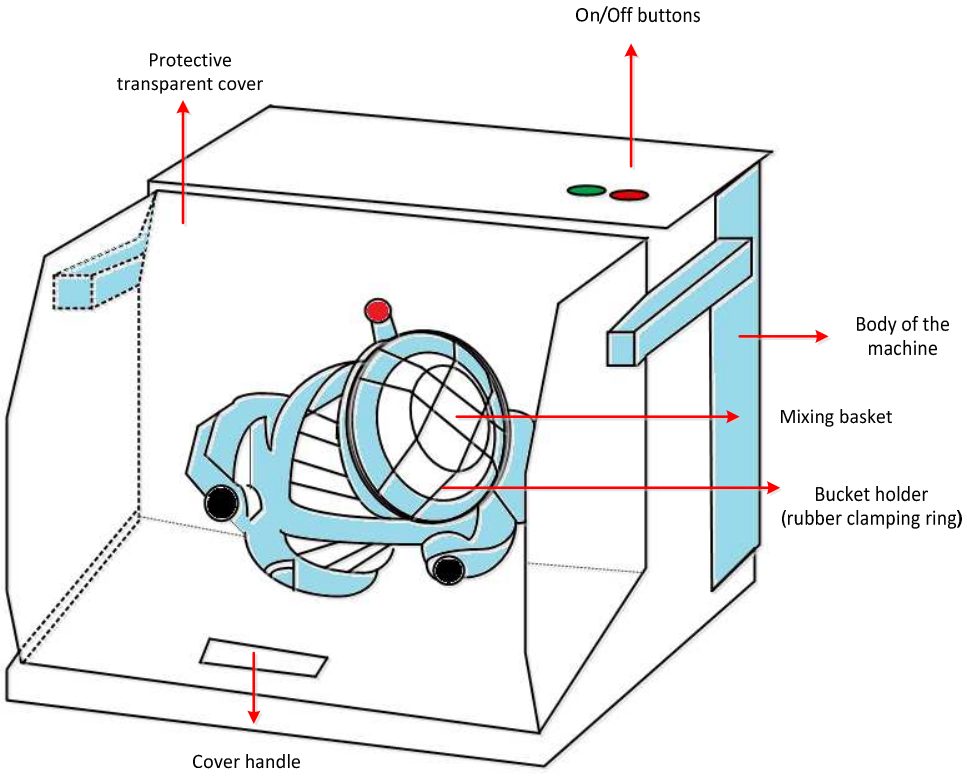

Figure 3.4: Turbula mixer used for dry mixing.

3.2.2.3 Tapping

In this process, 4.2 g of salt beads were first poured into the cavity of a 22 mm diameter tool steel die (with the bottom punch in place) as seen in Figure 3.5. The upper punch weighs 246 g, and the bottom, 163 g, along with the main die which weighs 1252 g. The bed of salt beads in the cavity was levelled off by 10 taps to disperse the beads evenly in the cavity. 9 g of dried PEEK powder was added to the salt beads and distributed evenly onto the salt bead surface. After the PEEK/salt bead mixture layer was developed in the die cavity then it was transported to the same Autotap machine that was reported in section 3.2.2 and the die tools filled with the mixture were setup firmly on the tapping plate with the upper punch was inserted. The whole assembly was tapped by the

machine, which employs a simple lifting and dropping action (dropping through a height of 5 mm), stopping after a pre-determined number of cycles (as many as 10,000 taps, tapping at 215 taps per minute).

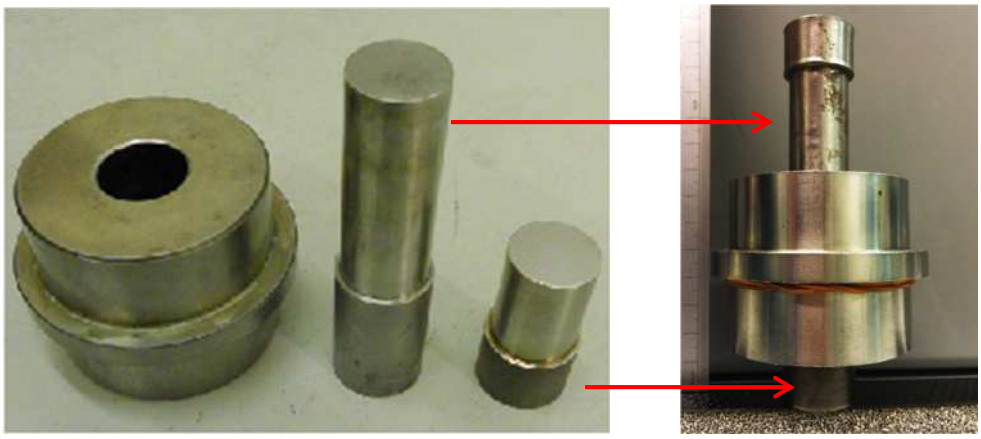

Figure 3.5: (a) The cylindrical metal die set; (b) The assembly of the die set. The arrows show the position of the punches in the die cavity.

The tapping tools consist of a cylindrical metal die and punches with the dimensional lengths depicted in Figure 3.6a. The die set consists of the cylindrical die of 22 mm inner diameter (Figure 3.6b) with 55 mm height along with its upper punch and the lower punch (Figure 3.6c). Inside of the die cavity die are salt beads (the green shading) and PEEK powder (the yellow shading).

In several cases, the progression of tapping was investigated by measuring the thickness changes of the materials in the cavity as a function of the number of taps. In order to follow the progression of packing of the beds, digital Vernier callipers were used to measure the thickness of the mixed bed indirectly, by

placing the upper punch in the die on top of the bed and measuring the distance it protruded from the die and repeating the process at set tapping intervals.

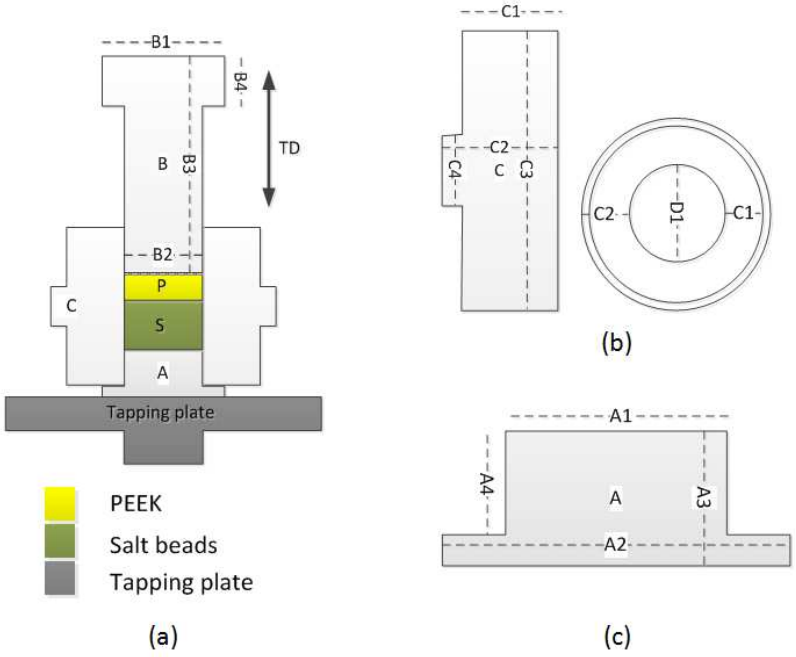

Part A (Lower punch) – A1 (22 mm); A2 (28 mm); A3 (50 mm); A4 (30 mm); 163 g
Part B (upper punch) - B1 (28 mm); B2 (22 mm); B3 (80 mm); B4 (17 mm); 246 g
Part C (die) – D1 (22 mm); C1 (20 mm); C2 (26 mm); C3 (55 mm); C4 (10 mm); 1,252 g

Figure 3.6: (a) Schematic of the powder layers including the dimensions of the upper punch, (b) the dimensional lengths of the die and (c) the lower punch dimension. The arrow shows the tapping direction; A, B, and C are the lower and upper punch and die respectively.

3.2.3 Compaction

When compacting wet or dry mixtures, the same 22 mm cylindrical die set as was used for tapping (see 3.2.2.3) was cleaned with Industrial Industrial Methylated Spirit (IMS), a solvent for the cleaning of the tools. 4.9 g of the mixtures were poured into the die cavity with the bottom-punch in place. The upper punch was then inserted into the die and then compacted using a 40 Ton mechanical press, loading using pre-sets of 30, 70, 140 and 190 kN. Only one

loading set was then applied (70 kN set) throughout the experiment which was considered to give good compact samples based on their density. The actual loads, corresponding stresses and the height, diameter and mass of the compacted samples (after ejection from the die) were recorded. Compaction resulted in a robust "composite" pellet of PEEK/salt beads. Tapped structures were transferred from the Autotap machine and compacted in the same way.

3.2.4 Sintering

This step is to alter the solid PEEK pellets from compaction by heat without melting them to the point of liquefaction. Before the pellets were introduced into the chamber of the furnace; they were placed on a tray (Figure 3.7) which was already coated with an aluminium foil covered with a spray coating of a boron nitride spray supplied in an easy-to-use aerosol can - HeBoCoat 401E (details in Appendix 2). The coating was used to prevent the pellets from sticking to the aluminium foil covered-tray surface at high temperature. Sintering (or more correctly melting) of the PEEK was performed in a furnace using the following schedule. The heating cycle was started at room temperature and was raised at 5^{o}C/min up to 300^{o}C, dwelling for 30 min, and then was raised at 5^{o}C/min to 380^{o}C dwelling for another 30 min. The furnace was then switched off and although set to cool at 5^{o}C/min, cooling to room temperature took up to 6 hours. The programmed heating and cooling profile is shown in Figure 3.8.

Figure 3.7: Pellets on a tray covered with a boron nitride- coated aluminium foil.

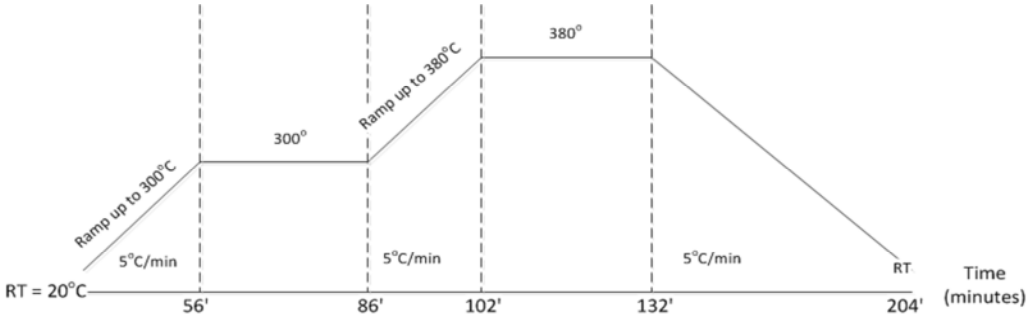

Figure 3.8: Heating profile for the "sintering" process

3.2.5 Dissolution and drying

The sintered "composite" pellets were immersed in water to remove the salt. An ultrasonic bath (James Sonic 3000) with a capacity of 2l was used, setting the water temperature to 50^{o}C. The pellets were immersed for periods of up to 3 days, changing the water every 30 - 60 minutes in the first 2 hours and subsequently twice a day. After water changes several times (or day 3), clear water and floating pellets indicated sufficient leaching time that the leaving salt had created cavity and the density of samples reduced (lower than water density). The PEEK scaffolds were finally dried in a drying cabinet at 90^{o}C for 3 hours, weighed and their dimensions were measured.

3.3 Material characterisation

3.3.1 Materials, pore and window morphology

PEEK powder, salt beads and coated salt beads were prepared separately, dried at 90^{o}C for 30 minutes, and stored in different sealed plastic bags prior to mounting. For SEM examination, specimens were mounted by dispersing and distributing powders and particles evenly on a stub which was already covered with a double-sided sticky carbon tape.

Prior to SEM imaging, all specimens were coated with platinum using a sputter coater, applying 2.0 V and 2.0 – 4.0 mA plasma current in an argon gas atmosphere for 90 seconds. After that, samples were observed through a Philips XL 30 SEM, operated at 15 – 20 kV in Secondary Electron (SE) mode.

For the case of wet mixture, Energy Dispersive X-ray (EDX) Spectroscopy was conducted in order to be able to distinguish between PEEK and salt elements from the black and white image of the SEM. The point analysis of EDX was chosen since the surface of the sample observed not completely flat.

The observation of the porous PEEK was firstly performed by using a stereoscopic microscope, Nikon SMZ-10A, coupled to a Nikon Digital camera DXM1200F, using a dedicated image capture software of ACT-1. The preparation of some porous PEEK fragments was facilitated by either simply scoring and snapping large pieces or sectioning using a cut-off disc to reveal the internal structure. Before examination, an air spray was used to remove any debris from the fracture surfaces.

To image the surface and internal structure of porous PEEK at higher magnification, SEM images were also produced. Samples were sectioned in the same way as for preparation for optical microscopy and mounted and coated in the same way as for particulate materials (described in section 3.4.1.1). The observation was performed by using the same Phillips XL 30 SEM and imaging conditions to those reported earlier.

Image analysis software, ImageJ was used to quantify structural parameters using imported images from optical and scanning electron microscopy. The digital (tiff) images were rescaled in ImageJ to match the resolution and then transformed into an 8-bit format and thresholded in order to apply measurements.

3.3.2 X-ray computed tomography

Detailed structural quantification was performed using micro computed X-ray tomography using a Scanco MicroCT 40 unit. Porous PEEK samples were dried and cleaned using an air spray and placed securely in a 36 mm diameter sample holder (limitation of the available equipment). For the purpose of obtaining actual porosity, an intact sample was simply placed at bottom of sample holder base. The position of the sample was with the top surface facing up. The MicroCT 40 was operated at a voltage of 70 kVp and a current of 145 mA. Samples were scanned at 30 μm voxel (3D pixel) resolution (machine capability) with an integration time of 300 ms to produce the 2D and 3D tiff files using the same threshold value (35). Parameters, such as the 2D and 3D

scaffold porosity, mean pore size, strut thickness and other key parameters, were then generated by the dedicated Scanco software.

In some cases, 2D images from the MicroCT 40 were analysed using ImageJ (see section 3.4.2) but, owing to the limiting resolution, only features larger than 30 μm were analysed. Image analysis was used to identify and quantify the levels of residual salt particles in the porous PEEK from image stacks by adjusting the brightness to enable a clear distinction between the salt particles and PEEK structure. Alternatively, the observation of salt residue were conducted by sample observation under SEM and optical microscopy.

3.3.3 Mechanical testing

Porous PEEK pellets were prepared before testing by grinding (with the salt in place) to produce parallel faces. The grinding process was also applied when preparing for moulding integration between porous and solid part in 6.1.1. The resulting specimens were disc shaped with typical thicknesses of 5-6 mm and 22 mm in diameter and a minimum of 5 samples was prepared. A mechanical testing machine, Instron 5969 was used to compress the samples at a speed of 0.5 mm/min, up to 80% strain or a 5 kN load limit and two flat metal plates were used to hold the pellets. The compressive load and the displacement were recorded to define the compressive yield strength (the first peak of the compressive stress–strain curve). In this test the twin linear variable differential transducers (LVDTs) were used to accurately measure the strain.

Chapter 4: The Comparison of Porous PEEK Scaffolds Made by Wet, Dry and Tapping Routes

4.1 Observations of the rounded salt beads and the PEEK powder

4.1.1 Rounded sodium chloride beads

The rounded salt beads were produced using a method explained in section 3.2.1. The structure of the beads is shown in Figure 4.1 for rounded salt beads of 1.0 – 1.4 mm diameter, where it can be seen that the bead shapes appear rounded with a few appearing slightly elongated. Quantitative analysis of images such as that presented in Figure 4.1a shows the degree of anisotropy to be between 1.15 and 1.19. The structure of the beads was also observed by SEM as seen in Figure 4.1b, showing that the beads are comprised of an agglomerate of fine salt grains.

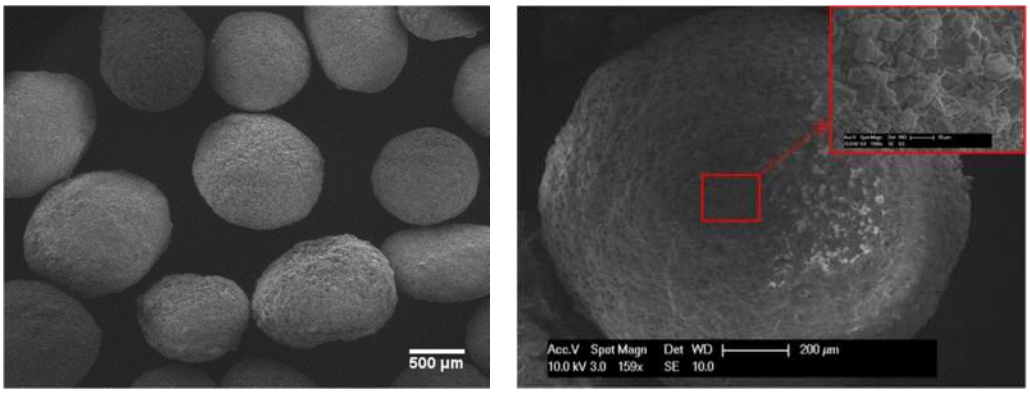

(a) (b)

Figure 4.1: (a) Rounded salt beads of 1.0 – 1.4 mm diameter; (b) An example of a typical rounded salt bead of 1.0 – 1.4 mm diameter accompanied with a zoomed area marked with a red squared line.

Figure 4.2 shows a 2D CT image of the salt beads, where it is clear that they contain (black) pores. The density of salt is 2.15 g/cc, and the rounded salt beads in the diameter range of 1.0 – 1.4 mm have a density of 1.65 g/cm^3 [40], thus containing 23% porosity (see section 3.1.1).

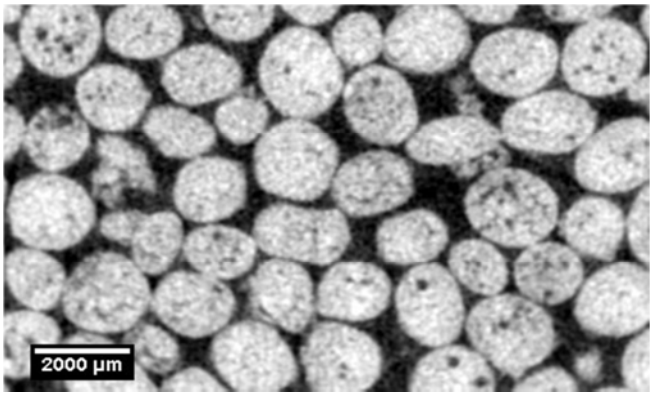

Figure 4.2: CT image of the salt beads. Pores are shown as black spots within the white beads

4.1.2 PEEK powder

Three types of PEEK were used in the early experiments; Vicote, LT1 and LT3 PEEK. They are compared in Figure 4.3a, b and c. The PEEK powders of Vicote, LT1 and LT3 generally appear similar in shape, rounded but irregular.

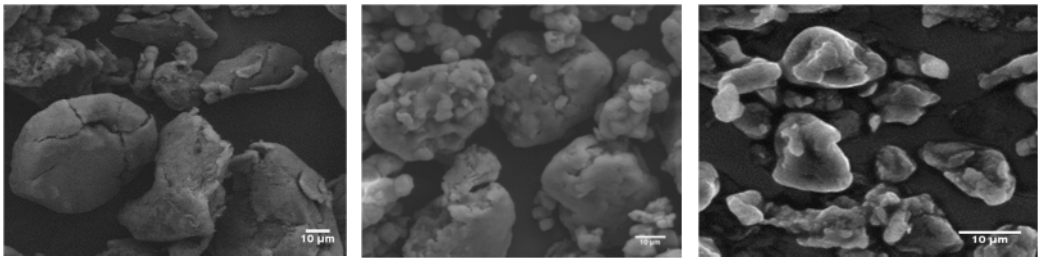

(a) (b) (c)

Figure 4.3: SEM images of (a) LT1 PEEK; (b) LT3 PEEK; and (c) Vicote PEEK.

The size distribution of the PEEK particles is presented in Table 4.1. The table shows that the LT1 PEEK has a largest particle size and that the Vicote type

has the smallest size and narrowest particle distribution among the three. Typical plots of the PEEK particle size distributions are plotted together in Figure 4.4, with the volume average particle size (D_{50} - the volume median) of each type of PEEK at 11.4, 54.2 and 42.1 µm for Vicote, LT1 and LT3, respectively. Since the plots of the distribution of particle size are not fully symmetrical, median and mean values could be slightly different. Thus, D_{50} is more effective to explain the distribution of the particles. The complete outputs from the Mastersizer 2000 are included in appendix 3.

Table 4.1: Statistics of PEEK particle size distribution measured using a Malvern Mastersizer 2000 (3 times of measurement).

PEEK Type	Vicote	LT3	LT1
D_{10} (µm)	6.092	15.418	21.349
D_{50} (µm)	11.402	42.137	54.228
D_{90} (µm)	19.728	81.839	109.758

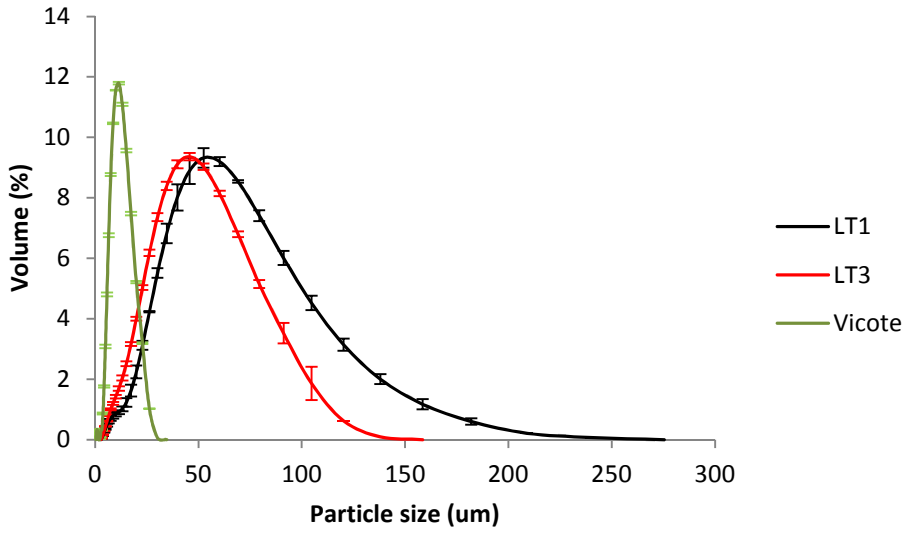

Figure 4.4: The comparison of the particle size distribution for the Vicote, LT1 and LT3 PEEK powder. Inserted images represent each type of PEEK used.

4.1.3 Apparent density and tapped density

The apparent and tapped densities for the PEEK powder and the 1.0 – 1.4 mm salt beads were measured and are shown in Figure 4.5 and Figure 4.6 along with the packing fraction (relative density) estimated from the bulk density of the beads and powders. The packing fraction here is associated with the value of relative density and is calculated by the bulk density divided by the density of the material. The packing fraction of the salt beads increased from 0.53 to 0.56, achieving a constant packing fraction after fewer than 500 taps. The initial packing fraction (of loose packing) for the PEEK was much lower (between 0.22 – 0.24) and was highest for the LT1 powder (Figure 4.5). The packing density increased with tapping (to between 0.26 and 0.32) with the densest packing again for the LT1 powder. Achieving a stable packed structure took much longer for the smaller PEEK powder than the large beads, taking between 1000 and 2000 taps (Figure 4.6).

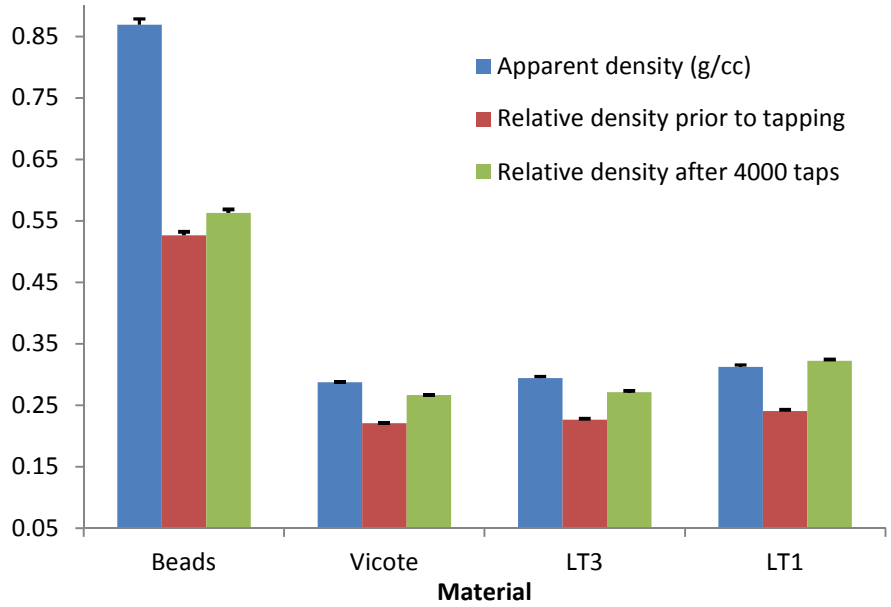

Based on 3 times of measurement using 40.4 g of the salt beads and 10.06 g of each PEEK type. *Relative density is compared to its material density whereas 1.65 g/cc for the 1.0 – 1.4 mm salt beads and 1.3 g/cc for the PEEK.

Figure 4.5: The comparison of the relative density of salt beads, Vicote, LT3 and LT1 PEEK with loose packing (no tapping involved).

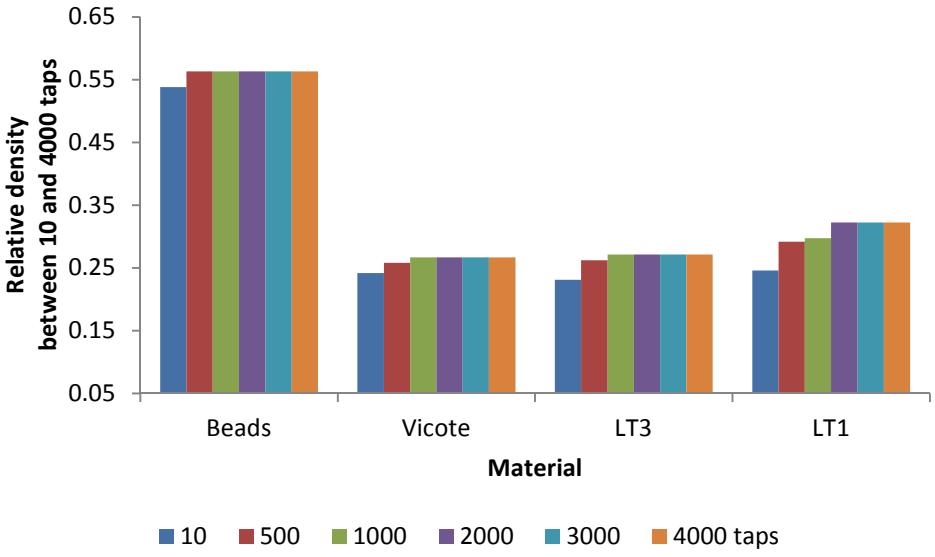

Figure 4.6: The progression of relative density (packing fraction) between 10 and 4000 cycle of taps (shown by different colour bars) for the salt beads and PEEK powder.

4.2 The Fabrication of porous PEEK scaffolds using wet, dry and tapping routes

4.2.1 Wet mixing route for porous PEEK scaffold fabrication

A batch of wet mixed powders was produced using 7 g of PEEK powder, 42 g of salt beads and 9-10 cc of water. The production was repeated four times to determine the consistency of the technique, relating it to the final yield of the mixture and that was left over after sieving, prior to compaction. Some key data were collected such as the mass of the beads and PEEK, water volume, mass of the mixture and the mass of PEEK lost after sieving (separated from NaCl beads) as shown in Table 4.2. Using the Vicote PEEK, the standard deviation in the average percentage yield was 0.5% indicating the process is repeatable.

Table 4.2 compares the efficiency of the wet-mixing route using Vicote, LT1 and LT3 in a 1/6 weight ratio of PEEK to the salt beads. Although Vicote PEEK appeared to stick better to the salt bead surface due to its smaller particle size, the recorded data, however, showed that using LT1 is more efficient, with the highest percentage of sieved mass for this mixture (90.76%) compared to the other two which were at 88% and 84% for LT3 and Vicote respectively.

Table 4.2: Comparison of the wet mixture from Vicote, LT1 and LT3 PEEK materials in 1/6 weight ratio of the PEEK to the salt beads.

No	Parameter/Sample type	Vicote	1L3	1L1
1	Mass of Beads (g)	42.00	42.00	42.00
2	Mass of PEEK (g)	7.00	7.00	7.00
3	Water (cc)	9.40 ± 0.05	9.44 ± 0.15	9.4 ± 0.13
4	Mass after mixing and drying (PEEK +Beads) (g)	48.73 ± 0.13	48.81 ± 0.02	48.72 ± 0.01
5	Sieved mass (g)	41.32 ± 0.20	43.22 ± 0.13	44.22 ± 0.12
6	The remainder of mixture sieved (<500μm) (g)	7.16 ± 0.27	5.14 ± 0.25	4.14 ± 0.23

Table 4.3: Data of the wet mixture prior to the compaction on the Vicote PEEK material in 1/6 weight ratio of the PEEK to the salt beads

PEEK type		Vicote				Average	STD
No	Parameter/Batch no	1	2	3	4		
1	Mass of Beads (g)	42.00	42.00	42.00	42.00	42.00	0.00
2	Mass of PEEK (g)	7.00	7.00	7.00	7.00	7.00	0.00
3	Water (cc)	9.36	9.46	9.37	9.42	9.40	0.05
4	Mass after mixing and drying (PEEK +Beads) (g)	48.88	48.74	48.57	48.71	48.73	0.13
5	Sieved mass (g)	41.27	41.12	41.30	41.60	41.32	0.20
6	The remainder of mixture sieved (<500μm) (g)	7.42	7.33	7.10	6.80	7.16	0.27

STD : standard deviation (n = 4)

PEEK-covered salt beads were observed in the SEM as seen in Figure 4.7. The PEEK adhered to the surface of the salt beads (Figure 4.7a, b and c) and the shape of the beads changed, making the surfaces rougher. Figure 4.7d shows 4 analysis points used for Energy Dispersive X-Ray (EDX) analysis, used for the elemental analysis of the sample. The dark regions at points 1 and 4 are oxygen and carbon-rich, and are thus PEEK and regions 2 and 3 are high in sodium and chlorine and are thus the salt beads. As the Vicote is the finest powder, this PEEK type coats the beads better than the other two in terms of the covered area.

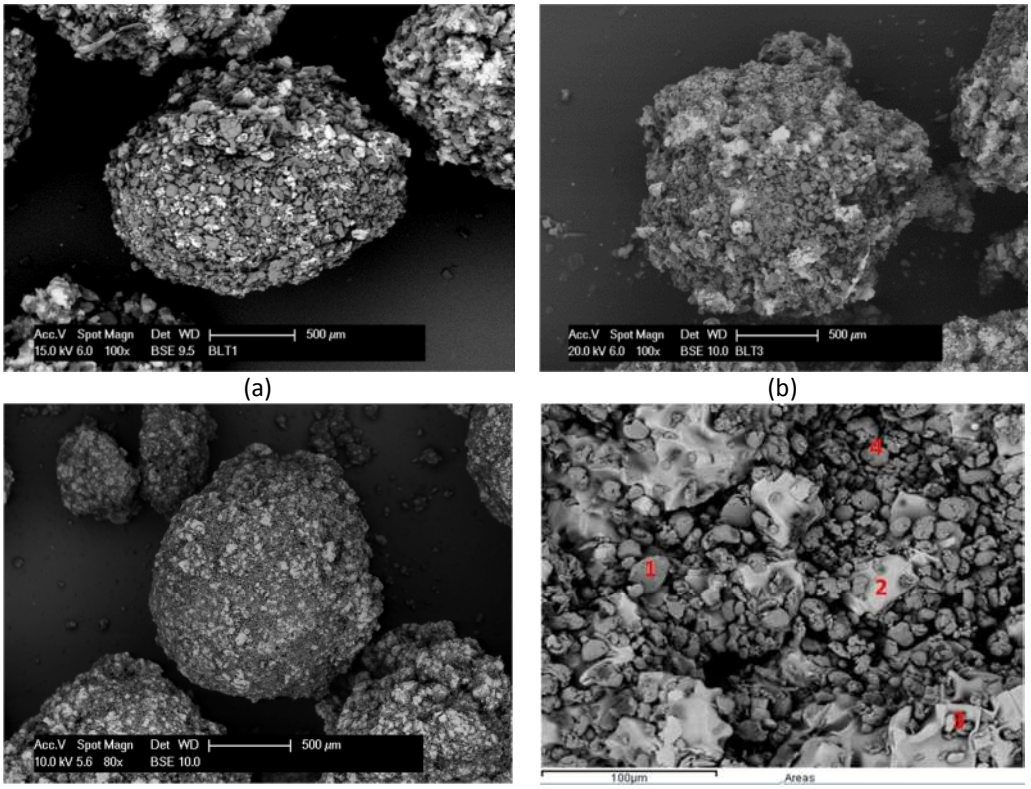

(a) (b)

(c) (d)

Figure 4.7: Typical salt beads covered by (a) LT1, (b) LT3, and Vicote (c) PEEKs after wet-mixing and drying and (d) Point locations identified by red numbers on the surface of Vicote/salt bead sample via the EDX attached SEM instrument.

EDX attaches to the SEM instrument of which specimen images of interest could be identified. The EDX generates some spectra showing peaks corresponding to the elements making up the true composition of the sample. Table 4.4 shows the quantification of chlorine element as a substance of NaCl. It was predicted that point 2 and 3 were dominantly salt as the quantification had more Cl element for both points than those of point 1 and 4.

Table 4.4: EDX analysis on the Vicote PEEK/Salt beads surface quantifying Chlorine (Cl) element to distinguish between NaCl and PEEK

No of point	1	2	3	4
Cl quantity (%)	13.87	41.8	54.5	6.17

In general, the wet-mixing based scaffolds appeared similar for all three powder types, shown in Figure 4.8, with the pore shapes replicating the bead shapes. Figure 4.9 presents a typical porous PEEK scaffold made from the wet mixture.

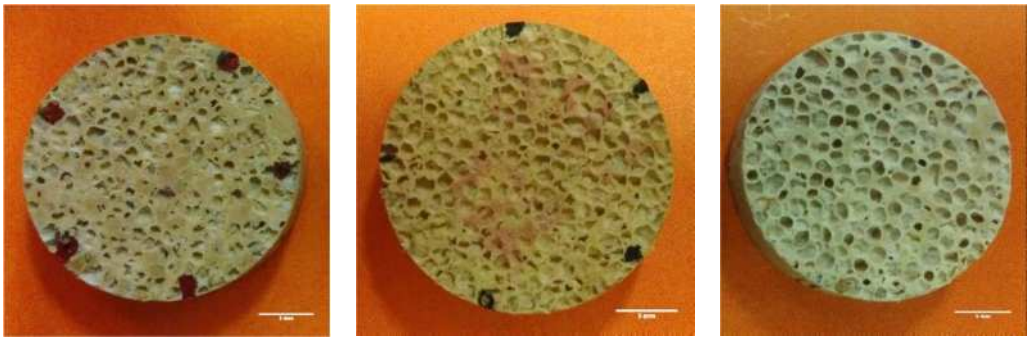

(a) (b) (c)

Figure 4.8: Examples of the (a) Vicote, (b) LT1 and (c) LT3 based samples made through the wet-mixing fabrication route. Each scale bar represents a 5 mm length.

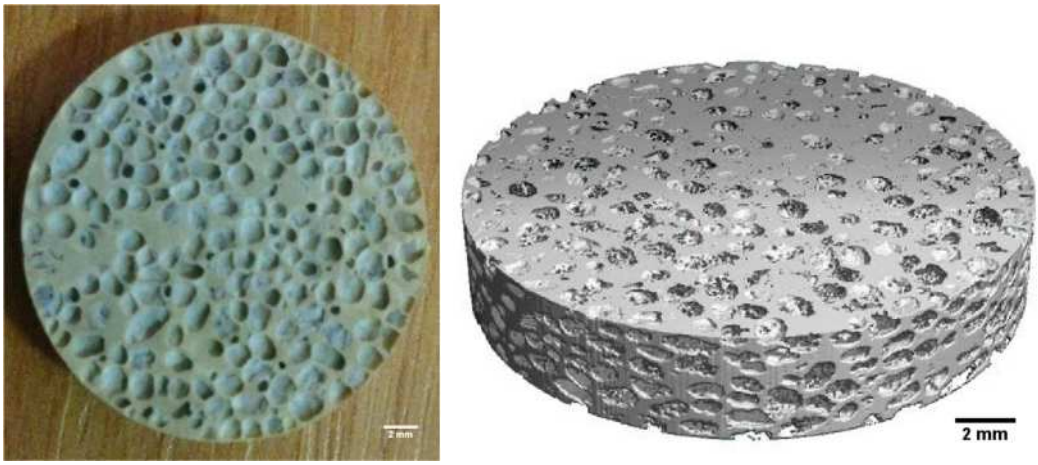

(a) (b)

Figure 4.9: Typical porous PEEK samples manufactured by wet mixing (a) digital photo; (b) MicroCT 3D construction

The porosity of these scaffolds was targeted at around 83% associated with a 1/6 weight ratio of the PEEK to salt beads. Measurements showed that the porosities were close to these targets, with 81.43 (±0.94)%, 82.23 (±0.48)% and 83.26 (±0.56)% porosity for the Vicote, LT1 and LT3 scaffolds,

respectively. Although similar, the smallest deviation in the porosity of these scaffolds was obtained using the LT1 powder.

The scaffold morphologies are shown in Figure 4.10. The structure is typified by large pores from the salt surrounded by small pores in the cell walls. Porous PEEK scaffolds made by wet mixing using all powder types exhibited similar structures in terms of the pore (Figure 4.10a, b and c) and strut shapes (Figure 4.10d, e and f) and pore walls (Figure 4.10g, h and i). The images show the pores of the scaffolds tend to be elongated perpendicular to the compaction direction.

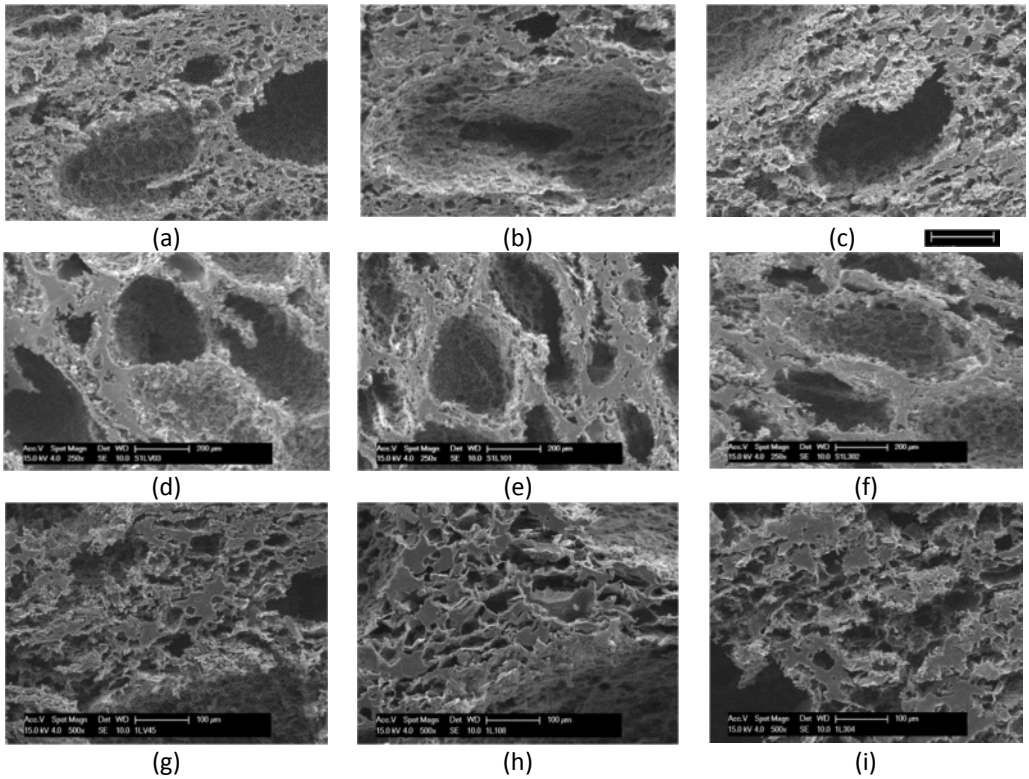

Figure 4.10: The cross-sections of porous scaffolds made by wet mixing using (a, d and g) Vicote, (b, e and h) LT1, and (c, f and i) LT3 at the same 1/6 weight ratio of the PEEK to the salt beads. The scale bars represent 200 µm length.

Figure 4.11 shows a coloured map of the pore size distribution created from CT data for the Vicote, LT1 and LT3 PEEK samples. The dark blue colouring

represents small pores (<100 µm) and the orange-red areas represent larger pores. The colour bar gives information of the range of the pore size distribution. The structure contains many small pores throughout the structure.

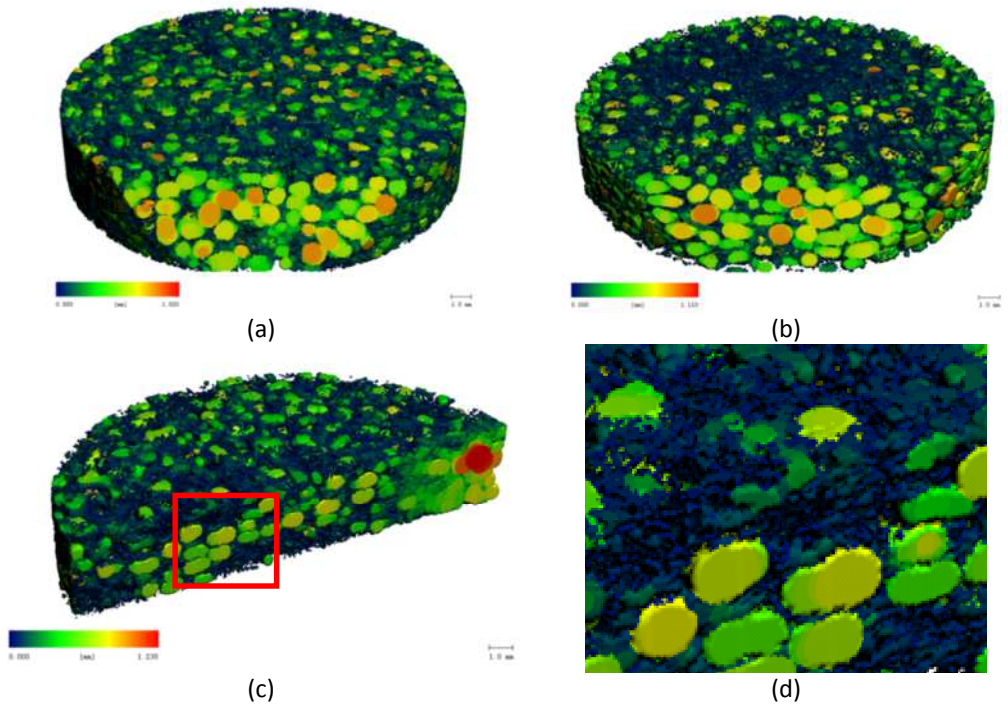

Figure 4.11: Colour maps of pores for the wet mixing based scaffolds from (a) Vicote; (b) LT3; and (c) LT1 PEEK shown as a cut part; the red square represents an area of interest; (d) the zoom version of (a); visualisation of the dark blue regions indicates fine pores of <100 µm.

The existence of small pores in the wet-mixing based scaffolds is also seen in the pore size distributions generated by the 3D evaluation. Figure 4.12 shows the distribution of the pore size for each scaffold type, measured by CT. The wet mixing based scaffolds show bimodal distributions of the pore sizes and they show a similar tendency. The red square represents the first mode of the pore size at around 120 µm, and this tendency occurs for all PEEK types processed through the wet-mixture route. The small pores are distributed throughout the scaffolds (as was shown in Figure 9). The black square defines the size of the second mode of the pore size distribution at around 630µm.

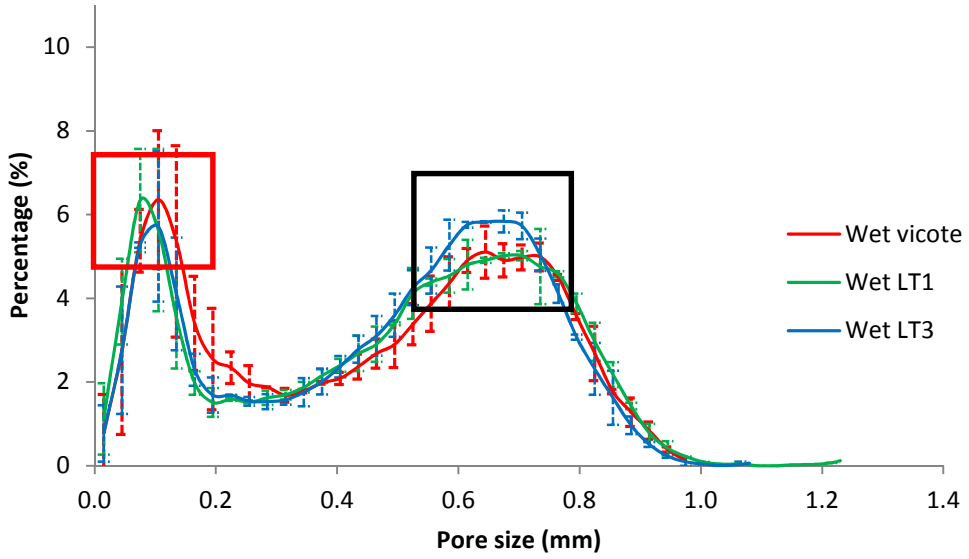

Figure 4.12: Typical pore size distributions of the wet mixed samples (n= 2) showing bimodal peaks of around 120 (red square) and 630 (black square) micron sizes.

Figure 4.13 shows the distribution of strut thickness for each scaffold type. The mean strut thickness ranges from 100 to 130 µm which is near the modal value. The maximum thickness of the struts was around 390 µm for each type of scaffold. Key structural parameters are clearly summarised for each PEEK type in Table 4.5 and include the degree of anisotropy (see 2.2.2 for a brief explanation), which increases compared with the original anisotropy of the as-received beads (see 4.1.1), and the connectivity density, referring to the trabecular number per mm^3. The target and actual densities are also shown. Scaffolds made from the wet-based route had broadly similar characteristics for the three PEEK types used.

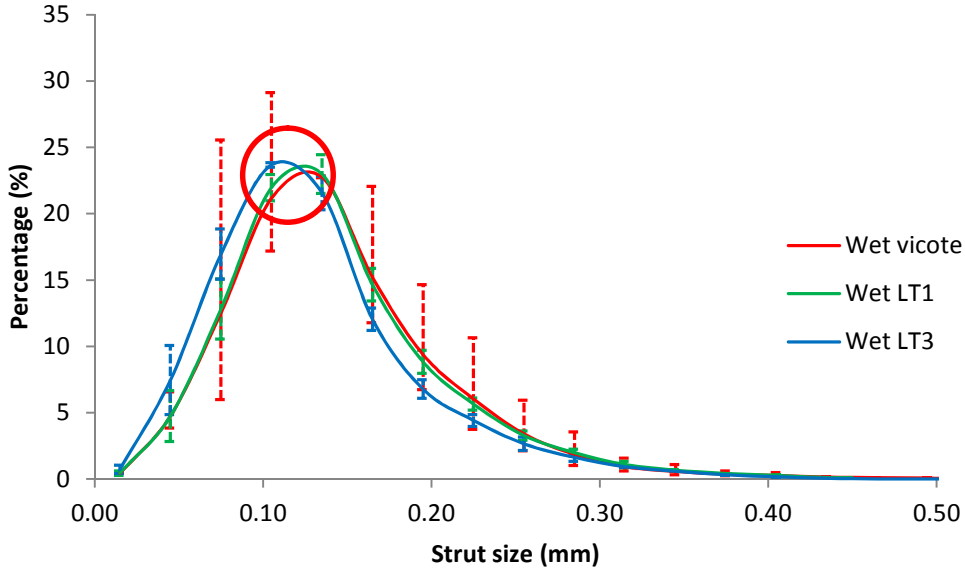

Figure 4.13: Strut thickness distribution for the wet-mixing based scaffolds (n=2); the red circle represents the location of the mean size of the strut thickness identified.

Table 4.5: Structural parameters for the PEEK scaffolds made by wet mixing

Parameter	Vicote	LT3	LT1
1st mode of pore size (µm)	120	90	90
2nd mode of pore size (µm)	630	690	690
Mean pore size (µm)(STD)	-	-	-
Maximum pore size (µm)	1,020	1,110	1,230
Mean strut thickness (µm) (STD)	100 (± 40)	120 (± 50)	130(± 50)
Strut thickness mode (µm)	120	120	120
Degree of anisotropy (DA) (1)	1.30	1.36	1.37
Connectivity density (1/mm^3)	72.72	68.75	78.49
Target porosity (%)*	82.76	82.54	82.54
Average actual porosity (%) (STD)*	81.43 (± 0.94)	83.26 (± 0.56)	82.23 (± 0.48)
Relative density (STD)*	0.186(± 0.009)	0.167(± 0.006)	0.177(± 0.005)

*non microCT measurement with standard deviation (STD) based on n = 10.

Figure 4.14 shows the distributions of 2D (areal) porosity over the thickness of the scaffolds. Between 25 and 75% of the thickness, LT1 and LT3 had higher porosity than their average 2D porosities and show low porosity regions at the

surfaces. The deviations of porosity over the thickness by this wet-mixing route are relatively large for the LT1 and LT3 PEEK, 8.8% and 11.4% deviation from the mean, respectively. The Vicote has a relatively small deviation, 2.5% of the average 2D porosity.

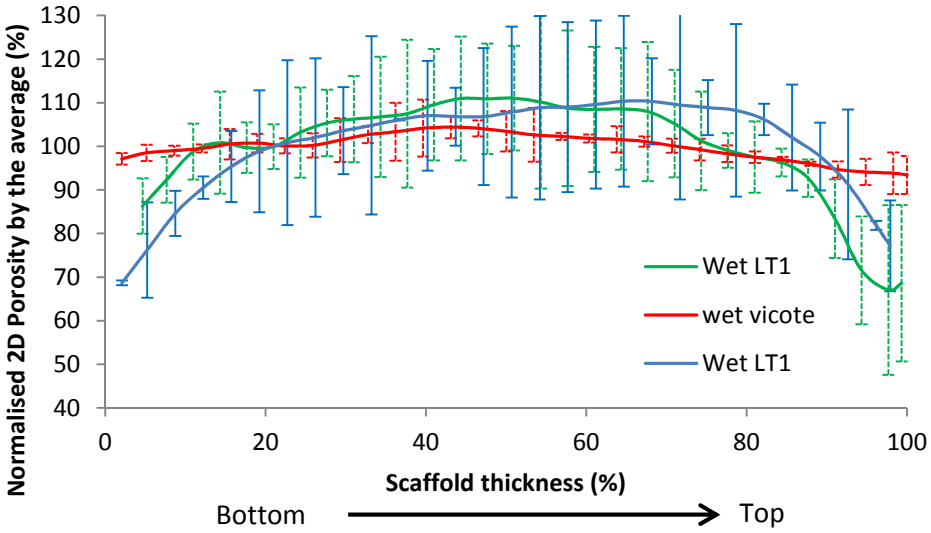

Figure 4.14: Normalised 2D porosity over the thickness of scaffolds (n = 2) made by wet Vicote PEEK mixture.

Figure 4.15 presents "transparent" CT images showing the residual salt through the whole thickness of scaffolds made by wet-mixing. The white spots are the residual salt particles and enlarged views of the areas marked by red boxes are also shown. The scaffolds made from LT1 (Figure 4.15c) and LT3 (Figure 4.15e) tend to show more salt particles around the edges as opposed to the internal regions.

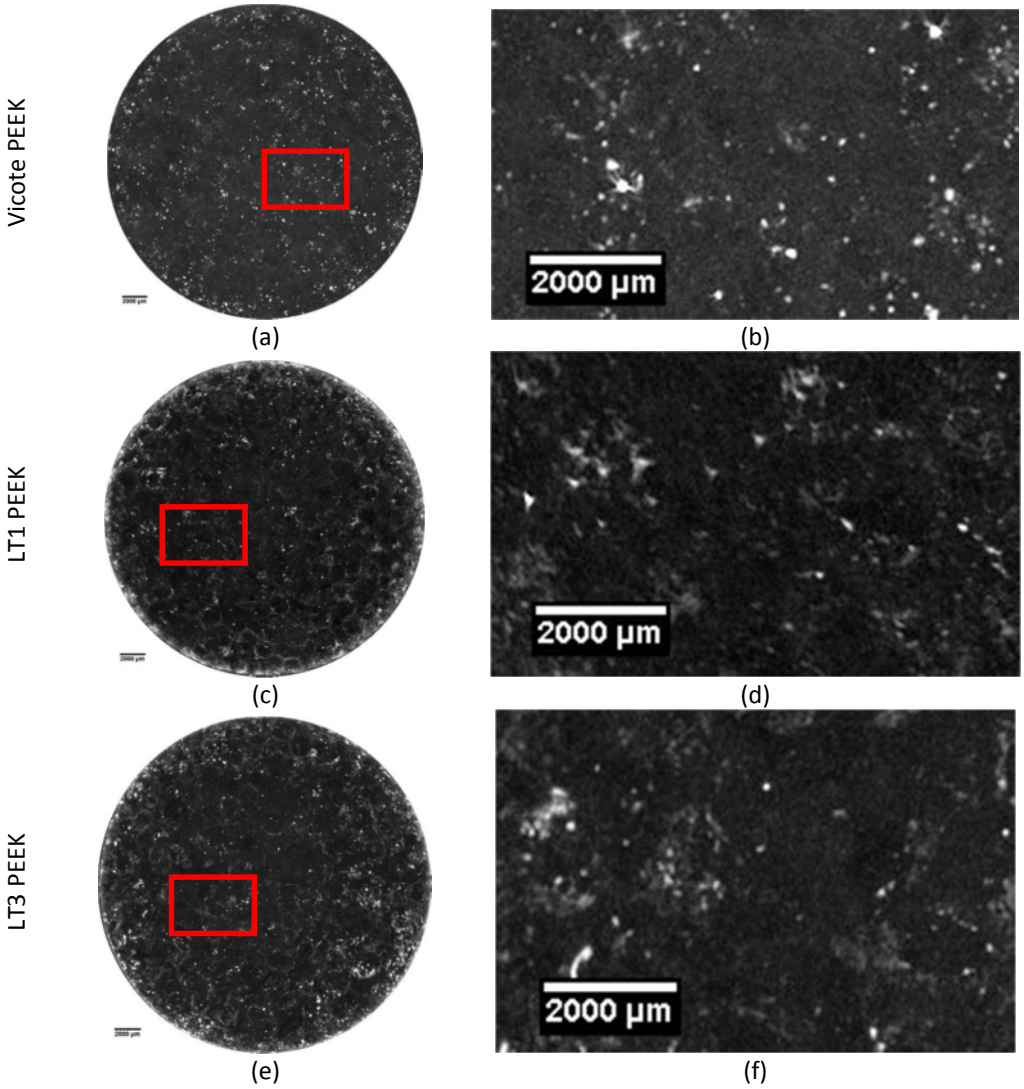

Figure 4.15: (a, c and e): The transparent 3D reconstructions of the residual salt in the wet-mixing based scaffolds viewed from the top. The salt particles are shown as white spots. (b, d and f): The red boxes represent zoomed areas.

The quantification of the volume fraction of the residual salt confirms that the Vicote had less residual salt with less than 0.1% by volume. While LT1 and LT3 scaffolds had more salt left in the structures, 0.2 and 0.9% by volume, respectively.

4.2.2 Dry mixing route for porous PEEK scaffold fabrication

Macroscopically, the porous PEEK scaffolds made by the dry-mixing fabrication route appeared similar irrespective of the powder used, as seen in Figure 4.16 and in Figure 4.17. The porosity of these scaffolds was again targeted at around 83% but the obtained porosity, for all PEEK types, was less than 81% (80.41 (±0.72)%, 79.25 (±0.75)% and 73.37 (±2.46)%, for Vicote, LT1 and LT3 scaffolds respectively).

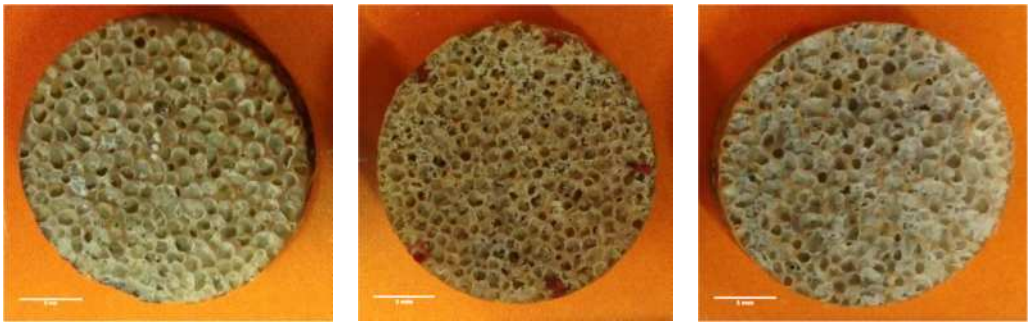

(a) (b) (c)

Figure 4.16: Examples of (a) Vicote, (b) LT1 and (c) LT3 based PEEK scaffolds made through the dry-mixing fabrication route. The scale bar is 5 mm.

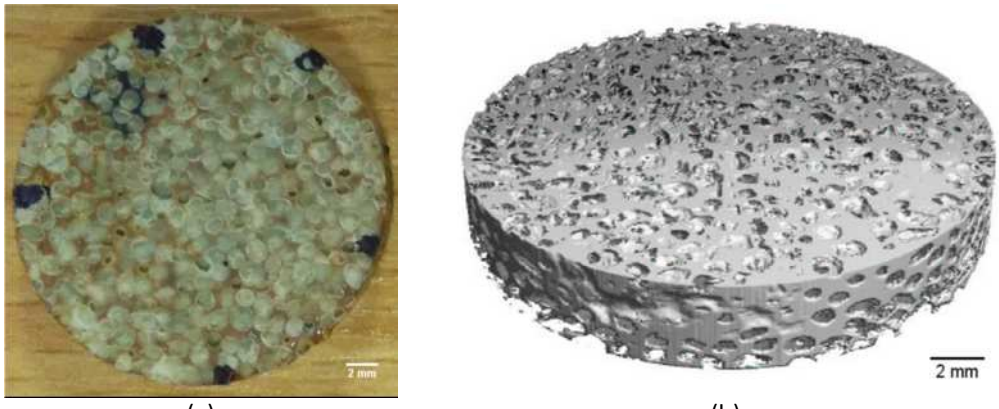

(a) (b)

Figure 4.17: Porous PEEK samples manufactured by dry mixing shown in (a) digital photo; (b) MicroCT 3D construction

Figure 4.18 shows scaffold morphologies typified by large pores from the salt with solid cell walls in between them. Similar structures were found in terms of

the pore (Figure 4.18a, b and c) and strut shapes (Figure 4.18d, e and f) and pore walls (Figure 4.18g, h and i). The images show the pores of the scaffolds tend to be elongated perpendicular to the compaction direction.

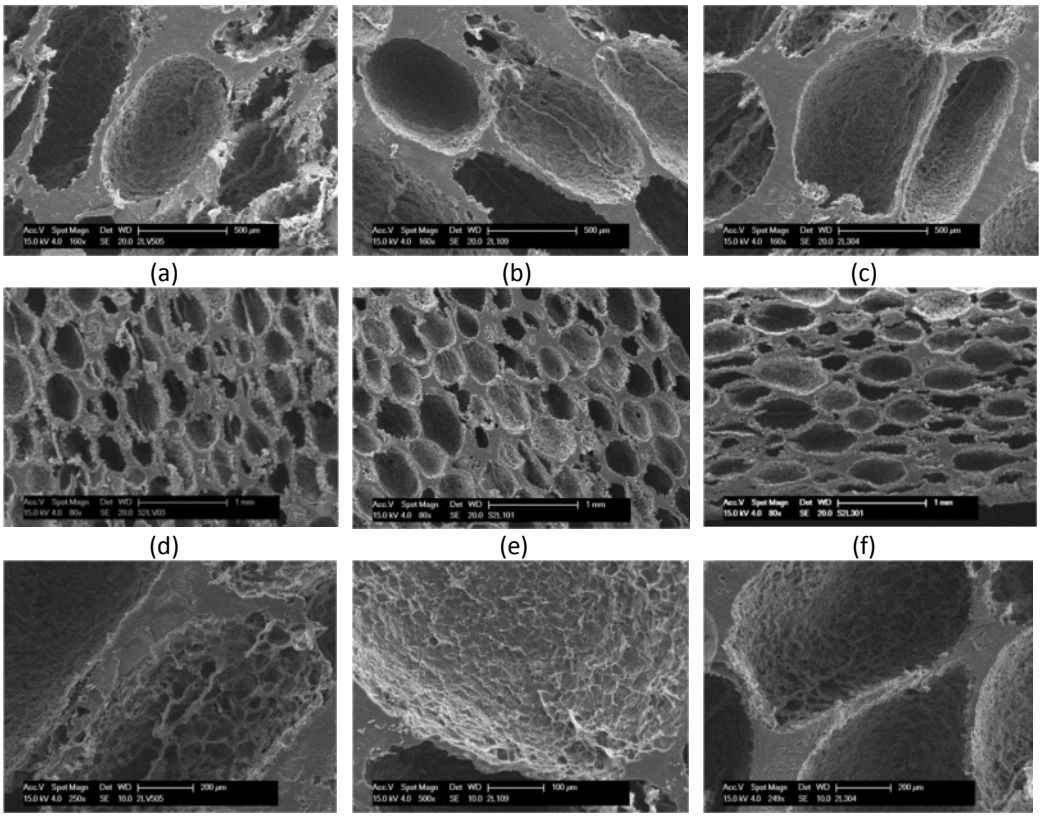

Figure 4.18: The cross-sections of porous scaffolds made by dry mixing using (a, d and g) Vicote, (b, e and h) LT1, and (c, f and i) LT3 at the same 1/6 weight ratio of the PEEK to the salt beads.

Figure 4.19 shows a coloured map of the pore size distribution created from CT data for the Vicote, LT1 and LT3 PEEK samples. The structure contains mostly large pores with a few small pores. The existence of larger pores in the dry-mixing based scaffolds is also seen in the pore size distributions generated by the 3D evaluation. Figure 4.20 shows the distribution of the pore size of each scaffold type, measured by CT. More, larger pores are indicated by the

skewed distribution where the modal size of the pores (shown by the red square representing a size of 600 – 690 µm) is larger than the mean size (450 – 600 µm). This tendency occurs for all PEEK types used through the dry-mixing route, with the tendency for the Vicote based scaffolds to have slightly larger pores.

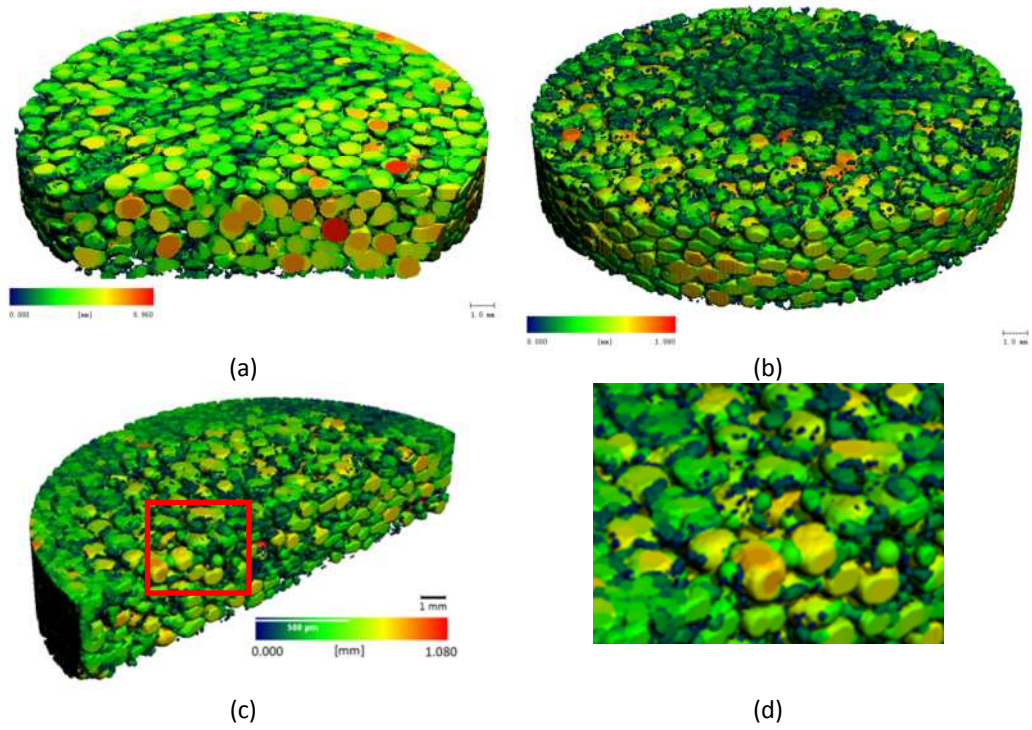

Figure 4.19: Colour maps of pore size for the dry mixing based scaffolds from (a) LT1; (b) LT3; and (c) Vicote PEEK as a cut part; the red square represents an area of interest; (d) The zoom version of (a); The visualisation of the dark blue spheres indicate pores < 100 µm.

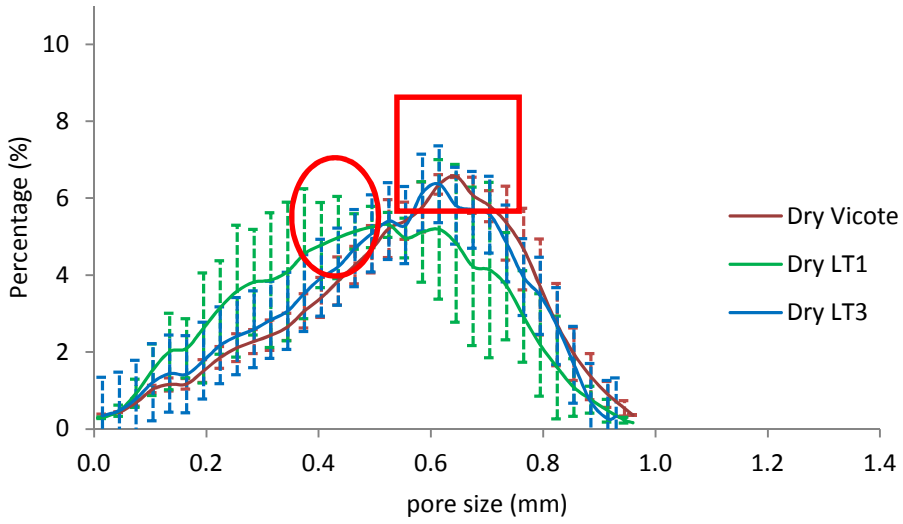

Figure 4.20: The pore size distribution for the dry mixing based-samples (n = 2) showing the mode position by the red square and the mean pore size by the red ellipse.

The distributions of strut thickness of each scaffold type are depicted in Figure 4.21. The mean strut thickness is larger than the modal size. The red square represents the modal size at around 120 – 150 µm and the red circle defines the mean size at around 170 – 180 µm.

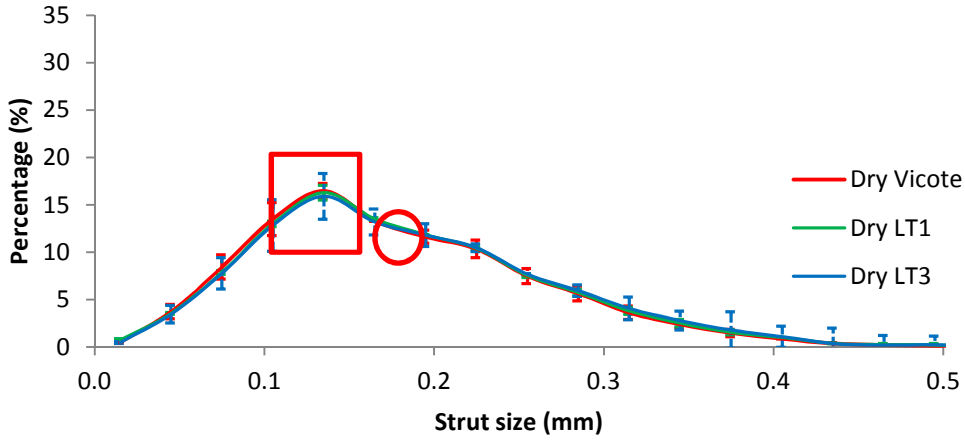

Figure 4.21: Strut thickness distribution for the dry-mixing based scaffolds (n = 2); the red box represents the location of average strut thickness. The red circle represents the location of the mean size of the strut thickness.

Table 4.6 presents key structural parameters, collected from measurement via microCT and other measurement methods, and includes the degree of anisotropy, again larger than the value for the as-received beads, and the connectivity density, which is considerably lower than for the wet-route.

Table 4.6: Values for experimental parameters and statistical results of microCT on the PEEK scaffold from dry mixtures

Parameter	Vicote	LT3	LT1
1st mode of pore size (μm)	690	600	630
Mean pore size (μm)(STD)	600 (±210)	530(±200)	450 (±190)
Maximum pore size (μm)	1,080	930	960
Mean strut thickness (μm) (STD)	170(±80)	180(±90)	180(±80)
Strut thickness mode (μm)	120	150	150
Degree of anisotropy (DA) (1)	1.57	1.62	1.64
Connectivity density (1/mm3)	9.82	11.61	7.66
Target porosity (%)*	82.76	82.54	82.54
Average actual porosity (%) (STD)*	80.41(± 0.72)	73.37(± 2.46)	79.25(± 0.75)
Relative density (STD)*	0.19(± 0.007)	0.26(± 0.002)	0.20 (± 0.008)

*non microCT measurement with standard deviation (STD) based on n = 10.

Figure 4.22 shows the distribution of 2D porosity over the thickness of the scaffolds. The Vicote sample has a higher porosity than the average 2D porosity between 15 and 70% of the thickness and shows low porosity regions at the surfaces. For about a half of the thickness, the LT1 sample has a lower porosity than the average, tending to increase towards the upper surface with a large increase between 60 and 70% of the thickness. Between 20 and 60% of the thickness, the LT3 sample has a higher porosity than the average 2D porosity and shows an unclear porosity tendency for the remaining area. The deviations in porosity over the thickness by this dry-mixing route are relatively large, 4.7%, 7.0% and 5.8% using Vicote, LT1 and LT3, respectively.

Compared to the wet-mixing route, the dry-mixing route has a significantly higher variation in porosity with position within the scaffold structure.

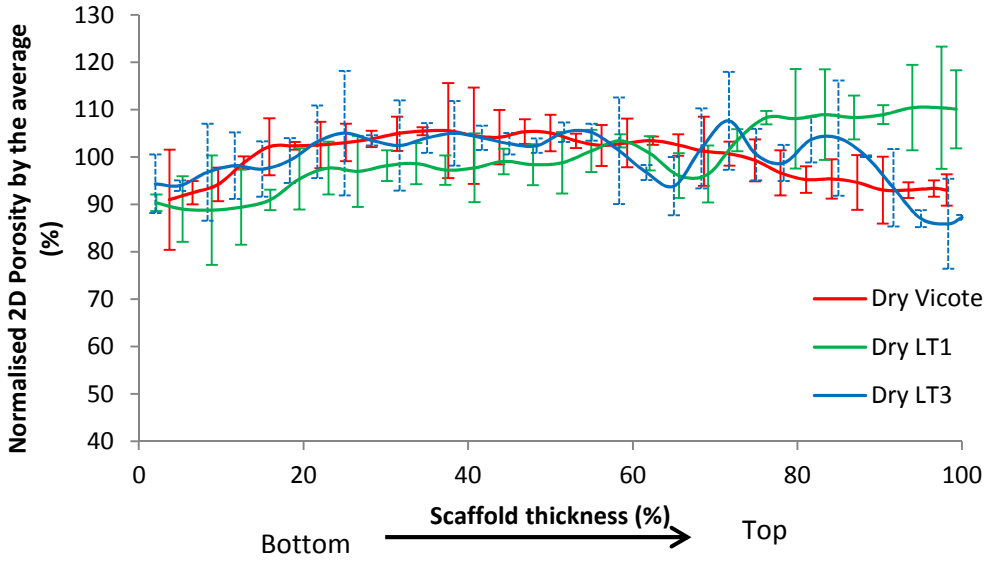

Figure 4.22: Normalised 2D porosity over the thickness of scaffolds (n = 2) for dry mixtures.

Figure 2.1 presents "transparent" CT images showing the residual salt through the whole thickness of scaffolds made by dry-mixing. The white spots are the residual salt particles and enlarged views of the areas marked by red boxes are also shown. Large, undissolved salt particles are clearly observed in samples made using LT1 and LT3 PEEK powder.

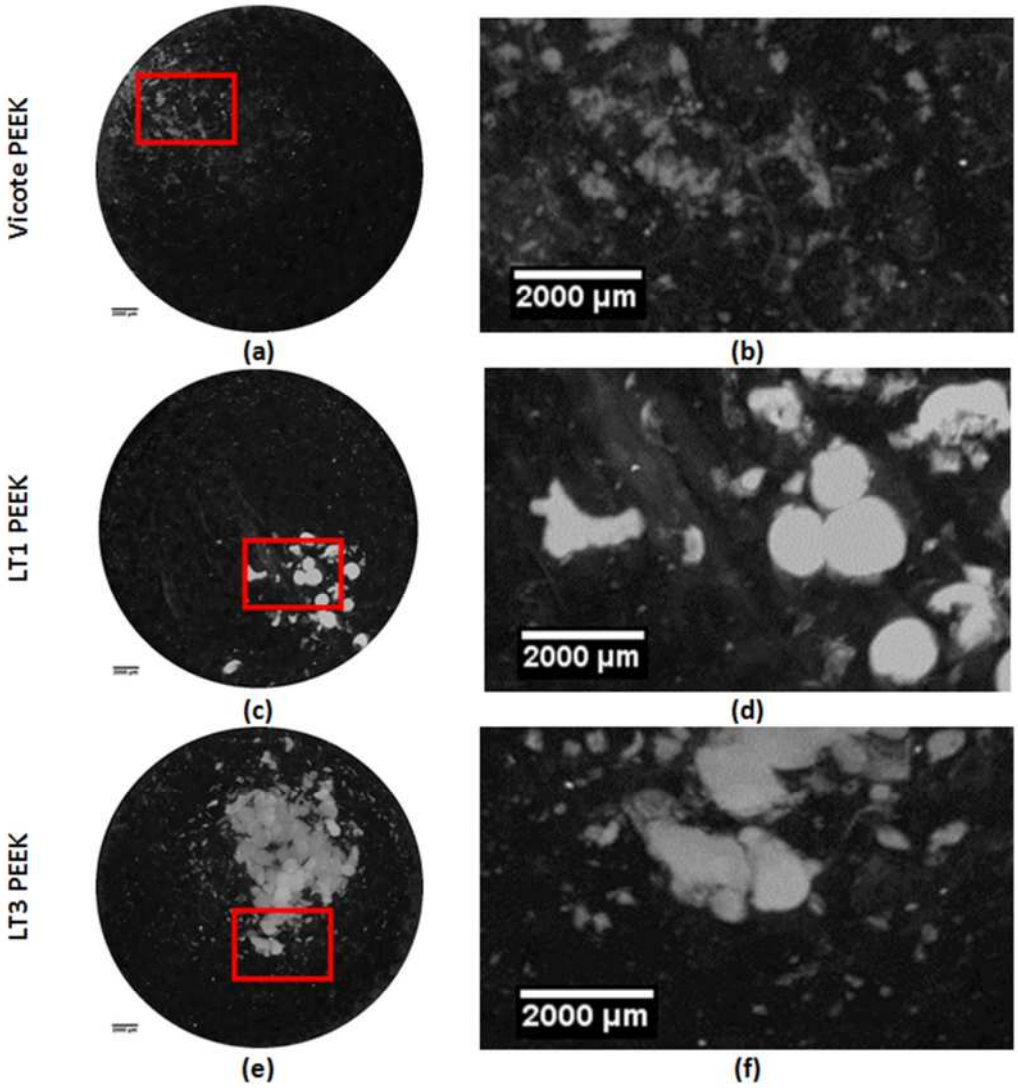

Figure 4.23: (a, c and e): The transparent 3D reconstructions of the residual salt in the dry-mixing based scaffolds viewed from the top. The salt particles are shown as white spots. (b, d and f): The red boxes represent zoomed areas.

The quantification of the volume fraction of the residual salt indicates that Vicote, LT1 and LT3 had 3.5, 4.8 and 15.30% by volume, respectively. In comparison to the wet fabrication route, the dry fabrication route retains significantly more salt in the scaffolds. The salt residue in the dry-mixture based scaffolds appeared agglomerated and concentrated in certain areas. While the salt residue in the wet-mixture based scaffold appeared distributed through the scaffolds in a smaller size.

4.2.3 Tapped mixing route for porous PEEK scaffold fabrication

Porous scaffolds made from all PEEK types generally had a similar structure regarding the regularity of the pore network, as shown in Figure 4.24, with open pores replicating the beads on the surface. Figure 4.25 presents a typical porous PEEK scaffold made by the tapping route.

(a) (b) (c)

Figure 4.24: Examples of the (a) Vicote, (b) LT1 and (c) LT3 based samples made through the tapped-mixture fabrication route. Each scale bar represents a 5 mm length.

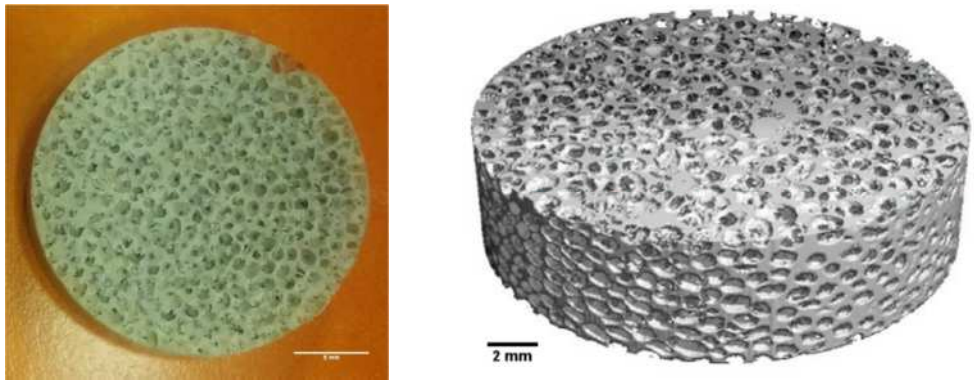

(a) (b)

Figure 4.25: Porous PEEK samples manufactured by tapping mixing shown in (a) digital photo; (b) MicroCT 3D construction.

The porosity of these scaffolds was targeted around 83%. High porosity, > 80%, was obtained by scaffolds fabricated through the tapping route. Vicote

and LT1 powders produced scaffolds with porosity slightly higher than the target (roughly 83%). LT3 had a lower porosity of close to 80%.

Figure 4.26 shows the scaffold morphologies. The structure is typified by large pores and dense struts. Porous PEEK scaffolds made by the tapping route resulted in similar structures relating to pore (Figure 4.26a, b and c) and strut shapes (Figure 4.26d, e and f) and pore walls (Figure 4.26g, h and i) irrespective of the powder used. The images show the pores of the scaffolds tend to be elongated perpendicular to the compaction direction and contain connecting small pores or "windows". These large windows of this process could provide between 2 and 6 windows visible in sectioned pores. For the LT1 powder a mean window size of roughly (204 $\pm$ 41) µm was estimated, with minimum and maximum window sizes of 105 and 451 µm using 5 SEM images evaluated by ImageJ. For the Vicote scaffolds, windows were less commonly observed.

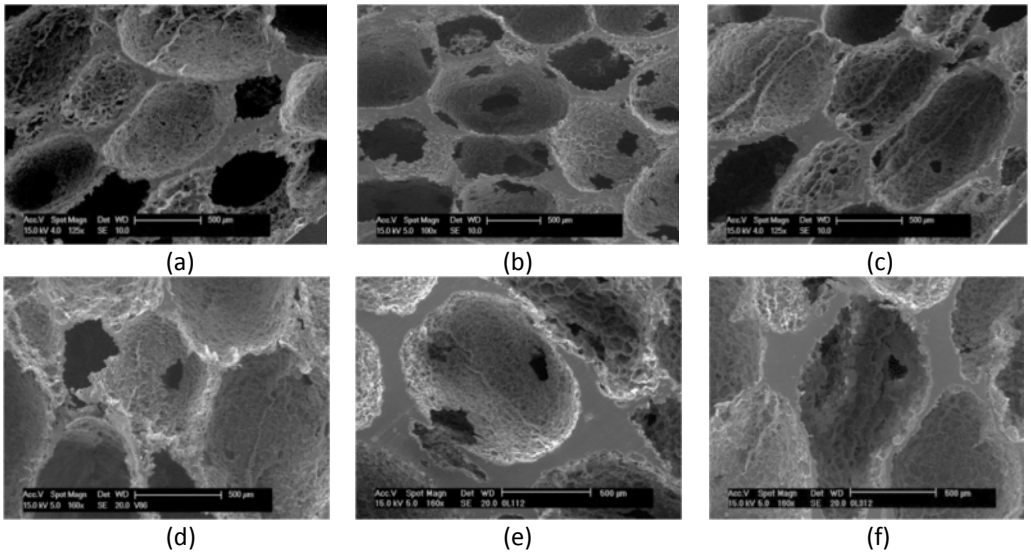

Figure 4.26: The cross-sections of the porous scaffolds from the tapped mixtures using (a, d and g) Vicote, (b, e and h) LT1, and (c, f and i) LT3 at the same 1/6 weight ratio of the PEEK to the salt beads. The red arrows indicate the compaction direction.

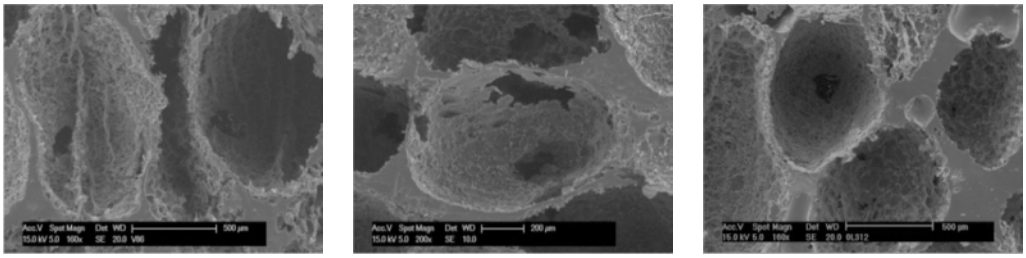

(g) (h) (i)

Figure 4.24 (continued): The cross-sections of the porous scaffolds from the tapped mixtures using (a, d and g) Vicote, (b, e and h) LT1, and (c, f and i) LT3 at the same 1/6 weight ratio of the PEEK to the salt beads. The red arrows indicate the compaction direction.

Figure 4.27 shows coloured maps of the pore size distribution created from CT data for the Vicote, LT1 and LT3 PEEK samples. The colour scale shows that the structure contains regular and large pores throughout the bulk of the structure, with small pores generally only on the surfaces where pores have been sectioned.

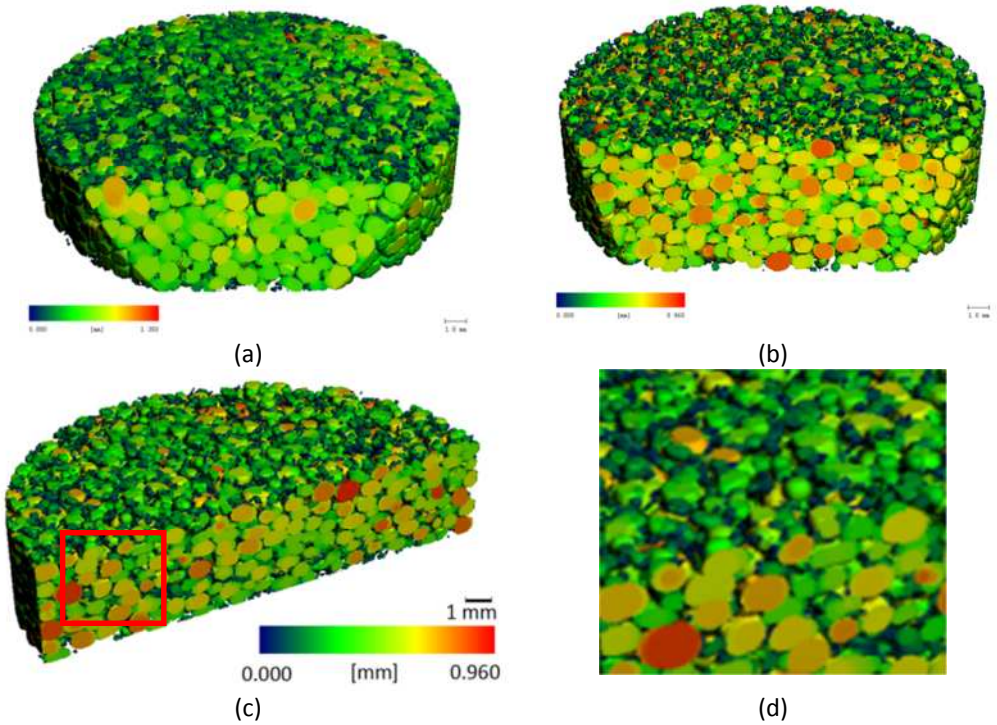

(a) (b)

(c) (d)

Figure 4.27: Colour maps of pore for the dry mixing based scaffolds from (a) LT1; (b) LT3; and (c) Vicote PEEK as a cut part; the red square represents an area of interest; (d) The zoom version of the (a); The visualisation of the dark blue spheres indicate pores < 100 µm

The more uniform distribution of pore sizes in the tapping-route based scaffolds is also seen in the pore size distributions generated by the 3D evaluation.Figure 4.28 shows the distribution of the pore size for each scaffold type, measured by CT. The tapping route based scaffolds show near-symmetrical distributions, indicated by close values between the mean (560 – 630 µm) and modal size (630 µm), and they show a similar tendency for each powder type.

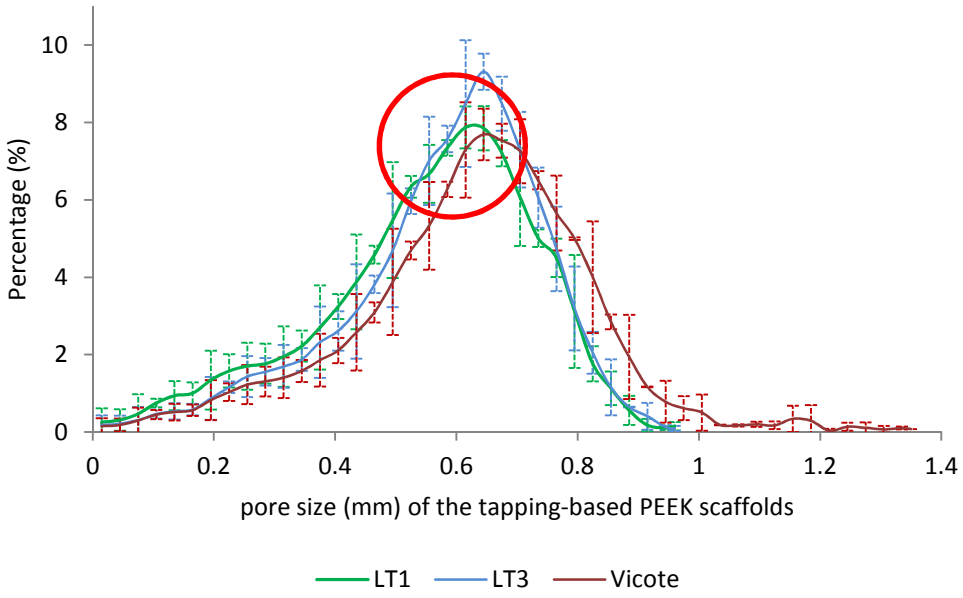

Figure 4.28: The pore size distributions for PEEK scaffolds (n = 2) made from tapped mixtures. The red circle represents the mean size of the pores.

Figure 4.29 shows the distribution of strut thickness for each scaffold type. The mean strut thickness ranges from 150 – 180 µm which is slightly larger than the modal value. Key structural parameters are clearly summarised for each PEEK type in Table 4.7. The degree of anisotropy (DA) for the scaffolds fabricated by the tapping route ranged from 1.53 – 1.62 which was close to the

DA for the scaffolds from the dry route (1.57 – 1.64) and higher than those of scaffolds from the wet route (1.30 – 1.37). The degree of anisotropy is one of parameter generated by microCT, which refers to length of longest divided by shortest axis (vector) fitted in a measured object shape. The connectivity density for scaffolds made by the tapping route was between 7 and 10/mm^3, similar to that for the dry mixture based scaffolds (7 – 12/mm^3) and well below those from the wet route (68 – 79/mm^3).

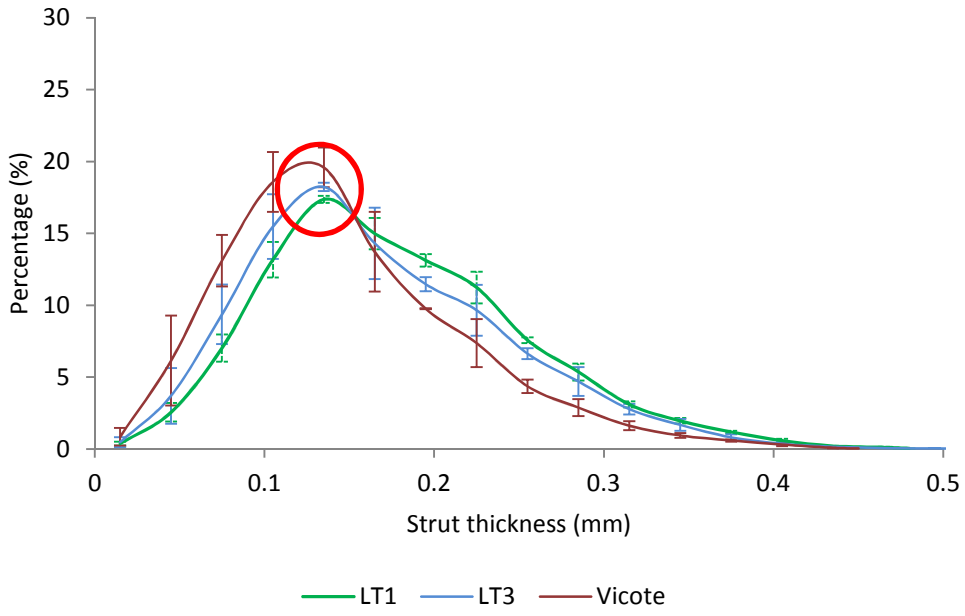

Figure 4.29: Strut thickness distribution for scaffolds (n = 2) from tapped mixtures. The red circle shows the mean strut thickness.

Table 4.7: Values of experimental parameters and statistical results of microCT on the PEEK scaffold made from tapped mixture

Parameter\PEEK scaffold	Vicote	LT3	LT1
1st mode of pore size (µm)	630	630	630
2nd mode of pore size (µm)	-	-	-
Mean pore size (µm)(STD)	630 (±190)	580(± 160)	560 (± 180)
Maximum pore size (µm)	1350	960	960
Mean strut thickness (µm) (STD)	150(± 70)	170(± 80)	180(± 80)
Strut thickness mode (µm)	120	120	150
Degree of anisotropy (DA)	1.62	1.62	1.53
Connectivity density (1/mm^3)	7.6	9.04	9.39
Target porosity (%)*	82.76	82.54	82.54
Average actual porosity (%) (STD)*	84.24(± 2.59)	80.26(± 0.58)	83.54(± 0.74)
Relative density*	0.16 (± 0.003)	0.20(± 0.006)	0.179(± 0.007)

*non microCT measurement with standard deviation (STD) based on n = 10.

Figure 4.30 shows the distributions of 2D porosity over the thickness of the scaffolds. Between 25 and 65% of the thickness, all the samples tend to have a higher porosity than their average and all samples tend to show a lower porosity at the top surface.

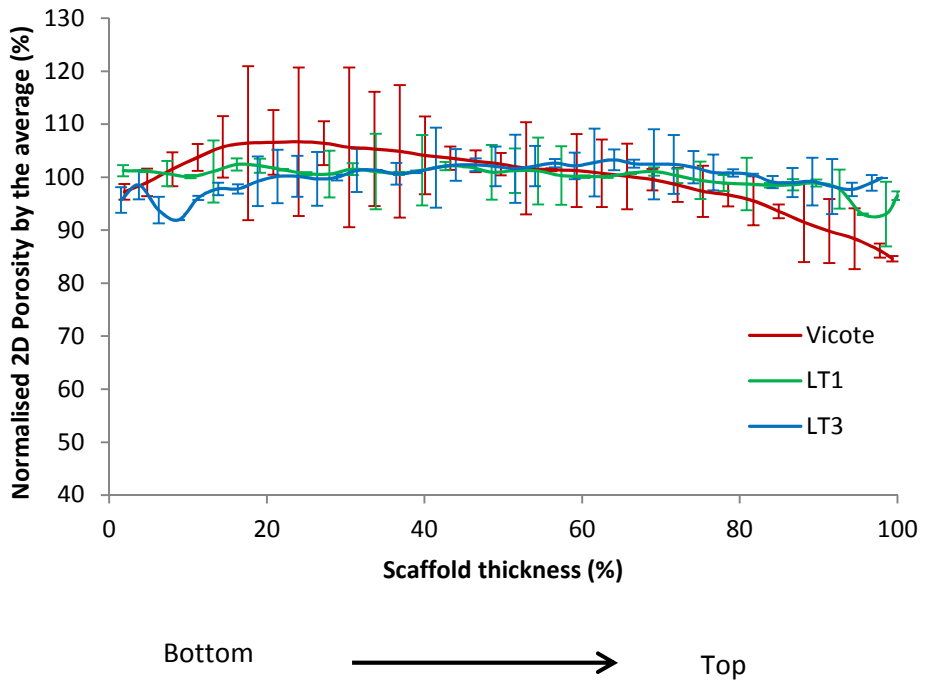

Figure 4.30: Normalised 2D porosity over the thickness of scaffolds (n = 2) for tapped mixtures.

Figure 4.31 presents “transparent” CT images showing the residual salt through the whole thickness of scaffolds made by tapping-mixing. The scaffolds made from LT1 (Figure 4.31 c) and LT3 (Figure 4.31 e) tend to show salt scattered evenly throughout the structure in small size.

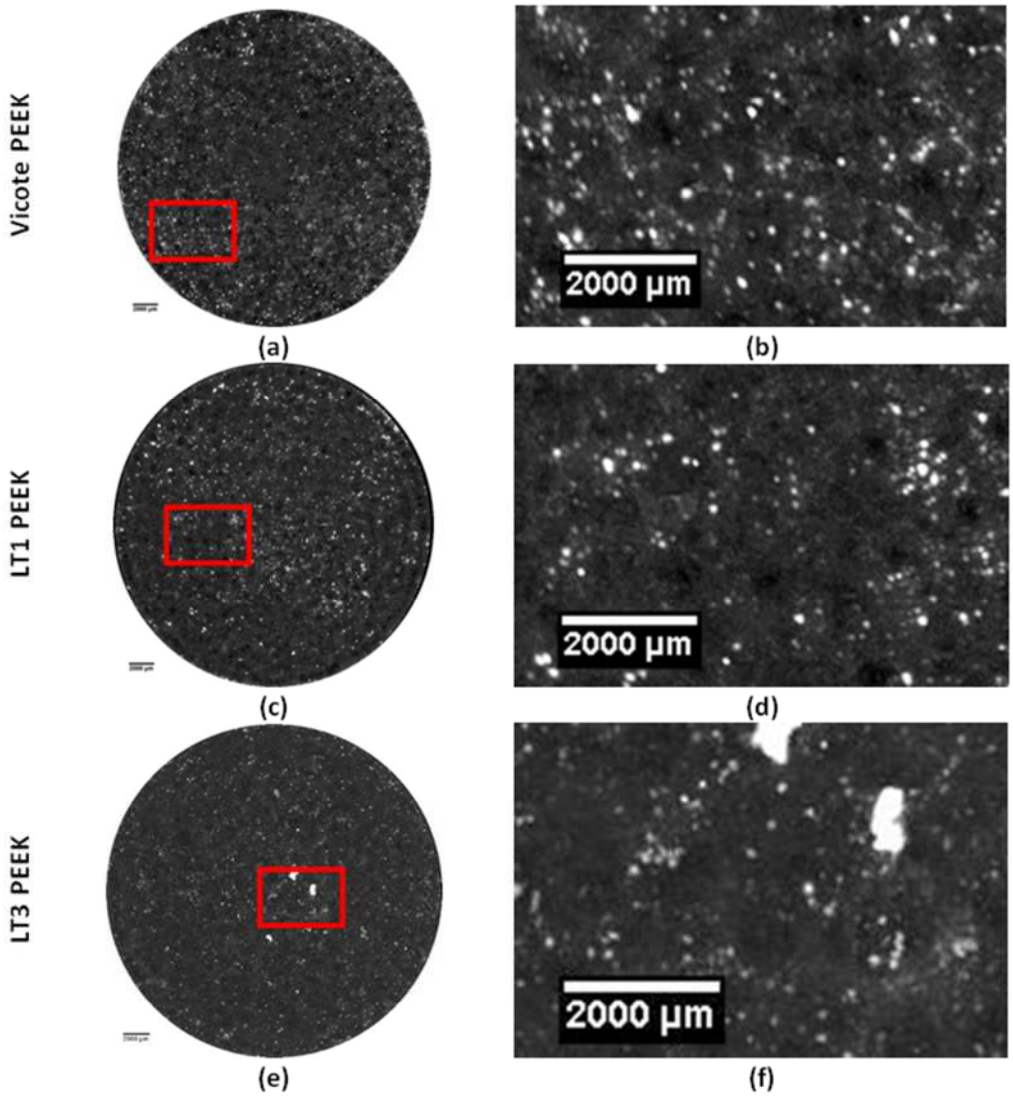

Figure 4.31: (a, c and e): The transparent 3D reconstructions of the residual salt in the tapping-mixing based scaffolds viewed from the top. The salt particles are shown as white spots. (b, d and f): The red boxes represent the zoomed areas.

The residual salt of the scaffolds was quantified using the same method applied to previous fabrication techniques. The LT1 had less residual salt, around 0.5% by volume, Vicote and LT3 had more salt left in the structures, but still less than 1%. These levels are similar to those in scaffolds made by the wet route, and much lower than those made by the dry mixing route.

4.3 Discussion of the influence of production route

4.3.1 Structural characteristics of the porous PEEK scaffolds

In theory, the porosity of the scaffolds can be controlled by the addition of varying amounts of NaCl beads to the mixture. Scaffolds were produced at theoretical values of 83% of porosity, however upon analysis, the actual porosities do vary from this target. The samples from the wet route and the tapping route were close enough, within scatter and experimental variation to the porosity target, ranging from 80 to 84% (Table 4.8). The samples from the wet route, when taking error into account, appear to have closer values to the targeted porosity (Ellipse A in Figure 4.32) indicating that the wet route is very good for producing scaffolds of specified porosities. One reason for this could be the generation of PEEK-coated salt beads which allows good control of the composition of the mixture.

It was difficult to the dry route to produce scaffolds with porosities close to the target and they appear to be below the target (70 – 80%, Ellipse B in Figure 4.32). In the case of LT3 PEEK, the dry route based scaffolds exhibit the highest deviation in porosity. The lower porosity (or more accurately higher density) obtained by samples from the dry route is likely to be due to the

retention of unleached NaCl in the porous structures. Poor mixing of the dry powders results in isolation of the NaCl beads from their neighbours and thus they are unable to be leached from the structure during immersion. This leads to a high density which can be falsely interpreted as a low porosity. Measured values for salt residue are shown in Table 4.8. It can be seen that the wet and tapping routes have similar residual salt levels and that the level of residual salt is much higher for the dry route.

It should be noted that since samples with high porosity were prepared, the porosity must be interconnected, on some level, in order for the salt to be dissolved from the structure. It was noted that salt removal took three days from the wet-route samples and only a few hours for the tapping route.

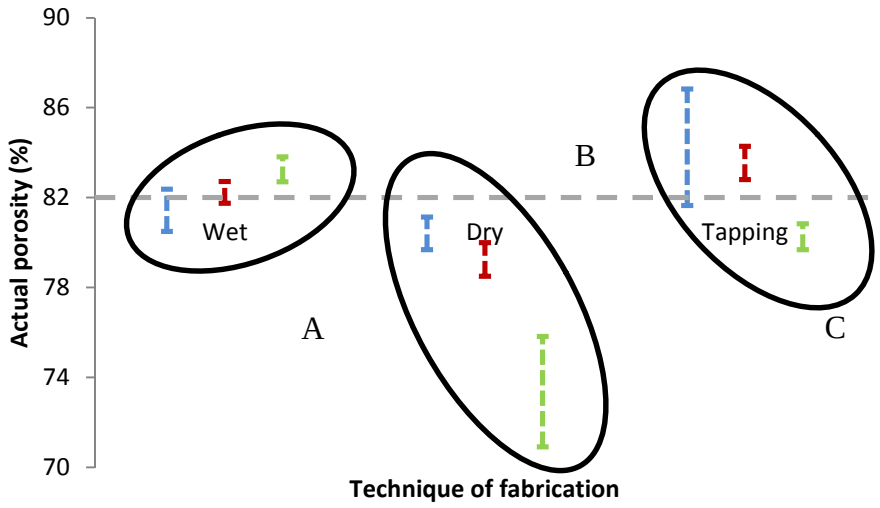

Figure 4.32: The distribution of actual porosity for the PEEK samples made from wet, dry and tapping techniques represented by black ellipse lines of A, B and C, respectively. The dashed line at 82 is the target porosity. The blue, red and light green dashed lines present the standard deviation of the actual porosity for Vicote, LT1 and LT3, respectively.

Table 4.8: Salt residue in the samples made from the wet, the dry and the tapping routes and the range of actual porosity achieved.

Fabrication route	Wet	Dry	Tapping
Salt residue range(%)	0.1 – 0.9	3.5 – 15.3	0.5 – 0.7
Actual porosity range (%)	80 - 84	70 - 82	80 - 87

Some researchers, by combining the salt leaching technique with injection moulding to fabricate PEEK scaffolds, achieved low porosities of < 70% [16] [21] [18] [19] due to the limitation of the production techniques. The wet and dry routes are able to obtain high porosity close to 80% and for the tapping route, the porosities of the samples were close and slightly higher than the target value, from 80 to 87%. Higher porosities via the tapping route are likely to be a result of requiring the PEEK powder to flow into and then pack in the spaces between the salt beads. Although this packing is increased during consolidation, there is likely to be less powder present in the inter-particle gaps than is the case for the other two methods. This is supported by the presence of excess powder on the surface of the tapped samples. Especially high porosities for the Vicote powder may then be a result of a lower packing density for this finer powder (as was shown in Table 4.2). Less complete penetration of PEEK into the structure also contributes to the formation of incomplete scaffolds (Figure 4.33a) and excessive PEEK at the top surface (Figure 4.33b) or fragile structures with thin struts (Figure 4.33c) and frequently appears on Vicote samples although the same tapping treatment is applied.

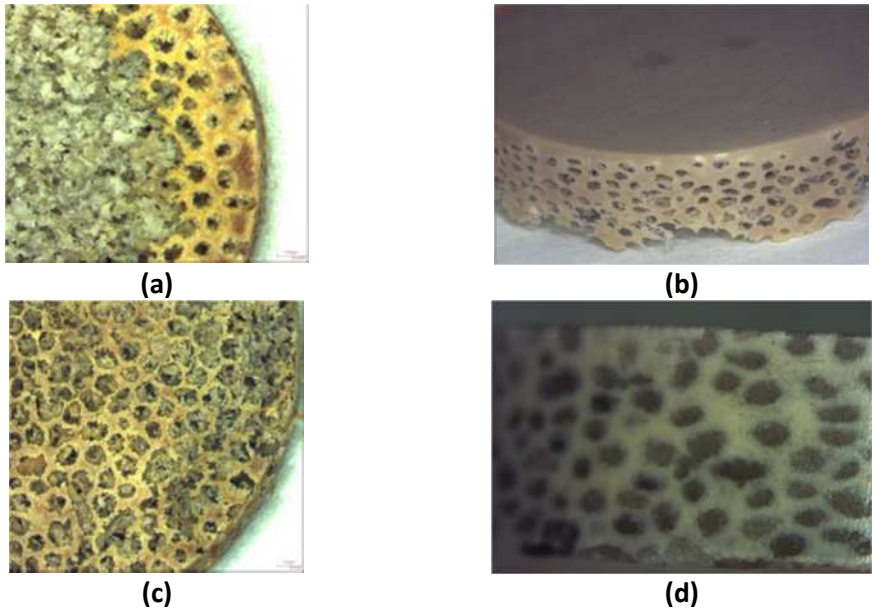

Figure 4.33: (a) An incomplete scaffold, (b) the excessive layer of PEEK at the top region, (c) a fragile structure and (d) good network of the compacted PEEK/salt beads.

2D porosity distributions comparisons (in Figure 4.34) show that samples from the wet and dry routes exhibit a wider deviation, 12% and 11%, respectively, in comparison with 8% standard deviation for the tapping route samples. Although only measured for a single sample, less uniform porosity distributions in the wet mixed powders are surprising given the prior attachment of the PEEK powder to the beads (affected by a "glueing effect" due to partial, surface dissolution of the salt in the water and then recrystallization of the salt). Non-uniform coating might give a small difference, but low porosity at the surfaces might be a result of compaction effects.

Reduced uniformity of porosity in the sample produced from the dry mixture is expected due to the mixing and die filling process allowing the beads and PEEK to be freely distributed in the die cavity. As poor mixing is expected for large and small powder mixes, an uneven distribution of porosity is expected.

In most cases the finer PEEK powder was seen to accumulate at the top surface of the dry mixed samples. The local level of porosity in the dry mixed samples is also highly influenced by trapped salt in the structure. Unleached salt (as a result of the poor mixing) yields lower levels of recorded porosity.

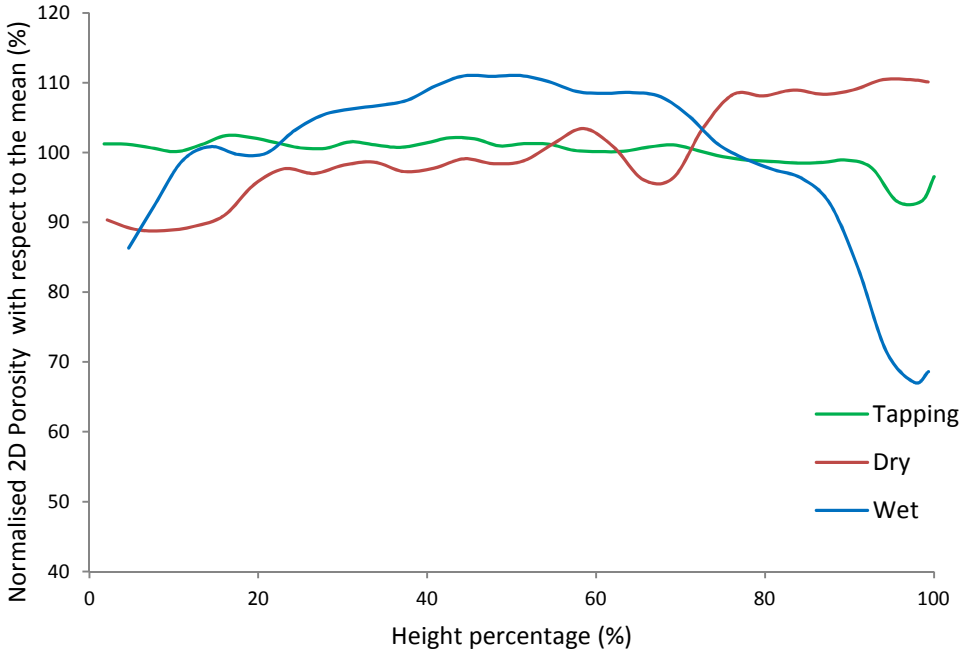

Figure 4.34: Porosity comparison for the samples using LT1 PEEK made by different routes.

More uniform porosity exists in the structure made by a tapping route although there is a decrease in porosity at the top region due to a slight excess of PEEK remaining at the top due to the a saturation of PEEK in the voids between the beads (Figure 4.35).

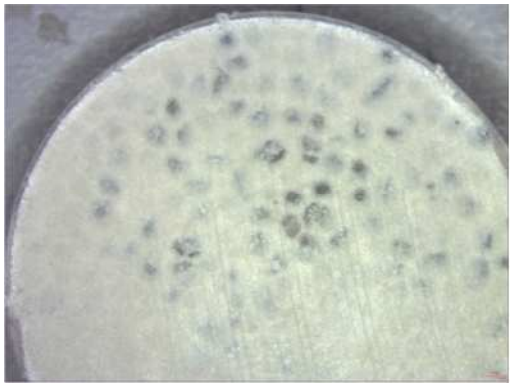

Figure 4.35: The remaining PEEK at the top region of tapped samples after compaction with appearing salt beads.

Figure 4.36 presents CT images clarifying the difference in the packing behaviour of the salt beads by the different routes. Figure 4.36a shows that the wet-route sample has evenly distributed beads, reasonably densely packed, but that the spaces between the beads contain dispersed porosity. This is a result of the PEEK being attached to the salt bead surfaces, preventing salt-to-salt contact but also because the PEEK is not free to move, not producing dense PEEK struts. Figure 4.36b, for the dry-route, shows more irregular packing with regions rich in beads and others rich in PEEK, resulting from poor mixing. Bead-to-bead contact is apparent in some regions and they appear (at least in 2D) to be isolated in other regions. The inter-bead region is, however, dense. An area is also shown which contains unleached salt which will raise the locally measured density. Figure 4.36c, for the tapped-route, shows dense and uniform packing of the salt beads (achieved prior to addition of the PEEK powder). Connections between salt particles are more numerous due to the pre-established interconnected salt bed prior to tapping. Tapping fills the gaps with PEEK but does not displace the contacting beads. The filling with PEEK is even and the struts (after consolidation) are dense.

The pore sizes for the different processes are compared in Table 4.9 and in Figure 4.37. It is clear that the modal pore sizes are broadly similar and that is to be expected as the same porogen was used to make all the scaffolds. What is apparent is, however, that the modal pore size of around 600 – 690 µm is in contrast to the original size of the beads, 1.0 – 1.4 mm.

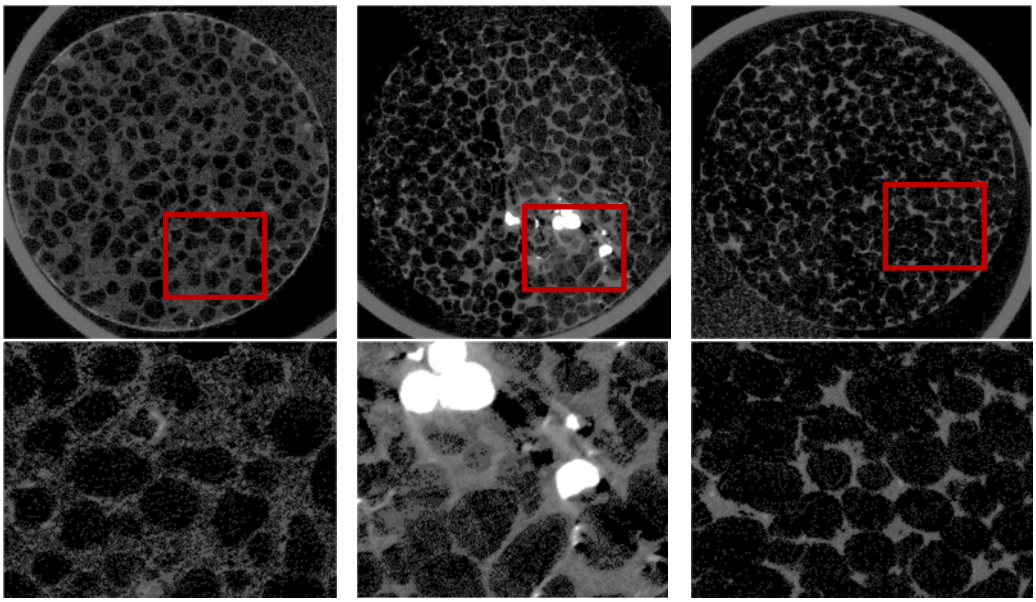

Figure 4.36: Typical 2D structure showing porosities for (a) wet-sample (b) dry-sample and (c) tapped-sample. The red boxes are the zoomed are provided bellow the structure images.

This discrepancy is a result of the measurement method. The CT software calculates the pore size by attempting to place a sphere into the pore space, regardless of its shape. Since compression of the porous beads changes their morphology, from rounded to elongated perpendicular to the compaction direction (as was shown in Figure 4.39), the measured diameter is actually a more accurate representation of the minor (Z) axis of the pores. Nevertheless, CT measurements do highlight the existence of small pores in the scaffold

made by the wet-route. Based on SEM measurement from cross-sections of each sample, the measured 'primary' pores are in the range of 645 – 1270 µm (Table 4.9) confirming that the measured pore sizes are still consistent with the real pore size range. It should be understood that the pore measurements on cross-sections are likely to underestimate the pore sizes.

Table 4.9: Summary for pore size PEEK scaffolds from wet, dry and tapping techniques

Manufacturing method	Wet	Dry	Tapping
Mean pore size (µm)	567 – 595[a]	450 - 600	560 - 630
Standard deviation of the mean pore size (µm)	163 – 173	190 – 210	160 – 190
Standard deviation of the mean pore size (%)	28 – 30	35 – 42	27 – 32
Mode of pore size (µm)	630 – 690	600 - 690	630
Minimum pore size measured by SEM analysis (µm)	739	645	669
Maximum pore size measured by SEM analysis (µm)	1270	934	1175

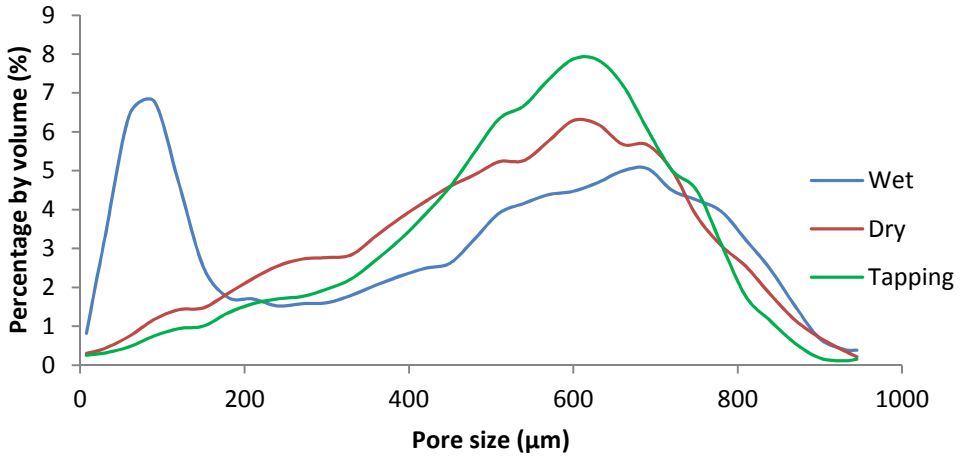

Figure 4.37: Typical pore size distributions of the PEEK scaffolds made by the wet, dry and tapping route techniques shown by the volume percentage.

The existence of very small pores in the sample structure from the wet route, also visible from the 2D image in Figure 4.36a, is most likely due to the way that the coated beads pack together, preventing close contact between the salt

particles and the formation of a dense PEEK strut. The small pores are manifested as fine porosity in the cell walls and struts (as was shown in Figure 4.39a and b). It was thought that the wet processing route might lead to fracture of the beads and hence the creation of a fine fraction of coated salt particles. Whilst there is some evidence of particle fracture when sieving to remove all particles below 500 µm was performed, although reduced (shown in Figure 4.38), a significant fraction of < 100 µm porosity remained.

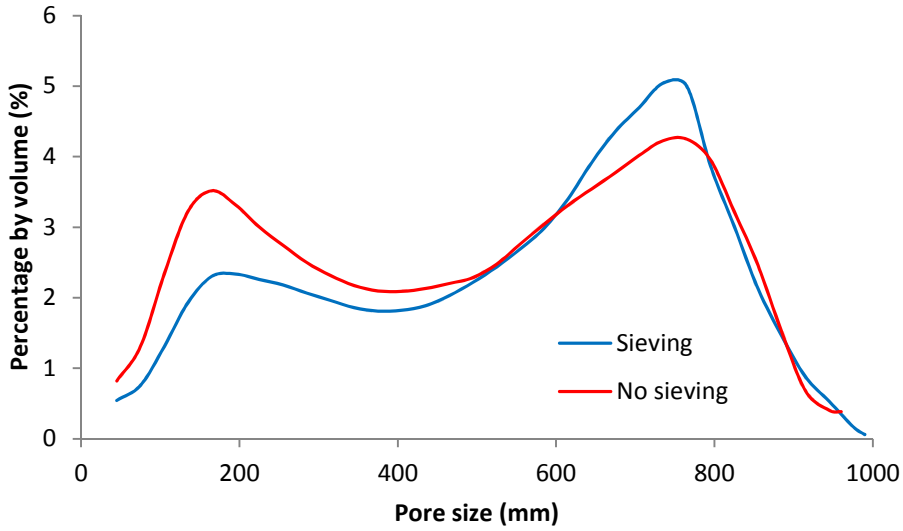

Figure 4.38: Distribution of pore size for the sample from the sieved wet mixture before and after screening with a 500 µm sieve.

The Degree of Anisotropy (DA) varies in the PEEK samples, it is noted that samples from the wet route (1.3 – 1.36) are lower than those from the dry (1.57 – 1.64) and tapping (1.53 – 1.62) routes. It is possible that the coated salt beads made by the wet route are more resistant to deformation when compacted and hence deform less, giving a lower DA value. However, it must also be considered that the overall measurement of the DA in the wet-route

sample also considers the significant fraction of small pores in the cell walls which have a much-reduced elongation.

As was stated earlier, the structures must have a high degree of connectivity in order that the salt escapes during dissolution. Simple observations of long immersion times being required for samples made by the wet and dry routes suggests a lower degree of connectivity in these structures.

Good connectivity is demonstrated by the sample made by the tapping route which shows large windows connecting neighbouring pores. Figure 4.39 highlights the difference in connectivity for the three processing routes. Connecting windows are rarely seen in the structure from samples of the wet route, as the result of covering the salt beads with PEEK which prevents salt-to-salt contact (previously highlighted in Figure 4.36). Instead, pore to pore connection is achieved through the fine porosity of the pore walls. The fine scale of this porosity accounts for slow salt dissolution rates. Connections in the sample made by the dry-route are more frequent but irregular (as was also shown in Figure 4.36) due to occasional but less regular contacts between neighbouring salt beads.

During the tapping route, the salt beads in the die form a dense, well-connected bead bed. Salt beads are supported by their contacting neighbours and when the PEEK is tapped through the structure it cannot disrupt these connections. The size of the windows is dictated by how well the PEEK can penetrate the contact area with smaller windows expected (and observed) for finer Vicote powder. The average window size is estimated at about 204 ($\pm$41) µm (the blue arrows

in Figure 4.39e) and is within the acceptable range for bone ingrowth [28, 89-92].

The number of windows present in the tapped structure is defined by the geometry of the packing. The tapping creates a bed of salt beads with a dense random packed arrangement (refer to table 4.1-3). Dense random packing results in an average co-ordination number (the number of touching neighbouring particles) between 6 and 7 [40, 124] and this corresponds well with the typical number of windows per pore.

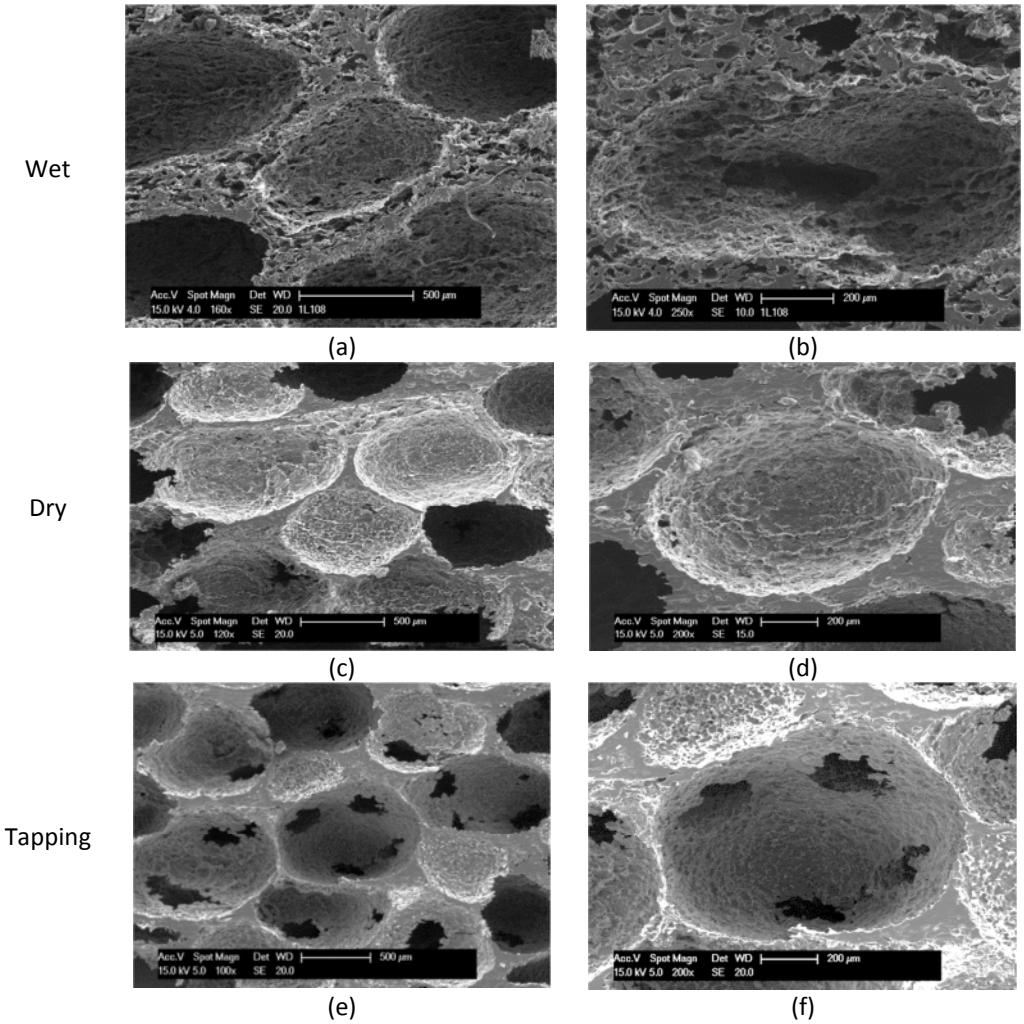

Figure 4.39: Pore structure and windows in the sample from (a, b) wet, (c, d) dry and (e, f) tapping routes. The red arrows show the compaction direction and the green ellipses show the windows.

The scaffolds from the wet route had values of connectivity density between 68 and 79/mm^3, much larger than samples from the wet and tapping routes (as seen in Table 4.10). It has been reported that vertebrae bone has a connectivity density around 2 – 15/mm^3 [100, 101]. Since the connectivity reports the number of redundant separations in a porous structure [102] the high value for the wet-route is most likely due to the small pores present in the cell wall structure. In normal cancellous bone, it has been suggested that the connectivity density may be a useful assessment of the elastic properties, where stiffness decreases with increasing connectivity [103].

Table 4.10: Summary of connectivity density for porous PEEK scaffolds from wet, dry and tapping techniques

Manufacturing method	Wet	Dry	Tapping
Connectivity density (1/mm^3)	68.75 - 78.49	7.66 - 11.61	7.6 - 9.39

4.3.2 Selection of the optimum processing route

In order to progress with the study, a single powder and process needed to be selected. The process of selection involved matching the observations made in this chapter to some key indicators. It was required that;

1. The process be repeatable with low deviation in porosity from part to part.
2. That an even distribution of porosity be present through the structure.
3. A good level of pore connectivity be achieved.
4. Appropriate sizes of pores and connecting pores are created to suit bone in-growth.

5. A low level of residual salt is present after a reasonable dissolution period.

From the five key indicators, a simple assessment could be performed by comparing the properties of the final porous samples through the processing routes. Table 4.11 shows a summary of the assessment by using Poor, Fair, Good and Excellent rating scales which are associated with quantitative numbers of 0, 1, 2 and 3, respectively along with a weighing factor of importance from 1 (least important) to 3 (most important). The assessment score is the sum of all multiplied ratings and weightings for the key indicators. From the assessment in Table 4.11 it is clear that the tapping route is the only possible route to meet the requirements.

Table 4.11: Assessment of the optimum processing route based on 5 key indicators

Weighting factor	Key indicators/Route of fabrication	Wet	Dry	Tapped
3 (most important)	Sizes of pores and connecting pores which suit to bone- ingrowth	Fair (1)	Poor (0)	Good (2)
2 (important)	Even distribution of porosity through the structure	Fair (1)	Poor (0)	Good (2)
2 (important)	Level of pore connectivity	Good (2)	Fair (1)	Excellent (3)
2 (important)	Repeatable process with low deviation in porosity	Good (2)	Poor (0)	Good (2)
1 (least important)	Level of residual salt	Good (2)	Poor (0)	Excellent (3)
	Assessment score	15	2	23

For the favoured (tapping) production route, scaffolds made using the slightly larger LT1 PEEK, showed the optimum size and number of connecting windows between the primary pores and thus the tapping process using LT1 PEEK has been developed further in this study.

4.3.3 Comparison of tapped structures with other porous PEEK structures

The original inspiration for this work was a prior study by Jinnapat and Kennedy (2010) who produced cellular solids via salt bead tapping but using aluminium powder. Figure 4.40 shows that, as expected, Al and PEEK porous structures made by the same route show very similar characteristics in regard to the pore shape, porosity and connectivity.

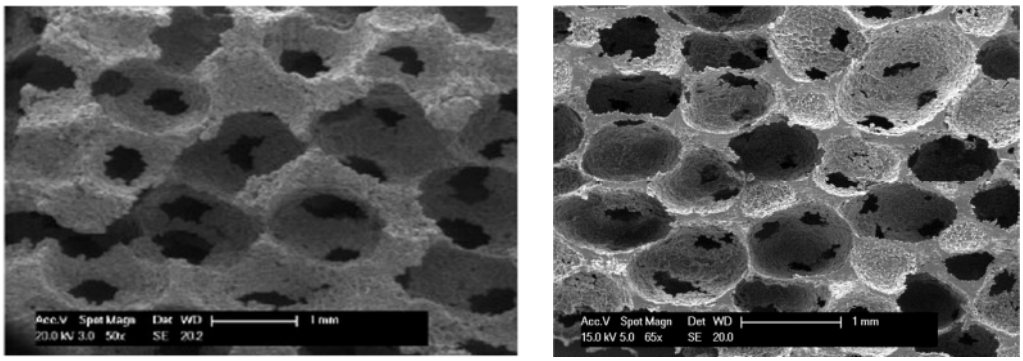

(a) (b)

Figure 4.40: Porous scaffolds made by tapping using (a) Al powder [104] and (b) PEEK powder.

Porous PEEK scaffolds have been made by a number of researchers and the processes used were summarised in the literature review in section 2.4. Table 4.12 summarises the shortcomings in the structural features (for example non-uniform or low porosity, poor pore connectivity, insufficient pore size and high residual salt) resulting from the methods used and re-presents images of the structures for comparison.

Considering these limitations, the technique presented in this thesis goes a long way to addressing the previous problems observed and results in porous PEEK scaffolds with excellent structural characteristics for medical devices.

Table 4.12: Comparison of scaffolds produced by tapping route and from the literature.

Method	Tapped mixing route	PEEK scaffolds by moulding process combined with salt leaching [16].	CNF-PEEK foams by injection moulding and $Al(HO)_3$ blowing agent [33, 122]	PEEK scaffolds by particulate leaching technique [21]	PEEK scaffolds by mould-salt leaching and vacuum melting under high temperature [18].
Characteristics	• 80 – 87 % porosity. • Uniform pore shape. • 2 – 6 windows seen from the observed side of the sample. • Good connectivity. • Low residual salt (<1%). • Good level of	• Low porosity (<50%) with small pore size of 70 µm and pore blocking due to salt residue. • The shape of pore size is non-uniform.	• Only contain pores in the centre with small pore size (69 – 121 µm), closed pores and low porosity	• Poor interconnectivity and low porosity (< 60%), porosity and pore shape not uniform with thick struts.	• Low porosity (24%), non uniform pore shape and lack of pore connectivity.
Scaffolds	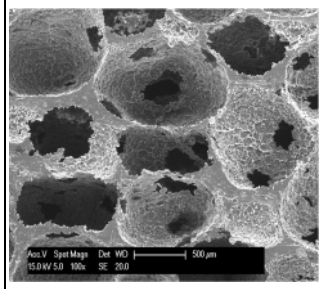	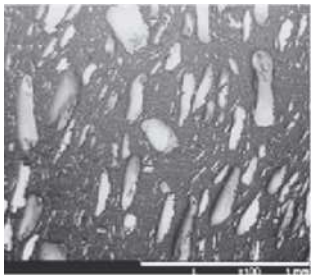	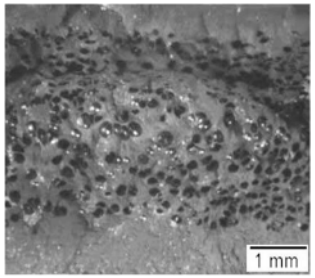	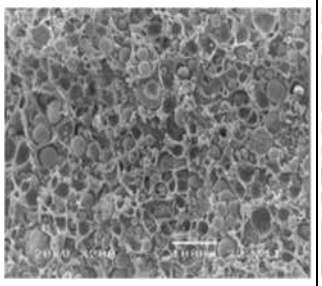	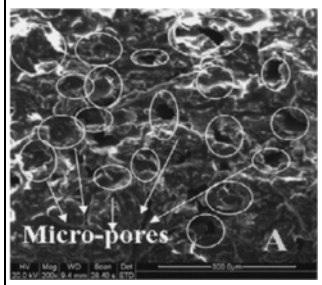

Chapter 5: Process Development For the Tapping Route

As the tapping route was identified as the most suitable route for producing porous scaffolds, this chapter looks in more detail at the tapping process with an aim to understanding and optimising the process.

5.1 Observations of the tapping process

There are essentially 3 stages to the tapping process; PEEK levelling, tapping and then achieving a stable state. Subsequent compaction follows the tapping process to obtain a compacted disc of the "composite". These stages are shown schematically in Figure 5.1.

First, the NaCL beads are poured into the cavity and levelled off by 10 taps in order to be easier to measure the height of the beads. The tapped NaCl bed height is measured using a Vernier gauge, with an estimated accuracy of $\pm$0.05 mm (parameter S1 in Figure 5.1) and then PEEK powder is loaded on top of the NaCl bed, and levelled off by light tapping. In the same way, the PEEK powder bed thickness can also be measured (parameter P1 in Figure 5.1). After the upper punch is inserted into the assembly, tapping is then started and then stopped at pre-determined points to measure the change in the height of the punch, from which the "composite" bed height can be determined (m1 and m2 in Figure 5.1). A stable condition is achieved when two or more consecutive measurements of the punch height differ by less than 0.3 mm.

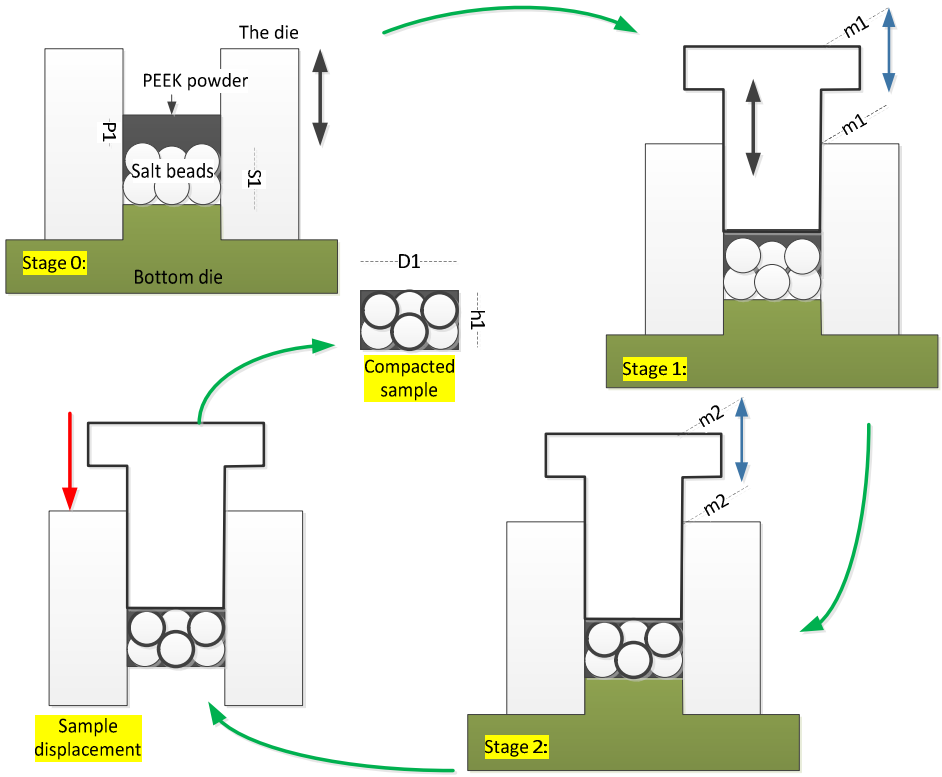

Figure 5.1: The tapping cycle to produce a tapped and compacted sample. Parameters S1 and P1 are the heights of the bed of spherical NaCl beads and PEEK powder in the cavity, respectively. Parameters m1 and m2 are the displacements of the punch during the tapping process. D1 and h1 are the diameter and the height of the compacted sample. Black, red and green arrows indicate tapping direction, compaction direction and cycle flow, respectively.

5.2 Tapping behaviour

5.2.1 The effect of different NaCl / PEEK ratios

Salt bead/PEEK composites were prepared in three ratios; 6/1, 8/1 and 10/1 by mass, using 1.0 – 1.4 mm salt beads. The mass and thickness of the salt bead bed were kept constant. Figure 5.2 shows the progressive change in height of the PEEK layer on top of the salt bead bed with the number of taps applied. In all cases, in the first 1000 taps the PEEK migrates quickly, but continually slowing down until reaching a stable height. The 10/1 mass ratio required 6000

taps to pack to a stable height while the 8/1 and 6/1 mass ratios required 7000 and 8000 taps respectively (Table 5.1).

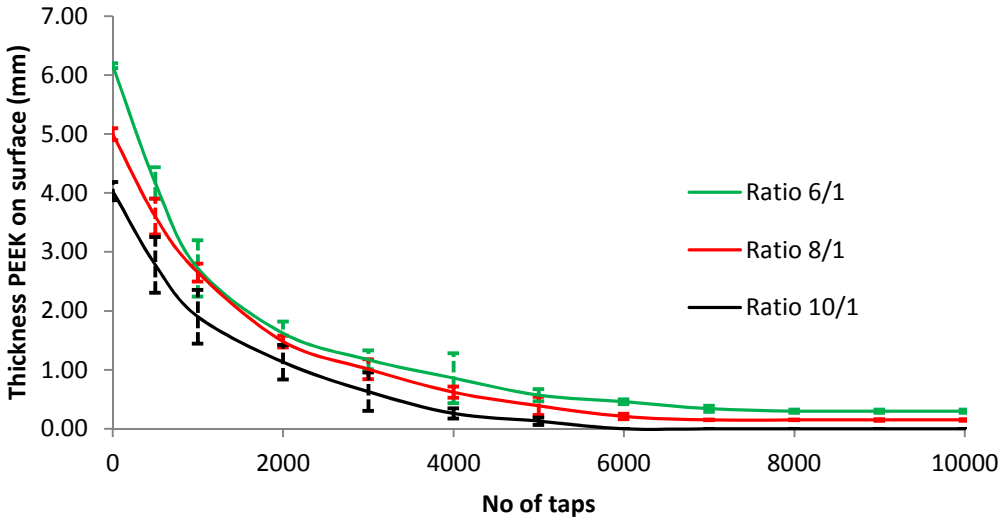

Figure 5.2: The change of PEEK bed height through tapping for salt beads of the size range of 1.0 – 1.4 mm for the salt beads/PEEK mass ratio of 6/1, 8/1 and 10/1 (The experiment was conducted 3 times).

Since the total mass of the salt beads in the composite remained the same, the 6/1, 8/1, and 10/1 ratio composites had the same thickness of salt bead bed (11.92 mm) and with different initial thickness of PEEK, 6.16, 5.00 and 4.03 mm for the initial PEEK bed corresponding to the 6/1, 8/1 and 10/1 ratios. After applying tapping and reaching their steady or stagnant height, the estimated thickness of PEEK on the composite surface was 0.30, 0.15 and 0 mm in respect to the increasing salt bead/PEEK ratio (Table 5.1). It should be noted that these values were calculated using the assumption that the salt bead bed height was not changing.

The validation of the measurement was conducted by observing the surface after tapping. Figure 5.3 depicts the conditions of the remaining PEEK on the

surface for each ratio. Figure 5.3a visualises some PEEK on the surface along with few salt beads for the 6/1 composite. This 6/1 composite has a predicted PEEK layer about 0.30 mm thick. For the 8/1 composite in Figure 5.3b, the measurement for the PEEK layer on the surface was 0.15 mm, and the tops of the beads were more visible, while the 10/1 composite (Figure 5.3c) exhibited beads on the top surface and very little PEEK (considered as 0.0 mm of PEEK on the top) indicating that the 10/1 ratio composite had insufficient PEEK.

(a) (b) (c)

Figure 5.3: The top surface of mixtures from (a) 6/1, (b) 8/1 and (c) 10/1 ratios of the salt beads to the PEEK.

Table 5.1: The thickness of PEEK on the surface in the die cavity before and after tapping using different ratios.

Mass Ratio	6/1		8/1		10/1	
Tapping	Before	After	Before	After	Before	After
PEEK bed on the surface (mm)	6.16	0.30	5.00	0.15	4.03	0.00
Required number of taps	8000		7000		6000	
PEEK (g)	0.71		0.54		0.43	
Salt beads (g)	4.29					

5.2.2 The effect of different bead sizes

For a constant mass ratio of 6/1, different bead sizes, of 1.0 - 1.4 mm, 1.4 – 2.0 mm and 2.0 – 2.5 mm were used at constant bead mass. Figure 5.4 depicts, as before, that PEEK migration is initially rapid but that a steady height of the PEEK layer takes longer to achieve as the bead size decreases (1.0 – 1.4 mm salt beads requires 8000 taps, 1.4 – 2.0 mm 7000 and 2.0 – 2.5 mm beads only 5000 taps). Figure 5.5 shows the surface of the tapped composite using different bead sizes. The 1.0 – 1.4 mm composite still contains PEEK on the top surface after tapping and very few beads were visible. More beads appear on the surface for the composite using a bigger bead size. The measurement of the PEEK layer after tapping shows that the 1.0 – 1.4 mm composite contains 0.30 mm of PEEK remaining on the top surface, while for the other composites using larger salt bead sizes, the PEEK layer thickness was very thin and close to zero (Table 5.2). No composite suffers from a lack of PEEK. For the 1.0 – 1.4 mm beads the rate of PEEK movement was slower than the rate for the 1.4 – 2.0 and the 2.0 – 2.5 mm (Figure 5.4). It was observed from the PEEK bed using 1.0 – 1.4 mm beads, that after 1000 taps, the PEEK layer thickness reduced by 56%, while for the 1.4 – 2.0 mm beads the change was 88% and 93% of the 2.0 – 2.5 mm beads.

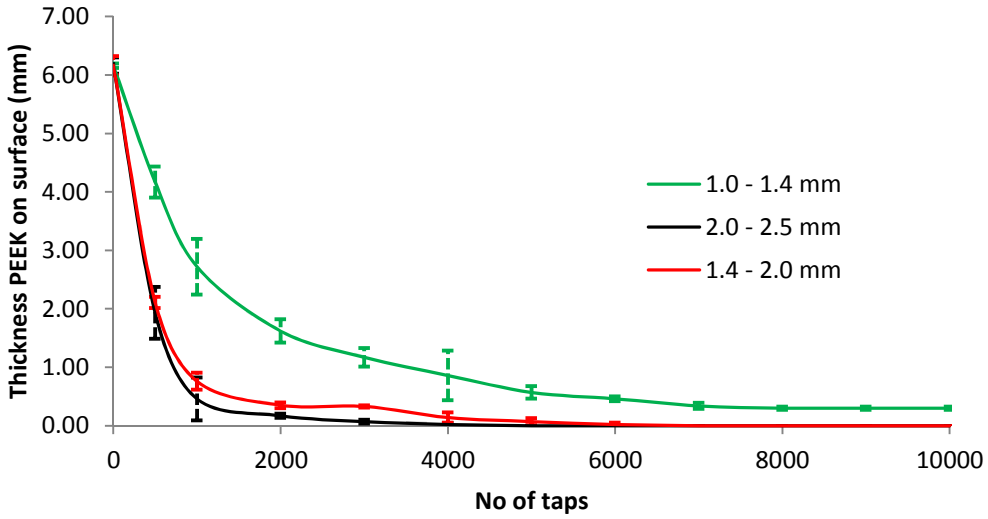

Figure 5.4: The change of PEEK bed height through tapping of a 6/1 ratio of salt beads to PEEK and NaCl beads of 1.0 – 1.4 mm, 1.4 – 2.0 mm and 2.0 – 2.5 mm. (The experiment was conducted 3 times).

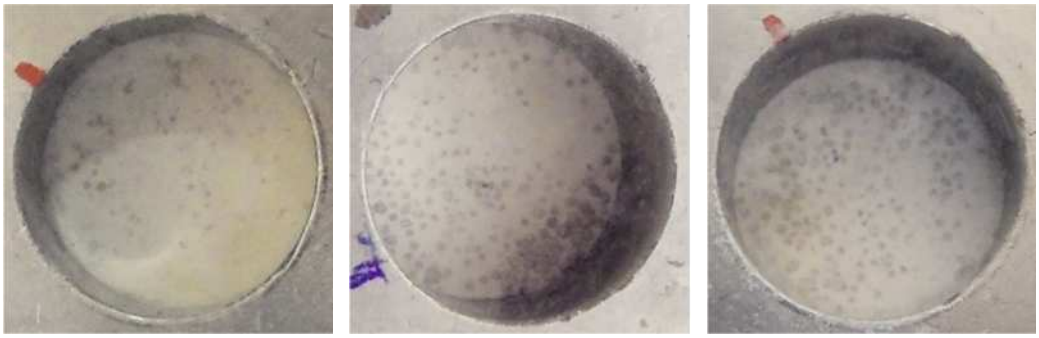

(a) (b) (c)

Figure 5.5: Typical surface of the PEEK layer on the top of salt beads for a 6/1 ratio and using (a) 1.0 – 1.4 mm, (b) 1.4 – 2.0 mm and (c) 2.0 – 2.5 mm beads, after 10,000 taps.

Table 5.2: The thickness of PEEK on the surface in the die cavity before and after tapping using different bead sizes.

Bead size	1.0 – 1.4 mm		1.4 – 2.0 mm		2.0 – 2.5 mm	
Tapping	Before	After	Before	After	Before	After
PEEK bed on the surface (mm)	6.16	0.30	6.16	0	6.16	0
Salt bead bed (mm)	11.92		12.84		13.17	
Required number of taps	8000		7000		5000	
PEEK (g)	0.71					
Salt beads (g)	4.29					

5.2.3 MicroCT study of tapping

A complementary experiment using a 20 mm diameter microCT sample holder was performed to see how the PEEK powder/salt beads packed during tapping. Due to the sample holder capacity, only 4 g of 6/1 NaCl/PEEK (1.0 – 1.4 mm bead size) was tapped. The progression of the PEEK powder height was studied by taking 2D radiographs of an interrupted tapping experiment measured from images such as those in Figure 5.6 and plotted in Figure 5.7. The graph shows that the tapped composite started with a PEEK thickness of around 5 mm and gradually decreased until it reached a steady thickness of 0.02 mm after 8000 taps. The trend is similar to that observed in Figure 5.2 for the metal die, but it is expected that the measurements of the various bed heights in this experiment are more accurate. The very small PEEK layer thickness indicates that there was little to no excess PEEK.

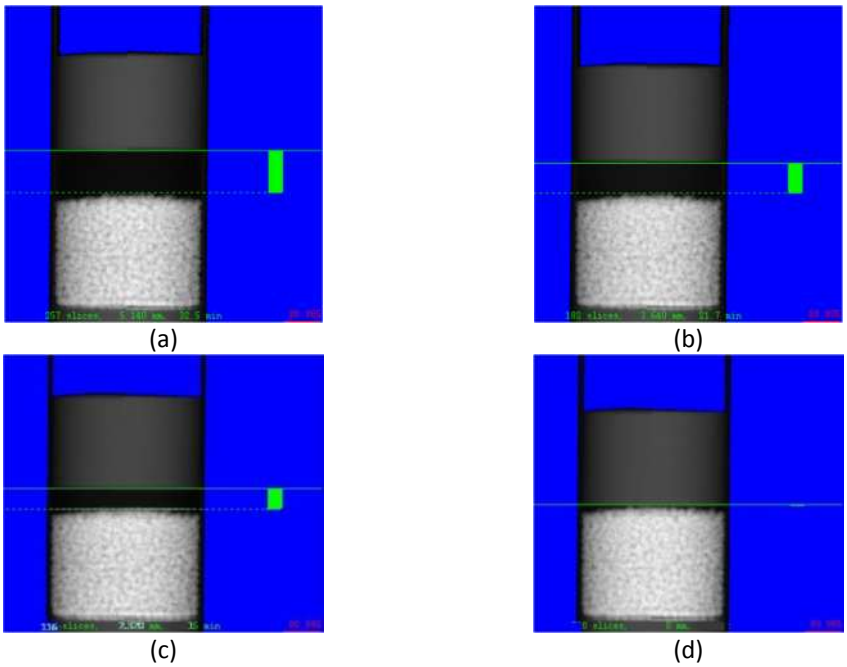

Figure 5.6: X-ray radiographs showing the progression of the PEEK bed (the black region in the middle and marked by green line bars) in the 20 mm microCT sample holder; (a) at 0, (b) 50, (c) 1000 and (d) 10000 cycles of taps.

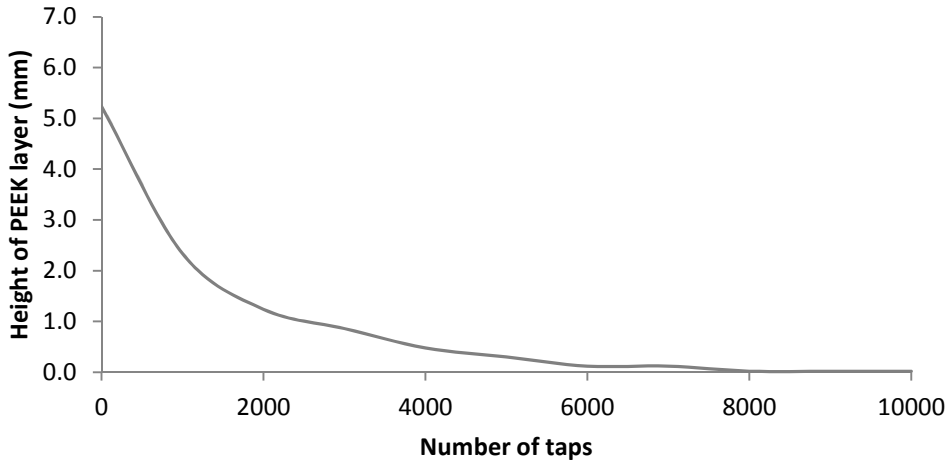

Figure 5.7: The change in PEEK layer height for salt beads of the size range of 1.0 – 1.4 mm for the salt bead/PEEK mass ratio of 6/1, using a 20 mm microCT sample holder (1 measurement).

5.2.4 Powder migration

To see the flow of the fine powder through the salt bead network in the cylindrical die, Ti powder of size <45 μm was used so that it could be more readily imaged through microCT scanning. From the 2D CT images inFigure 5.8, the packing of salt beads is clear. The observable depth of salt bead bed changed after tapping from 15 mm to 14.58 mm. According to 3D ImageJ measurements (threshold 94), the volume fraction of salt bead bed is 0.53 $\pm$ 0.02 for loose packing and 0.56$\pm$0.03 after tapping, agreeing well with previous bulk measurements.

Concentric circles were constructed to measure the radial packing fraction (Figure 5.9, Table 5.3). The radial packing fractions were measured for each bead size, in each track and for increasing radii expanding from the centre, summed over the full height of the sample. The results in the table show that for all particle sizes the packing fraction near the wall is slightly higher than it is closer to the centre.

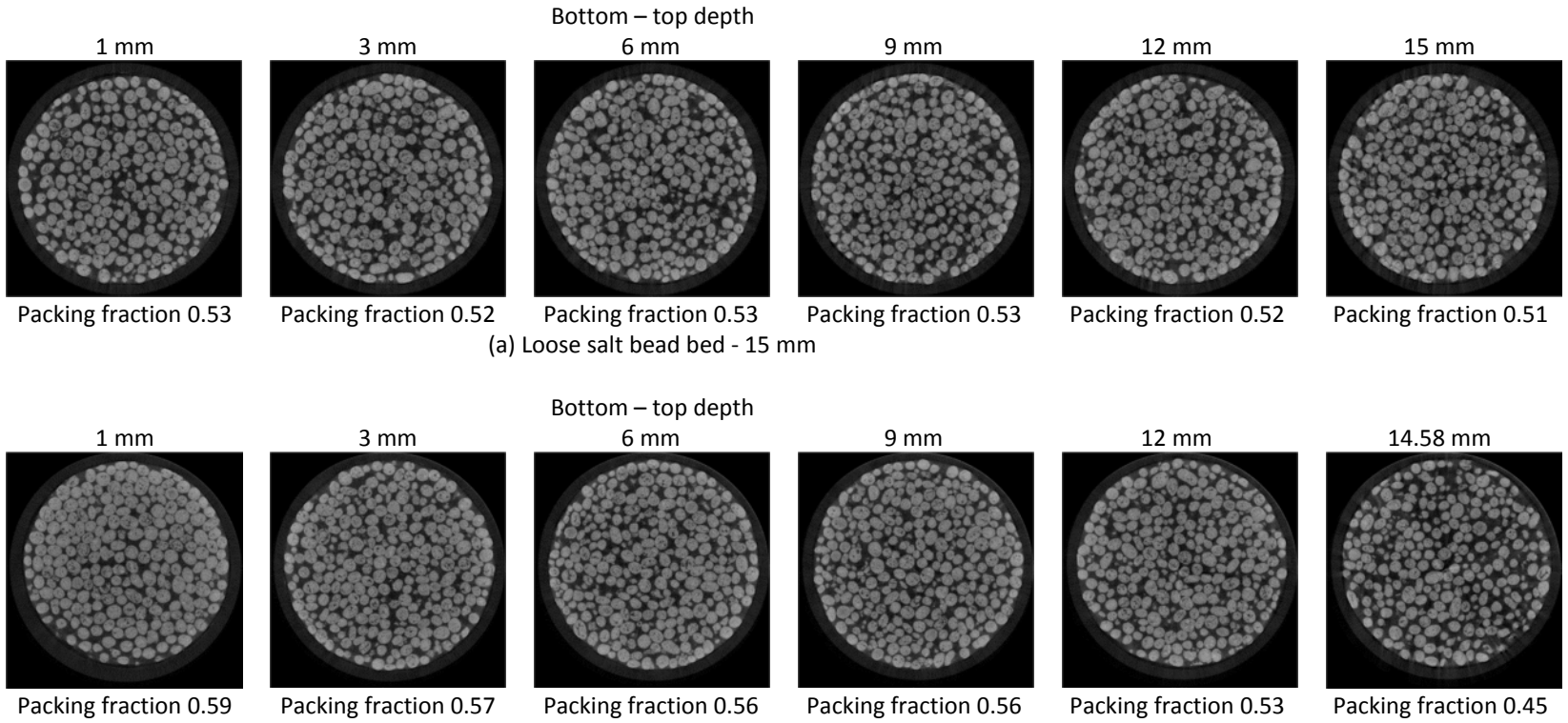

Figure 5.8: 2D slices of the salt bead network from tapped and loose packing in a 20 mm cylindrical microCT sample holder (distance from the bottom is shown).

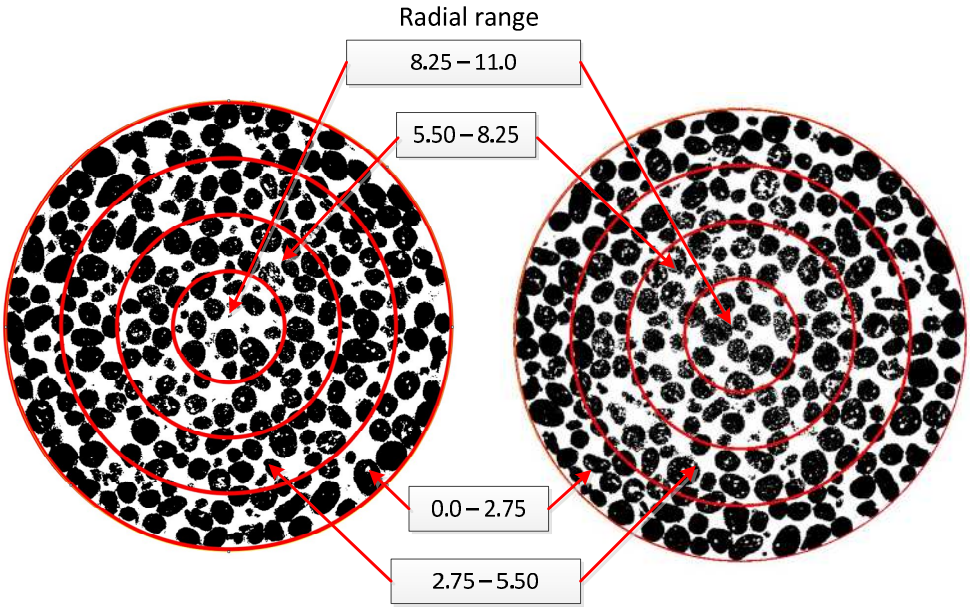

(a) Radial fraction of loose packing (b) Radial fraction of tapped packing

Figure 5.9: Radial tracks used to determine local variation in salt bead packing using (a) loose packing and (b) tapped packing of the salt beads.

Table 5.3: Packing fraction with radial position for tapped salt beads in a cylindrical vessel for different size ranges.

Packing fraction based on circle region			
Radius (mm)	1.0 - 1.4 mm	1.4 – 2.0 mm	2.0 - 2.5 mm
0.0 - 2.75	0.55	0.46	0.48
0.0 – 5.50	0.55	0.50	0.49
0.0 – 8.25	0.55	0.53	0.53
0.0 – 11.0	0.56	0.52	0.53
Packing fraction based on circle circuit			
Radius (mm)	1.0 - 1.4 mm	1.4 – 2.0 mm	2.0 - 2.5 mm
0.0 - 2.75	0.54	0.46	0.47
2.75 - 5.50	0.54	0.51	0.50
5.50 - 8.25	0.54	0.55	0.56
8.25 - 11.0	0.57	0.53	0.54

The initial loading of Ti powder prior to tapping is captured in Figure 5.10. Unlike for the PEEK, the small Ti particles penetrate the bead bed through the

accessible voids on the wall side, even before tapping starts, while in the middle area (yellow shading) unfilled voids are observed. Figure 5.11 shows the structure after 400 taps showing unfilled areas in the upper region of the salt bead bed (red shading).

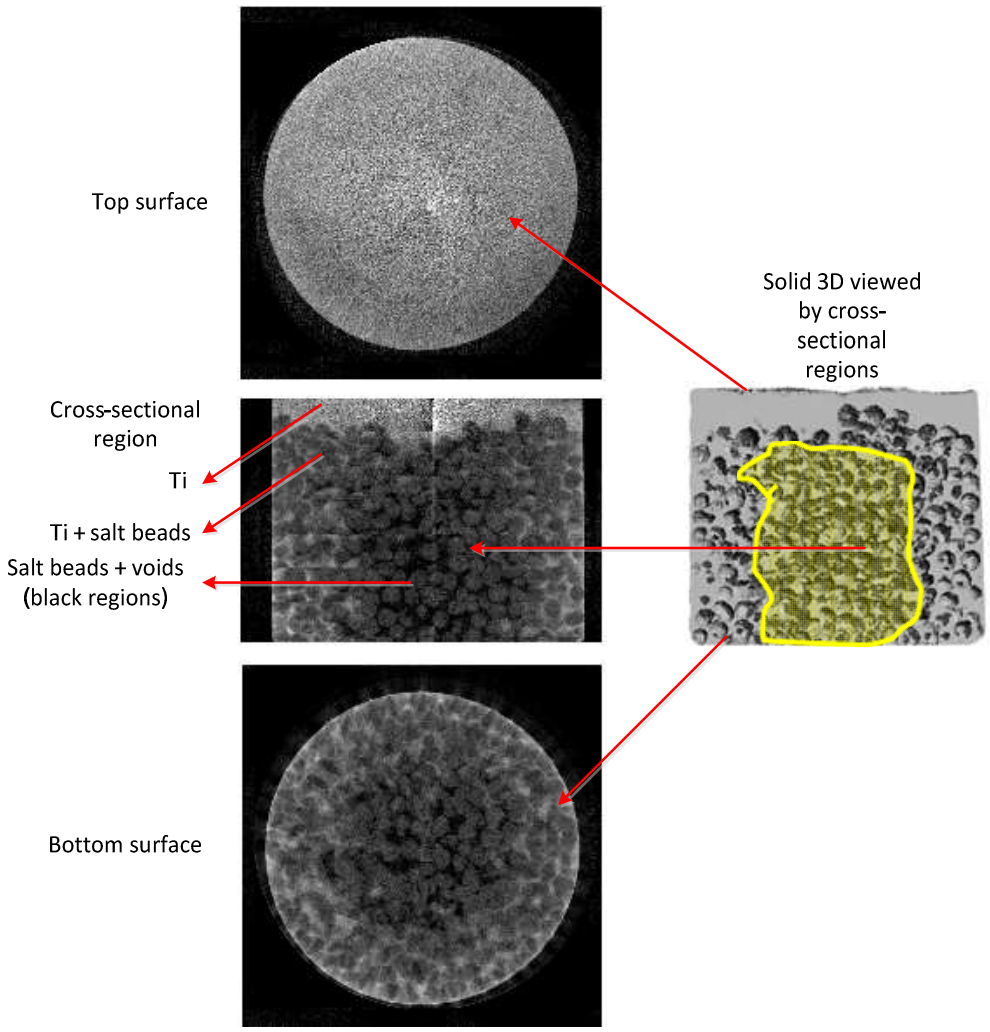

Figure 5.10: Cross section of a 3D image of salt beads/Ti composite coupled with top, bottom and cross-sectional regions prior to tapping. The top surface is covered by titanium powder. The yellow shading represents empty salt bead gaps before tapping and the red shading presents empty salt beads after tapping. The black region between salt beads and titanium in the cycle indicates voids.

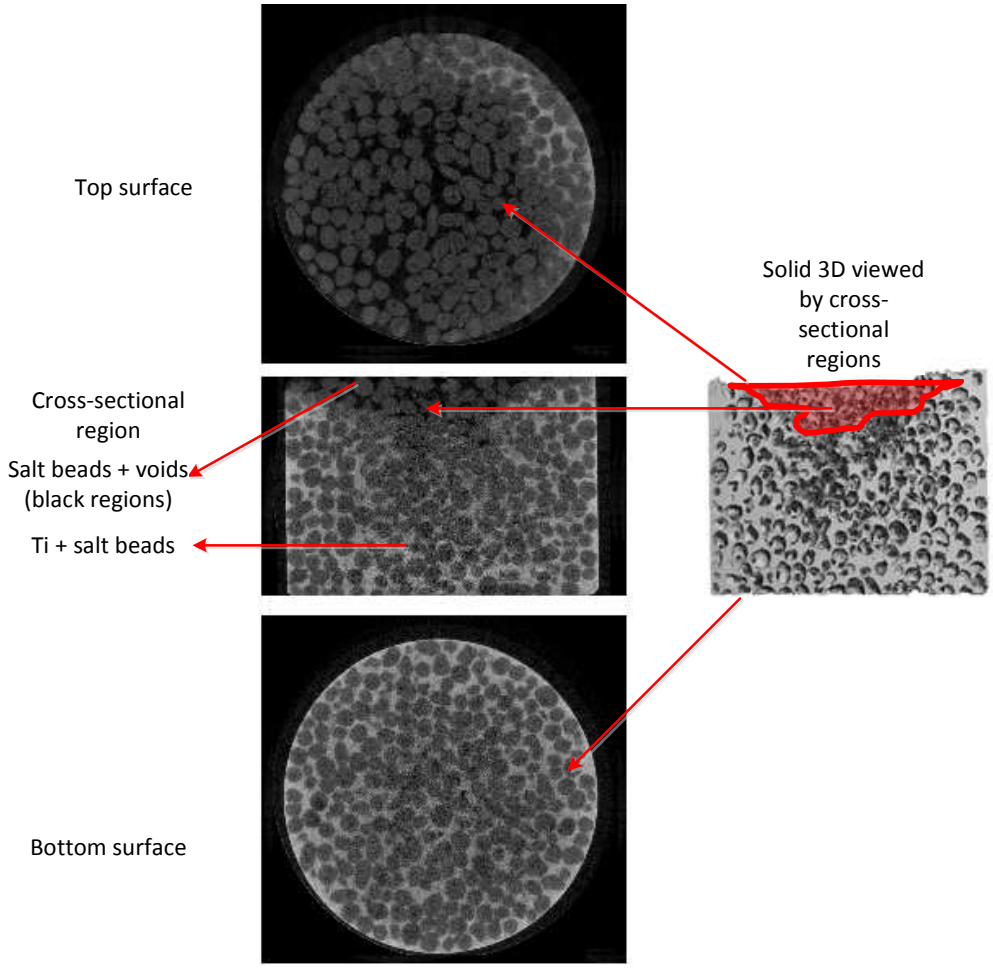

Figure 5.11: Cross section of a 3D image of salt beads/Ti composite coupled with top, bottom and cross-sectional regions after 400 taps. The red shading represents empty salt beads after tapping. The voids (black region in the cycle) only appear on the top surface.

The filling process can be seen in more detail in Figure 5.12 by comparing 2D slices taken from top to bottom after a different number of taps (0, 10, 100, 200, 400 and 1000). Figure 5.12 shows the progress of the Ti particles through the salt bead bed. When loading in the container, powder percolates through the bead bed by filling the wall area (loaded composite, in Figure 5.12) while the rest remained on the top. The bottom region was densely filled after 200 taps and the centre of the bead bed was filled after 400 taps. Excessive tapping (1000 taps) leads to the disaggregation of the salt beads on the top surface. It should be noted that as the Ti powder has heavier particles (larger and higher

density than PEEK), the Ti/NaCl bead composite was fully packed in fewer taps that for the equivalent PEEK sample.

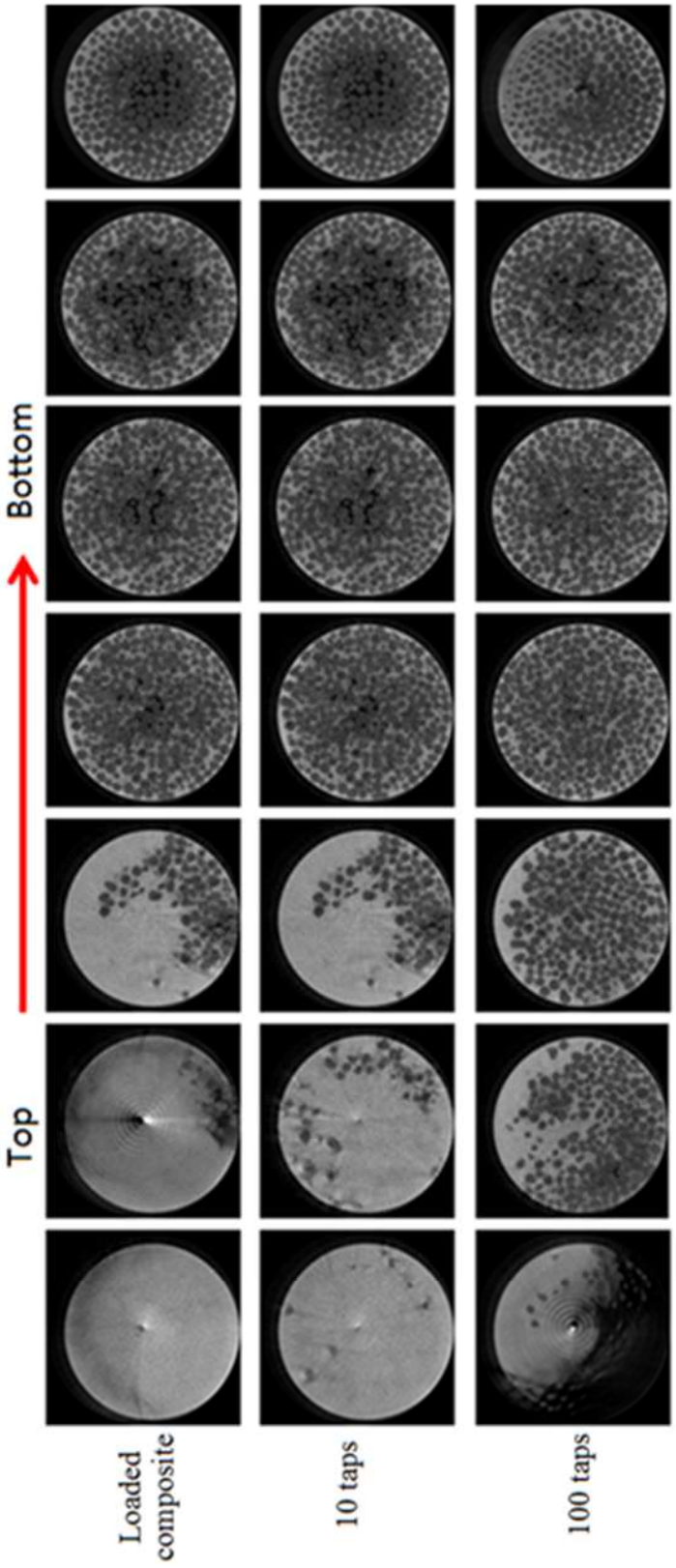

Figure 5.12: 2D CT slices of Ti powder (bright) and salt beads (dark grey) and voids (black regions) in the objects. The row series of images shows positions from top to bottom.

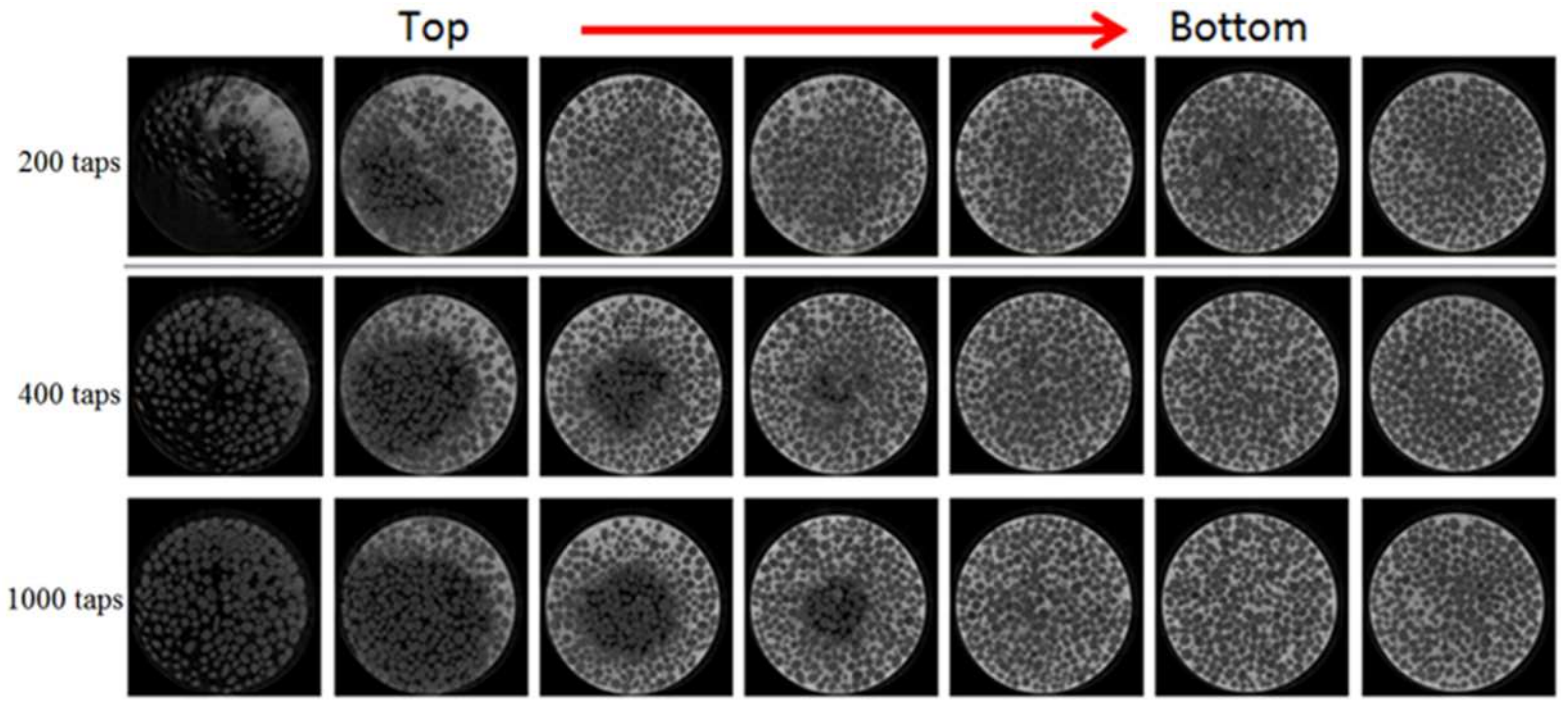

Figure 5.11 (continued): 2D CT slices of Ti powder (bright) and salt beads (dark grey) and voids (black regions) in the objects. The row series of images shows positions from top to bottom

5.2.5 Effects of inadequate tapping

Observations show that inadequate tapping results in less dense network of PEEK (not melted as it was prior to sintering process) in the NaCl bead gaps, indicating that the filling is not optimum, leaving bead gaps with a sparse network of PEEK (Figure 5.13a and c). In Figure 5.13c marked in a red circle, the PEEK network (shown by white region) is not even due to only few PEEK flow to that region. On the other hand, adequate tapping provides adequate dense network of PEEK appearing to separate the adjacent salt beads (Figure 5.13b and d). In Figure 5.13d marked in a red circle, the PEEK network appears to surround the beads.

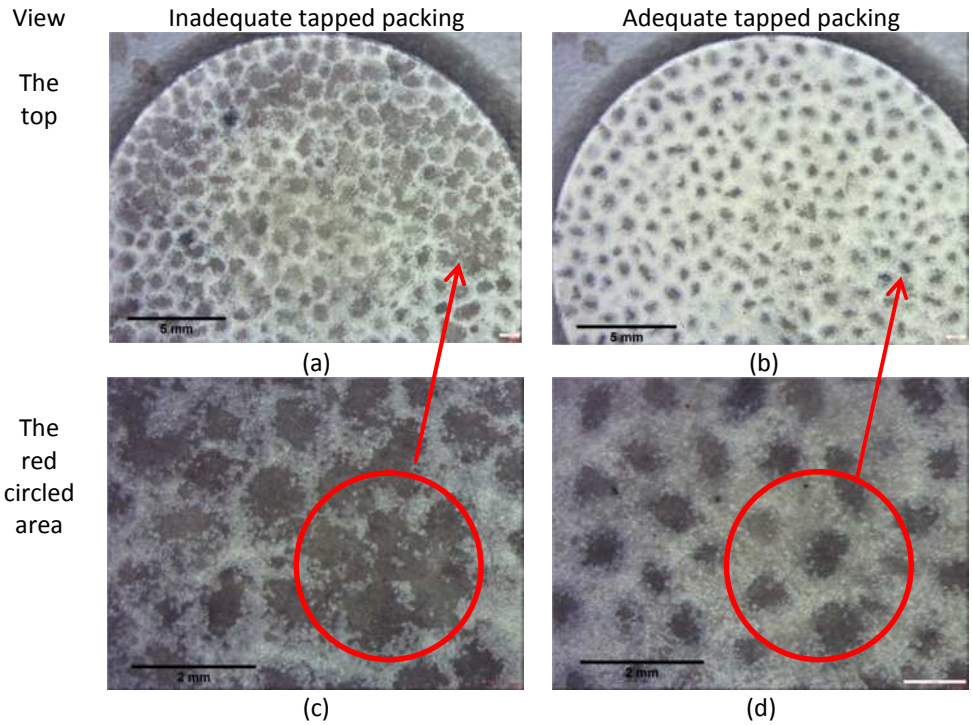

Figure 5.13: The comparison of tapped samples with a lack of required number of taps (a and c) with less dense PEEK between salt bead gaps compared to of the adequate tapping (b and f) as shown from the bottom surface. The red circles represents the area of interest to be compared.

Insufficient tapping also leads to an incomplete PEEK network as seen from the side wall where PEEK is only able to partially penetrate the bead bed (Figure 5.14a) causing a thick layer of excess PEEK at the top. Adequate tapping allows PEEK to uniformly percolate the bead gaps from the top to bottom areas (Figure 5.14b). In the figure, it appears sphere against the wall as a result of the compaction and also indicates that the salt beads are not fully spherical.

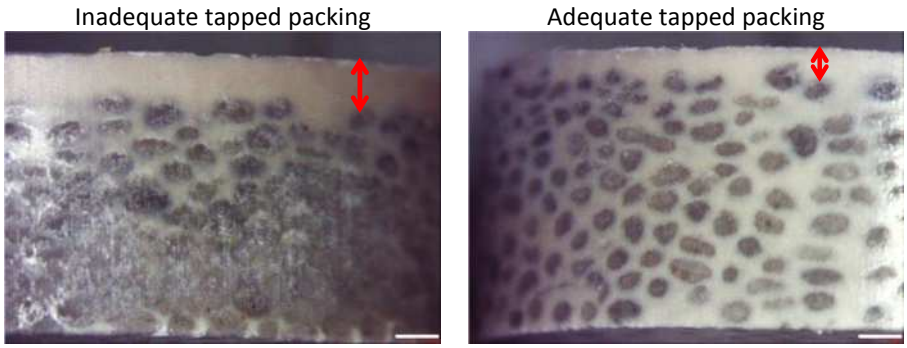

Figure 5.14: Sidewall views of samples made with a) insufficient tapping indicated by the excessive PEEK on the top but lower region with very little PEEK exist and b) adequate tapping indicated by distribution of PEEK between the salt beads and thin layer of PEEK on top surface. The 1 mm white scale bars in the right bottom are shown in the figures.

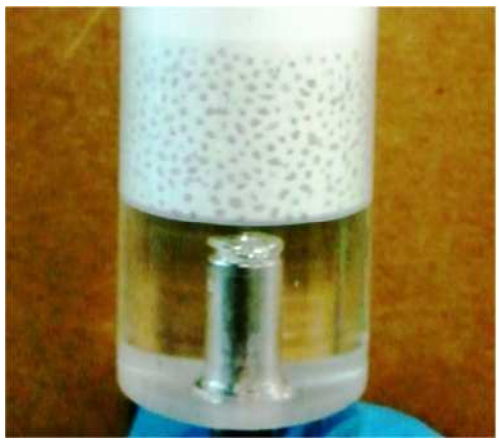

Figure 5.15: Salt beads and PEEK powder in a transparent container after the same tapping given. The wall of container also looks similar with bead composition after the compaction indicating that PEEK prevent a salt bead from experiencing in full contact with surrounding beads which could lead to deformation while being compaction.

Another indication of a good sample is a thin PEEK layer on the surface. Figure 5.16 shows typical good samples, at the bottom and on the wall side, the salt bead/PEEK arrangement is clear along with an acceptable skin thickness of PEEK at the surface where the salt beads are visible.

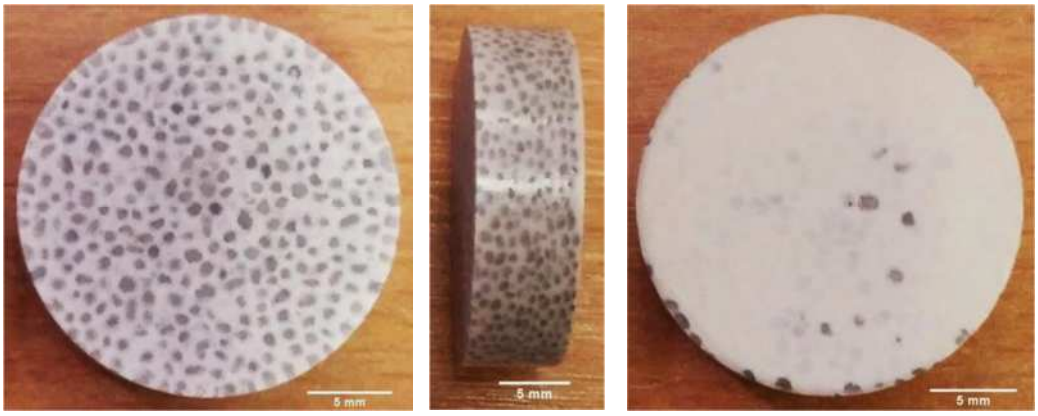

(a) (b) (c)

Figure 5.16: An example of a typical good sample after compaction applied to the salt bead/PEEK tapped mixture incorporating 1.0 - 1.4 mm bead size range. The sample are pictured from its (a) bottom, (b) side and (c) top surfaces.

Visualisation of compacted samples made using 1.0 – 1.4 mm beads is presented in Figure 5.17 showing a series of samples made with 4000, 6000 and 8000 taps. It can be seen that a thin and sparse PEEK network appears on the bottom of the sample after 4000 taps indicating the gaps were partially filled. The PEEK network at the bottom region becomes more established with the number of taps applied, and the salt beads appear clearly at the surface after 8000 taps (Figure 5.18).

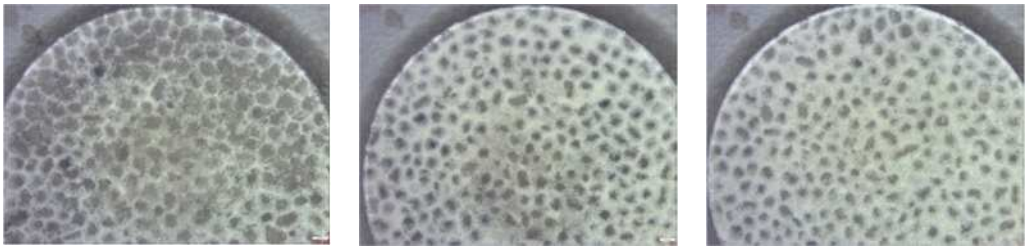

(a) 4000 (b) 6000 (c) 8000

Figure 5.17: Views on the base of tapped samples after 4000 – 8000 taps using 1.0 – 1.4 mm beads showing the dense of PEEK between the salt beads after (a) 4000, (b) 6000 and (c) 8000 cycles of taps. For the 4000-tapped sample, PEEK was not adequately filling the salt bead gaps indicated by less dense PEEK appear compared to the 6000 or 8000-tapped samples.

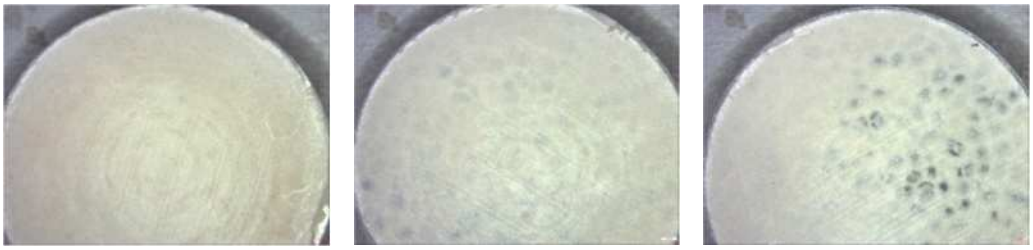

(a) 4000 (b) 6000 (c) 8000

Figure 5.18: Views on the top of tapped samples after 4000 – 8000 taps using 1.0 – 1.4 mm beads showing the dense of PEEK on the top surface after (a) 4000, (b) 6000 and (c) 8000 cycles of taps. For the 400-tapped sample, PEEK still remains on the surface and the salt beads are not as visible as the salt beads in other samples applied 6000 and 8000 taps.

After sintering and dissolution, the resulting salt-free samples obtained are shown in Figure 5.19 and Figure 5.20. Samples made with < 7000 taps are likely to contain voids or broken struts in the middle, edge, or surface areas (Figure 5.19 and Figure 5.20 shown by red lines). From the broken structure, linked pores are clear (dark spots). Rigid structures can be produced by applying 8000 to 10000 taps (Figure 5.20 e and f) and the pores of structure are clearer shaped with denser surrounding struts.

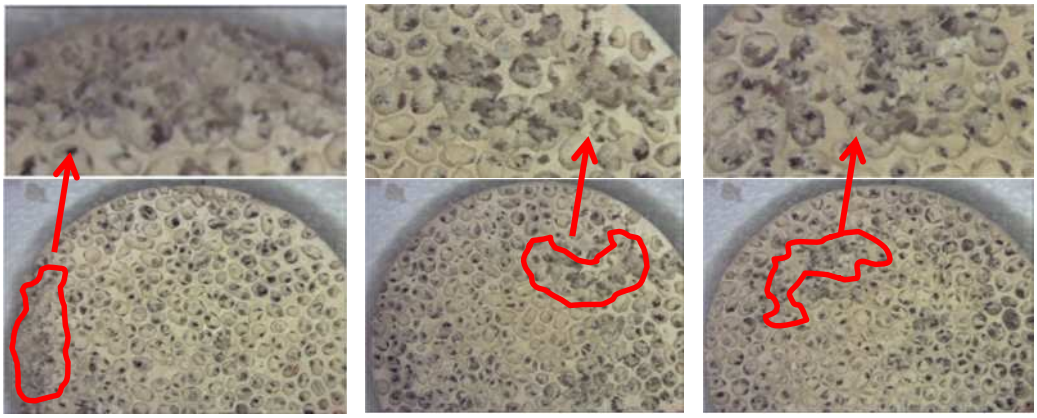

(a) (b) (c)

Figure 5.19: Some porous PEEK samples showing defects due to the lack of sufficient tapping. The red surrounding lines depict incomplete structures (broken struts) as a result of insufficient tapping process after (a) 4000, (b) 5000 and (c) 6000 cycles of tapping using 1.0 – 1.4 mm beads in the 6:1 ratio of the salt beads to the PEEK powder. The top images are the magnifications of the marked regions of the bottom images.

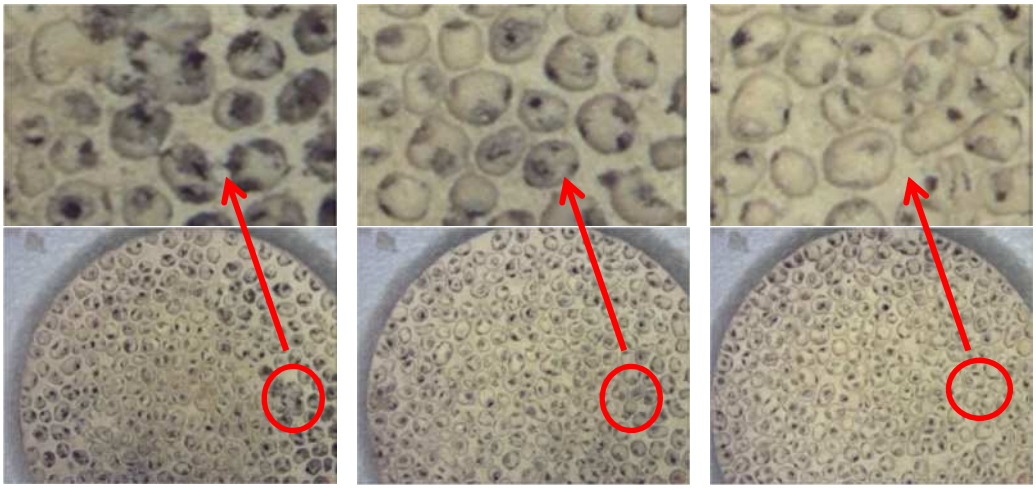

(a)7000 (b)8000 (c)10000

Figure 5.20: (a) A PEEK sample with broken struts made with 7000 cycles of tapping, and acceptable structures are obtained from the production applying (b) 8000 and (c) 10000 cycles of tapping using 1.0 – 1.4 mm beads in the 6:1 ratio of the salt beads to the PEEK powder. The top images are the magnifications of the marked regions of the bottom images.

5.3 Discussion

5.3.1 Particle packing

It was shown that for a 10/1 mass ratio there was insufficient PEEK added to fill all the inter-bead spaces. Experimental measurements (Table 4.3) showed the salt beads to have a packing fraction of 0.56, providing a void fraction of 0.44. Using PEEK (packing at a fraction of 0.32) to fill the salt bead gaps, the mixture could be depicted as in Figure 5.21. This idealised, maximum, packing fraction would be 0.70. From their packing volume and density, the "optimum" mass ratio can be estimated and is 5/1. Thus for all the ratios explored in this study, there should be insufficient PEEK.

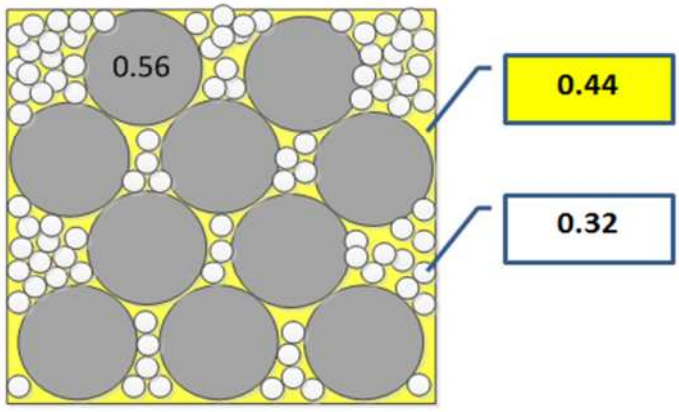

Figure 5.21: Illustration of packing fraction of salt beads and PEEK to meet an optimum composition.

An illustration of the packing condition is shown in Figure 5.22, assuming that the salt beads, grey objects, are fixed, while the PEEK quantity changes with the ratios. From the illustration, a 5/1 ratio should pack the PEEK into the salt bead gaps with 0 mm of PEEK on the surface, for the higher ratios, the level of

PEEK should reduce to lower levels in the salt bead bed (shown by black lines).

However, in practice, samples using 6/1 ratio (Figure 5.3a) still showed a thin layer of PEEK on the surface. This condition indicates that the PEEK packing fails to achieve the packing fraction for an "infinite" vessel owing to the constrictions of the shape and size of the spaces between the salt beads relative to the size of the PEEK powder. Assuming that the 6/1 ratio is optimum, (it was observed that higher ratios led to a noticeable increase in defects) and representing the fullest possible packing of PEEK between the salt beads (for the 1.0-1.4 mm bead size) the PEEK packing fraction is estimated to be 0.27.

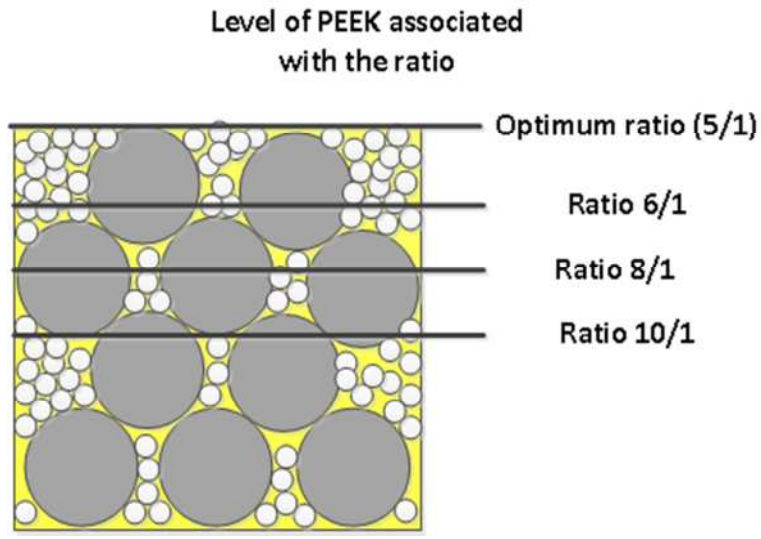

Figure 5.22: Illustration of mass ratio comparison using the same mass of salt beads and. The yellow regions show remaining voids in the packing.

According to [145], the 1.4 – 2.0 mm beads have a density of 1.61 $g.cm^{-3}$ and the 2.0 – 2.5 mm beads have a density of 1.57 $g.cm^{-3}$. The packing fractions for the 1.4 – 2.0 mm and 2.0 – 2.5 mm beads were close to 0.53 and lower than the packing fraction for the 1.0 – 1.4 mm (0.56). This observation agrees with

that of Zou (1995) [131] who saw that the packing fraction increases for a given vessel size as the particle size decreased, most likely due to a reduced influence of friction against the vessel walls, an effect also observed by Suzuki (2008) [131, 132].

The density for the salt bead/PEEK composite using the 1.4 – 2.0 mm and 2.0 – 2.5 mm beads can be estimated based on "perfect" packing of PEEK and are expected to be 1.04 and 1.02 $g.cm^{-3}$, respectively (shown in Table 5.4). The larger beads provide more void space after tapping and hence the optimum mass ratios for the 1.4 – 2.0 mm and 2.0 – 2.5 mm beads are 4.3/1 and 4.2/1, respectively (Table 5.4). This suggests the more completed filling for structures with large beads, albeit for a mass ratio of 6/1.

The model fits to spherical particles which is not the case in this thesis due to the rounded shape of the salt beads instead of being fully spherical. As a side not, the actual optimum packing would be different since not all PEEK was able to penetrate and fit the salt bead gaps perfectly and also, the salt beads are not fully spherical.

Table 5.4: Packing fractions and estimated densities for the salt beads, PEEK and their composite.

Estimated/material	PEEK	salt beads		
		1.0 - 1.4 mm	1.4 - 2.0 mm	2.0 - 2.5 mm
Packing fraction	0.32	0.56	0.53	0.53
Density ($g.cm^{-3}$)	1.30	1.65	1.61	1.57
Packing fraction of the composite-		0.70	0.68	0.68
Density of the composite($g.cm^{-3}$)		1.11	1.04	1.02
Optimum mass ratio of beads to the PEEK		5.0/1	4.3/1	4.2/1

It is also possible that the PEEK can be packed more efficiently into the larger spaces between larger particles. A simple illustration to show this is given in

Figure 5.23, where the gap between the salt beads for small (yellow) and big beads (green) are shown. Larger particles present fewer, larger inter-bead spaces. The size of these spaces controls the ability for the PEEK to pack in the contacting regions between the beads. The contact points between beads create inaccessible areas which increase as a fraction of the inter-bead size as the bead size decreases and as the powder size increases. Thus, for a fixed powder size, as is the case here, they will be able to make more efficient use of the inter-bead space for larger beads. It is worth noting that the size of the inaccessible region near the contact points will be what defines the size of the windows which interconnect the pores.

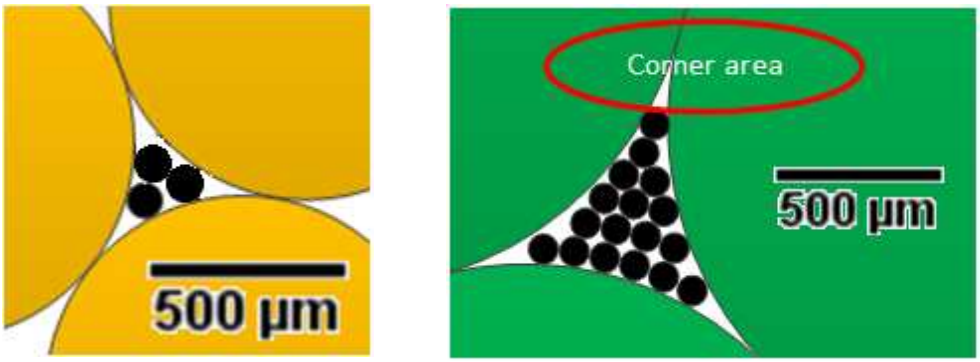

(a) small gap model (b) Big gap model

Figure 5.23: Illustration of the salt bead/PEEK packing for different bead sizes. Yellow, green and black circles are associated with (a) 1.0 – 1.4 mm beads and (b) 1.4 – 2.0 mm beads and PEEK particles as represented by yellow and green adjacent circles, respectively.

5.3.2 Particle migration

The rate of migration of the powder was influenced by the mass ratio and the salt bead size. The influence of different mass ratios on the number of taps required to reach the steady height (Figure 5.2) is principally due to the

different quantities of PEEK needed to be migrated. The more PEEK, the longer the time needed. With increasing bead size, not only does the void fraction increase slightly but we expect the size of the interconnecting channels to also increase.

A simple comparative model presenting three circle group sizes (1.0 - 1.4, 1.4 - 2.0 and 2.0 - 2.5 mm) is used to show the relationship between the salt bead size and the gap between them (Figure 5.24). The red circles fitting to the gap can be calculated either using simple geometry or ImageJ measurement. The diameters of circles fitting the gap are 216, 310 and 387 µm for circles of 1.4, 2.0 and 2.5 mm diameter, respectively. The simple model informs that larger beads will create a less restricted flow of fine particles trying to migrate through the gaps between them. This, in addition to lower packing fractions for larger beads (which pack less well into the same sized container [131]) leads to faster rates of PEEK permeation through beds of larger particles.

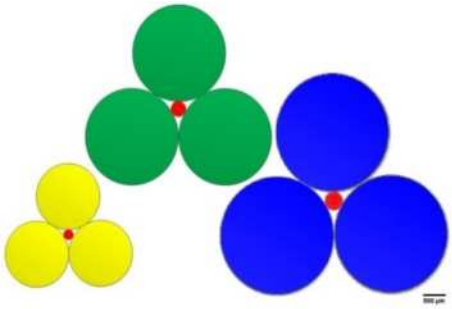

Figure 5.24: A circle model presenting 1.0 – 1.4 mm beads (yellow circles), 1.4 – 2.0 mm beads (green circles) and 2.0 – 2.5 mm beads (blue circles) with gap filled with small red circles.

It is well known that segregation or separation of different materials can be affected by vibration or tapping [141], which causes the smaller particles sift toward the bottom and the larger particles to rise to the top [139, 140]. More

detailed analysis of the process of particle migration when tapping fine powder through a bed of larger particles is, however, examined through the series of CT images in Figure 5.25. The images indicate that migration is not “plug” type flow with a horizontal migration front but that initial, rapid filling starts along and down the vessel walls (Figure 5.25a). It might be expected that this is due to lower packing densities in the wall regions. Although no such measurement was made to substantiate this in this study, it is expected that in the outer bead layers that packing, owing to the presence of the container wall, is poorer than in the central regions. The further percolation of the Ti powder can be speculated from void filling (in Figures 5.25b, c and d) where the flux of fine powder tends to be more strongly from the outside to the centre (at the base) and centre to the outside (at the top) than it does from the top to the base.

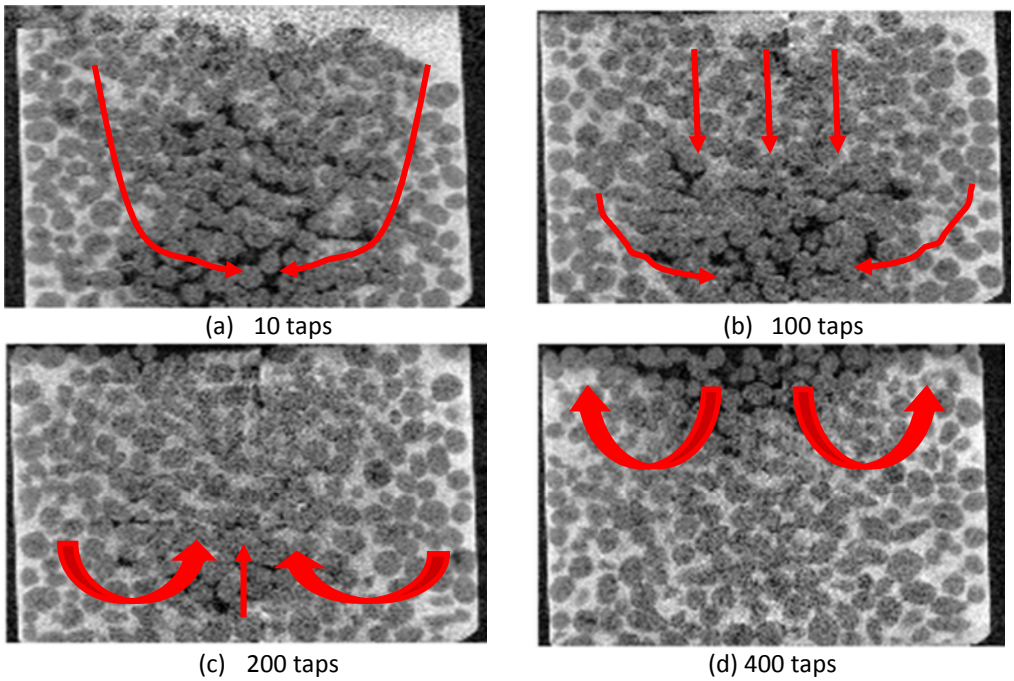

Figure 5.25: Cross sections showing powder migration after (a) 10 taps, (b) 100 taps, (d) 200 taps and (d) 400 taps. Red arrows present the tendency for Titanium migration (white objects) at different stages and salt beads are shown as rounded grey objects.

The convective nature of the flow is similar to the flow patterns predicted by Zhang (2001), Remond (2010) and Jain (2012) using the Discrete Element Method [137-139]. Their models showed that there is a circular motion of small particles during tapping [139] and this motion moves particles down the sides of the vessel and then up through the centre [143] which support to the estimated flow resulted in this thesis (Figure 5.25b and c). It shows that the strongest convection of powder from the outside to the inside tends to occur in the middle regions and the top rather than at the base. Despite rather speculative deductions about the flow from the CT images, the migration of the fine powder does seem to proceed in much the same way as predicted by DEM of similar processes. The effects are, however, expected to differ and be stronger for the much larger size differences used in this study.

5.3.3 Limitations of the tapping process

It has been seen that the tapping process can produce structures with the necessary features. Although it is a fairly simple process there are some limitations. These are highlighted below.

- The process in its current form is slow (215 cycles of tapping per minute based on the default machine set) and limited in production volume. There is a necessity to tap within a die and to tap for several thousand cycles.
- The porosity level is limited. Achieving good pore inter-connectivity requires the formation of a continuous network of beads. This can only be achieved in a narrow window of bead packing fraction. The quantity

of PEEK added must exceed (slightly) that required filling the network of voids.

- The filling process is not uniform from top to bottom and hence stopping the process before reaching the “steady state” is likely to produce defective samples with unfilled regions. A reduced number of taps cannot be used to increase the porosity in a “uniform” fashion. The tapping cycle must be completed to obtain a defect-free sample.
- There is a limit to the minimum pore size. The PEEK powder must be considerably smaller than the beads and the inter-bead spaces. As the size difference decreases, the rate of migration reduces, at some point the spaces will be too small to be filled efficiently with the PEEK powder. The use of finer PEEK can, in part, solve this problem but is likely to exhibit poor flow characteristics.
- The window size cannot be widely varied. The size of the windows connecting the pores is dictated by the packing of the PEEK into the spaces between the beads. This is a function of the sizes of the two particles and is not affected by processing.

Chapter 6: Integrating Porous PEEK Structures Into Injection Moulded Parts

This section aims to advance the technology for the use of porous PEEK in spinal applications (spinal cage). The investigation involves developing methods for integrating porous parts into supporting structures. The integrated parts were produced in order to be able to examine the potential for porous PEEK integration, to assess the strength of the resulting parts and to determine the feasibility of this route for the production of a spinal cage implant.

6.1 Processing methodology

The overall strategy was to prepare PEEK/NaCl "composite" inserts to be housed within the cavity of an injection moulding tool. Molten PEEK would then be over-moulded around the insert, using holes and partial dissolution of the salt within the insert to enhance the bonding between the insert and moulding. The details of the process are presented in the schematic in Figure 6.1. The key processes are described in the following section.

6.1.1 PEEK/NaCl "composite" insert preparation

The materials used were LT1 PEEK and 1.0 – 1.4 mm salt beads in the mass ratio of 6/1. The materials and their combination were examined in section 4 and it was shown that this could produce porosity higher than 80%, adequately meeting the requirement for cell growth [63, 95] and an acceptable pore size

range of 100 – 700 µm [1, 81] and pore window size at range of 70 – 150 µm [16, 28, 42]. The preparation process was explained in section 3.3.1.

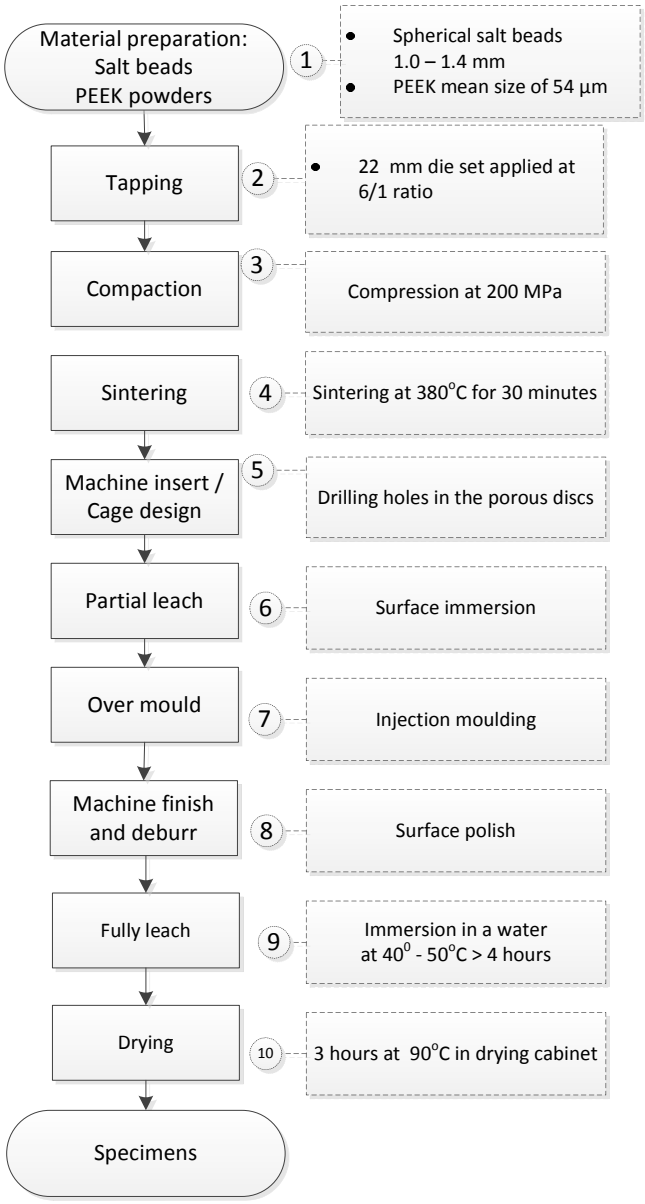

Figure 6.1: The fabrication process for the integrated porous PEEK parts.

Using similar processes to section 3.2.2.3, tapping was conducted using a 22 mm diameter die set applying 8000 taps. Due to the target disc thickness of 6 mm, the total mass of PEEK/salt beads composite was set at 5 g for the 22 mm

die along with compaction at 80 kN was applied after tapping, at a pressure of 200 MPa for the die. Sintering was performed as detailed in section 3.3.4.

In preparation for moulding, any excess PEEK on the sample surface was removed by grinding to give a final height of 6.00 mm. In order to provide shielding of the load to the porous PEEK sample, a number of through-holes were drilled into the PEEK/NaCl composites. The hole diameters were either 3.5 mm parallel holes or 6 mm tapered, countersunk holes and different numbers of holes were drilled in different samples. The countersunk holes were later to allow the molten PEEK to flow through the holes and turn into solid pillars as support. Examples of drilled inserts are shown in Figure 6.2.

Figure 6.2: 22mm diameter PEEK/NaCl composite samples with assorted drilled holes

To improve adhesion between the injection moulded PEEK and the insert, NaCl was partially removed from the surfaces of the inserts by brief insertion into water. An example of progressive salt removal, after 0, 2, 10 and 20 minutes in static water of 1 mm depth at room temperature is captured in

Figure 6.3. For the mouldings, the inserts were completely immersed in water at room temperature for 2 min with the target being to remove salt from at least one pore diameter from all surfaces.

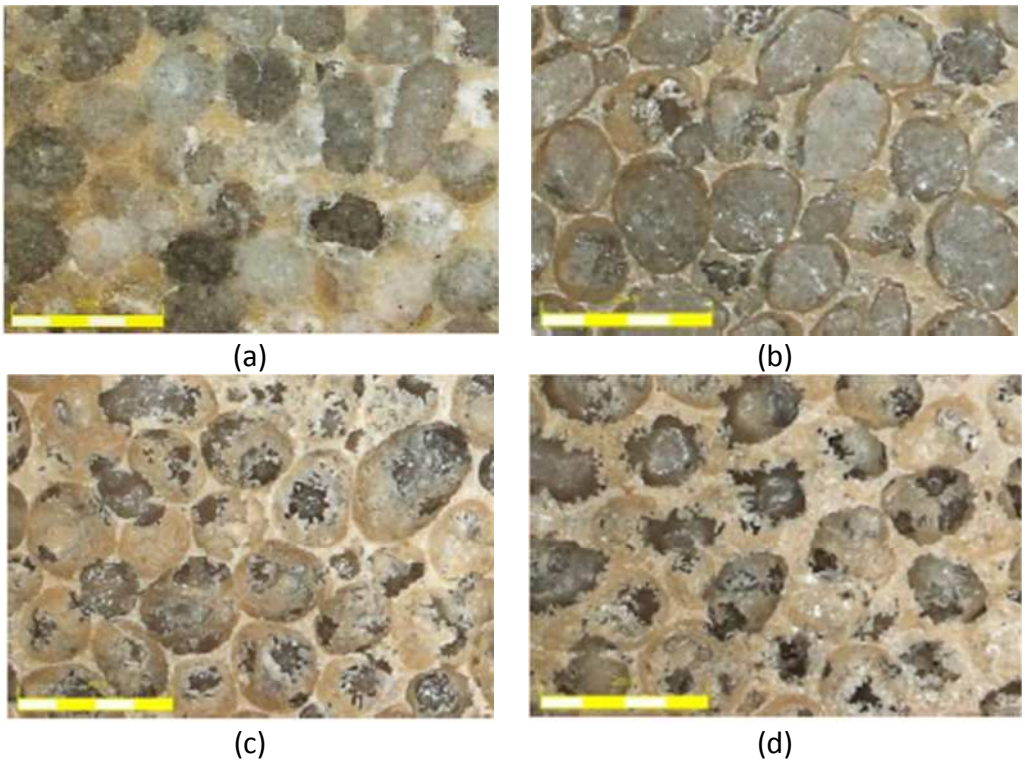

Figure 6.3: Images of (a) the structure prior to salt leaching, (b) 2 minute partial leaching, (c) 10 minute partial leaching and (d) 20 minute partial leaching (source: Invibio)

6.1.2 Moulding process

The moulding was performed using an Arburg injection moulding machine with constant injection temperature at 375 – 378^{o} C and injection pressure of 50 bar, performed at Smithers Rapra, Shawbury, UK.

The mould cavity was originally 52 x 52 x 10.5 mm and was used to make colour test plaques. This was modified using a close-fitting tool steel insert, 5.2 mm thick with a 22 mm diameter, 2 mm deep hole in the centre, placed on

the back face of the mould cavity in order to create a fixture for the PEEK composite inserts. The mould cavity is shown schematically in Figure 6.4. A "blank" moulding is shown in Figure 6.5 and the sprue and runner are labelled.

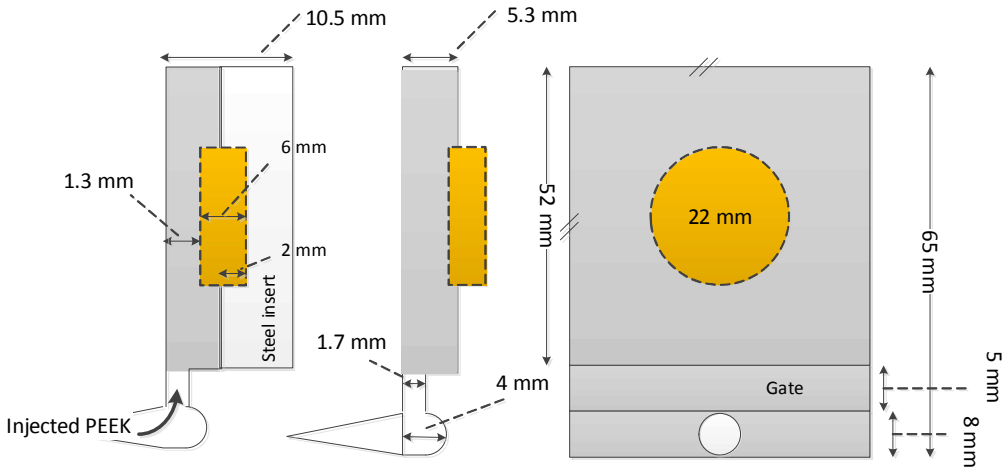

Figure 6.4: The schematic of mould cavity. The grey region presents the injected PEEK and the porous part is the orange region.

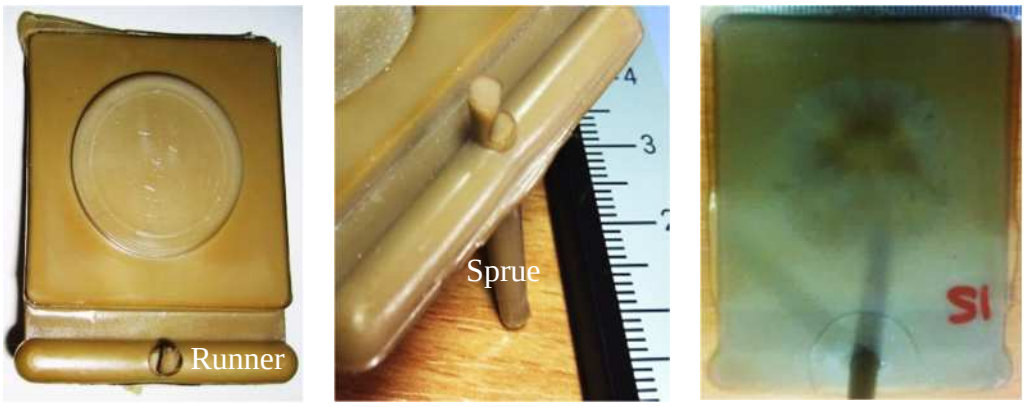

(a) (b) (c)

Figure 6.5: (a) A blank moulding showing the runner, (b)sprue, tab gate and (c) back of the moulding.

Inserts were preheated to 150^{o} C in an oven and transferred to the mould cavity. Figure 6.6 shows the injection moulder and a sample insert in the mould cavity. The depth of the hole to locate the insert meant that the insert

would protrude into the moulding by 4 mm and be encapsulated by a 1.3 mm PEEK layer below it.

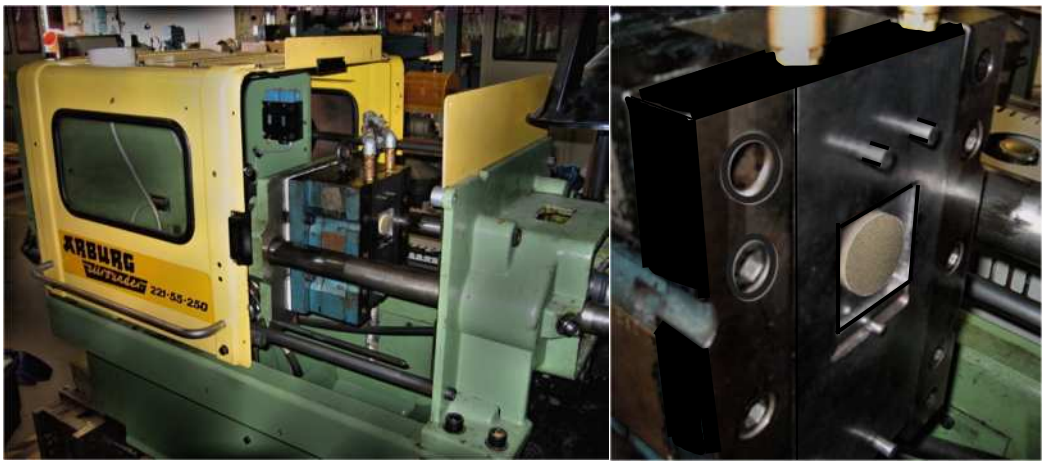

(a) (b)

Figure 6.6: (a) Moulding machine used to integrate the porous and solid part and (b) the mould cavity with PEEK/NaCl "composite" insert

6.1.3 Mouldings

Mouldings are shown in Figure 6.7 where it is shown that without dissolution of salt from the surface of the preform, adhesion between the moulding and the preform insert is poor and leads to falling out during ejection from the mould. Examples of successfully over-moulded parts are also presented in b) and c) this figure, where mere PEEK through the pre-drilled holes can be seen.

Figure 6.8 clearly shows the ingress of PEEK into the pre-drilled holes in the insert and also the infiltration of PEEK into the empty pores around these holes, created by the partial dissolution of the NaCl during the brief immersion in water. The penetration of the molten PEEK through the network of inter-connected porosity is apparent in Figure 6.9, after leaching of the NaCl. The infiltration direction can be seen from the shape of the PEEK front and there is

evidence of some compression of the empty pores as a result of the moulding pressure. It is clear that the ingress of PEEK into the porous surfaces of the insert will provide a mechanical "key" between the two components. It is obvious that the NaCl must remain in the bulk of the insert during moulding to ensure that the molten PEEK does not fill all the porosity, but the presence of the NaCl also preserves the pore geometry against the infiltration pressure.

(a) unsuccessful injected part (b) successful injected part

Figure 6.7: Examples of over-moulded inserts, a) without surface dissolution and b) with pre-drilled holes and pre-moulding surface dissolution.

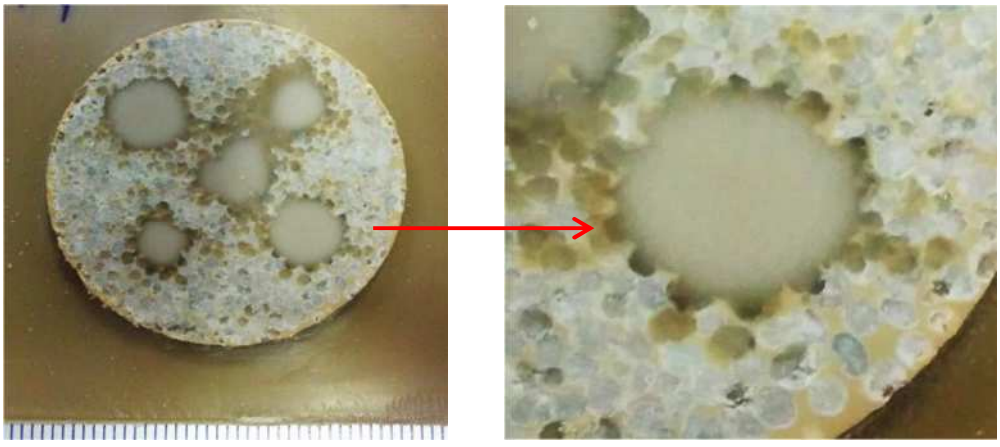

(a) (b)

Figure 6.8: (a) a moulded sample, after surface grinding, showing (b) the ingress of PEEK into the machined holes.

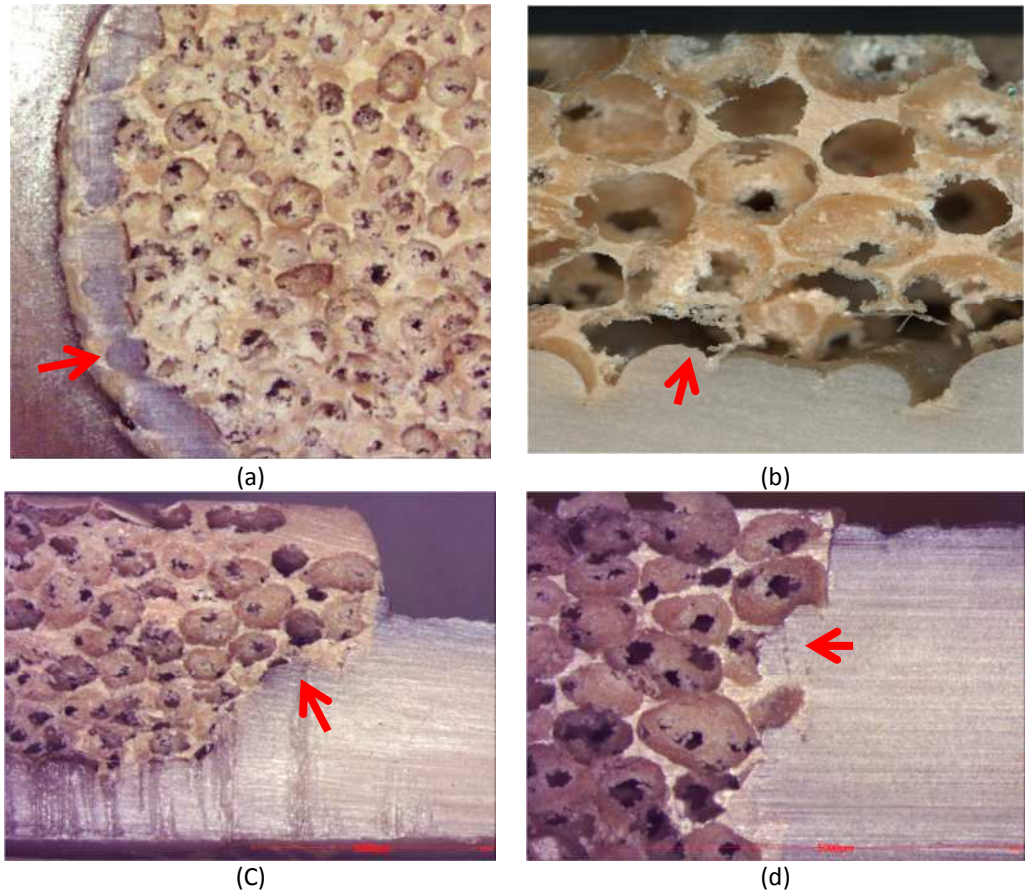

Figure 6.9: Cross-sections of PEEK disc after leaching showing (a) the injected PEEK infiltrating the porous sections from the top, (b) the cross-section of the middle region, (c) the cross-section of the porous-solid insert region and (d) the cross-section of the porous-solid non-insert region with the red arrows pointing the region of interest.

A small quantity of residual salt was detected post-leaching using SEM. The image in Figure 6.10 indicates that the ingress of PEEK into pores that have had NaCl partially removed from them can result in entrapment of residual salt. As this cannot be accessed by water, it is retained after leaching. As it is also unlikely to be removed in-service, so this entrapment might not be of concern.

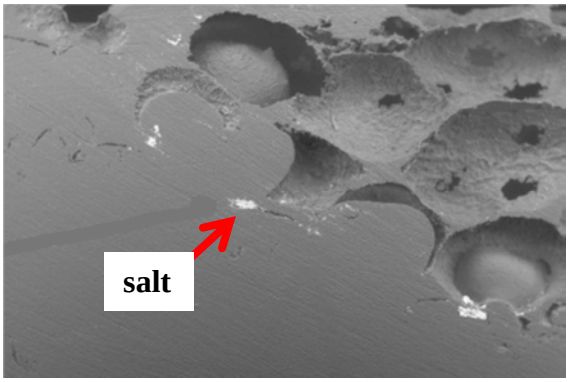

Figure 6.10: Entrapped salt caused by the ingress of PEEK into the porous surface

6.1.4 Compression testing of the mouldings

Injected moulded coupons with 22 mm inserts with 3.5 mm parallel drilled holes were prepared and are seen in Figure 6.11. To ensure parallel testing surfaces, the insert surfaces were ground flat, removing roughly 0.75 mm. All the salt was removed by immersion in water at 70^{o}C for 24 - 48 hours, followed by drying. Compressive testing was conducted on an Instron testing machine using twin LVDT's to accurately measure displacement. Samples were compressed at a speed of 0.6 mm/min. To ensure accurate pressing of the insert, a small cylindrical disc was placed on top of the insert (Figure 6.12a). The mechanical performance of the disc was characterised by the compressive yield strength and Young's modulus. The mechanical behaviour was also compared with a conventional porous disc, tapped using methods detailed in Chapter 3.

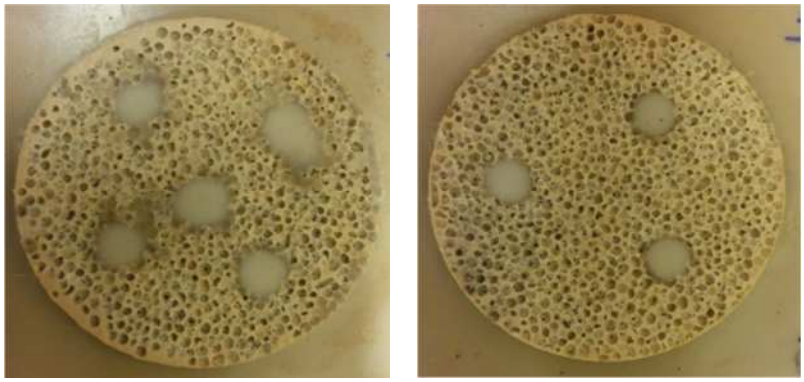

(a) 5 x 3.5 mm hole insert (b) 3 x 3.5 mm hole insert

Figure 6.11: Samples with 22 mm diameter porous inserts containing (a) 5 x 3.5 and (b) 3 x 3.5 mm holes filled with PEEK.

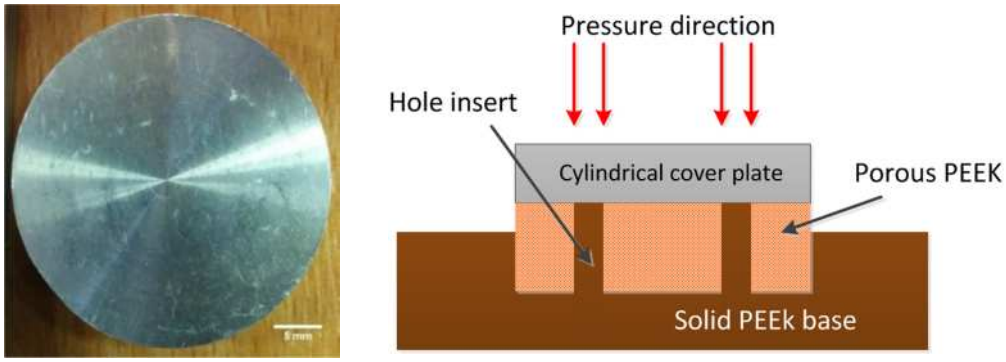

(a) Metal cylindrical plate for covering the top of tested specimen

(b) The disc and the covering base

Figure 6.12: (a) The cylindrical cover plate and (b) schematic of the porous-insert sample with a covering plate on the top surface used in compressive testing.

6.2 Mechanical behaviour

Figure 6.13 shows a typical stress-strain curve for a porous PEEK scaffold. It shows characteristic behaviour for a porous material, with a linear-elastic section to yield, a load drop and then a flat, plateau section before densification at high strain. Table 6.1 shows the average values for the mechanical properties for ≥ 7, 22 mm diameter samples, measuring a yield strength of 1.6 MPa and a Young's modulus of 40 MPa. This compares with 90 - 107 MPa

and 3.6 - 4.1 GPa for bulk PEEK [42, 72, 114, 115]. The strength and stiffness of the porous PEEK scaffold are very low compared with the bulk PEEK and compared with Evans' study [19] although scaffolds containing 67% porosity at top surface (Solid-porous PEEK with only 400 μm thick of porous layer at the top did not significantly decrease the strength of sample (8 mm in thickness and 16 mm in diameter) as measured at 71 MPa of the strength and 2.45 GPa of the Young modulus for the solid PEEK). It is understood that it is a problem to produce a high porosity part with good mechanical properties [23]. The low strength and stiffness are, of course due to the high porosity since they scale with relative density to the approximate power of 1.5 and 2, respectively [25] but also due to the tapping and sintering route and the weak struts that result from this [146]. The poor properties highlight the need to "shield" the porous component from the service load (typically lumbar stresses range from 0.3 – 2.3 MPa [113]).

Table 6.1: Mechanical property data for porous PEEK samples

Bead size (mm)	Elastic Modulus (MPa)	Compressive Yield (MPa)	Porosity (%)
1.0 - 1.4	40.12 $\pm$ 2.56	1.61 $\pm$ 0.19	82.75 $\pm$ 0.17

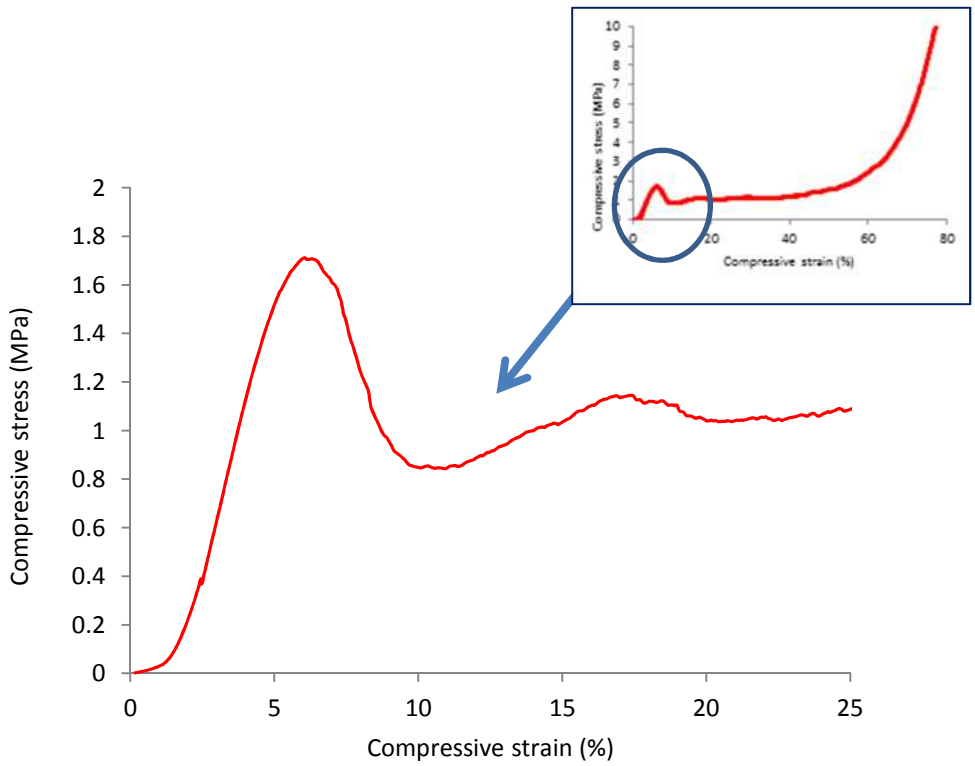

Figure 6.13: A typical compressive stress-strain curve for the PEEK scaffolds employing bead size range 1.0 – 1.4 mm for the first 25% of strain coupled with whole compressive-strain plot as an insert.

Stress-strain curves for inserts with filled holes which create "pillars" of PEEK are presented in Figure 6.14. They show clearly that the infiltrated holes greatly increase the effective compressive strength of the porous PEEK scaffolds, as it is these "pillars" which take the load. The compressive strength increases with the number of pillars, as the area of PEEK supporting the load increases. The effective stiffness of the porous insert increases in the same way. Adding 3.5 mm PEEK "pillars" increases the stiffness of the part from 40 to 255 and 374 MPa with 3 and 5 3.5 mm diameter pillars, respectively and the yield strength from 1.61 to 10.0 and 23.9 MPa for the 3 and 5 pillars, respectively. For both properties, the changes are tabulated in Table 6.2,

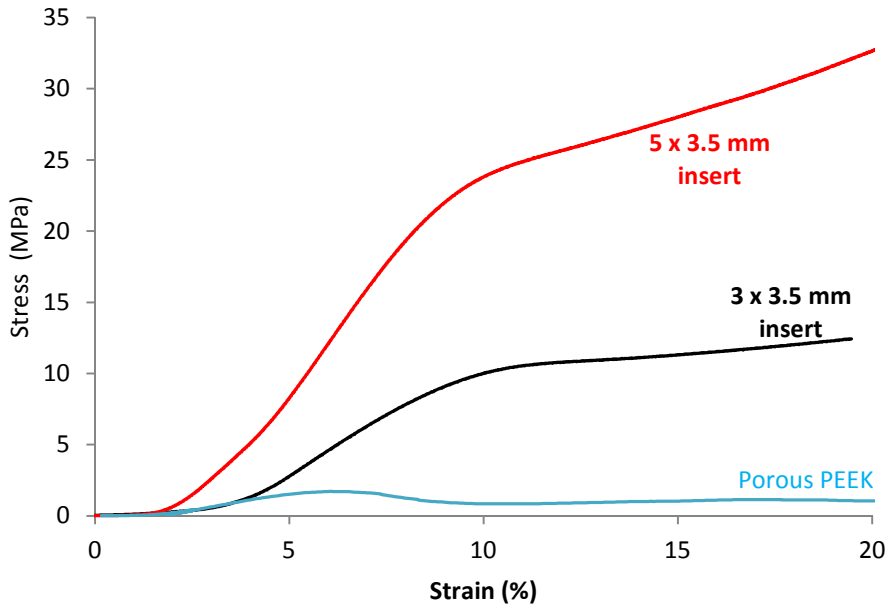

Figure 6.14 : Stress – strain curves for porous-solid PEEK parts. The red, black and blue dotted lines present parts with "pillars" of 5 x 3.5 mm, 3 x 3.5 mm and a porous part, respectively.

Table 6.2: Mechanical property data for the solid-porous part, porous and bulk PEEK

Porous-solid PEEK part	Modulus (MPa)	Yield (MPa)
3 x 3.5 mm insert (n = 1)	255	10.0
5 x 3.5 mm insert (n= 1)	374	23.9
Porous PEEK (n = 7)	40.12 $\pm$ 2.56	1.61 $\pm$ 0.19
Bulk PEEK [42, 72, 114, 115]	3 – 4 (GPa)	90 - 107

If it is assumed that the "pillars" are supporting all the applied load, the stress upon them at yield can be determined from the "global" yield stress and the ratio of the cross-sectional areas of the insert to the "pillars". The stiffness of the pillars can be estimated in the same way. These simple calculations reveal that the estimated stresses at global yield are 132 and 189 MPa, above those for yielding of PEEK and that the stiffness of the "pillars" are between roughly 3-

3.5 GPa. Despite inaccuracies in the exact diameter of the “pillars” this suggests that the transition to plastic deformation is dictated by yielding of the PEEK pillars rather than by buckling, a failure during the compression test, (which might be expected given their relatively low aspect ratio of < 1.5). This enables suitable geometries and the number of “pillars” to be designed for a particular application and the forces that go with it.

6.4 Case study: manufacture of a prototype hybrid porous PEEK-solid PEEK, spinal cage (Confidential)

PEEK/NaCl discs of 22 mm in diameter were manufactured at Nottingham and supplied to Invibio Ltd for them to make a demonstration part. 2 pieces per part were used in an injection moulding process (using the same principles of partial salt removal, mould inserts and over-moulding) to produce a prototype spinal cage with dimensions of 22 x 10 x 13 mm^3, shown in Figure 6.15. Post-moulding, and before removal of the salt, the saw-tooth fins were machined into the sample.

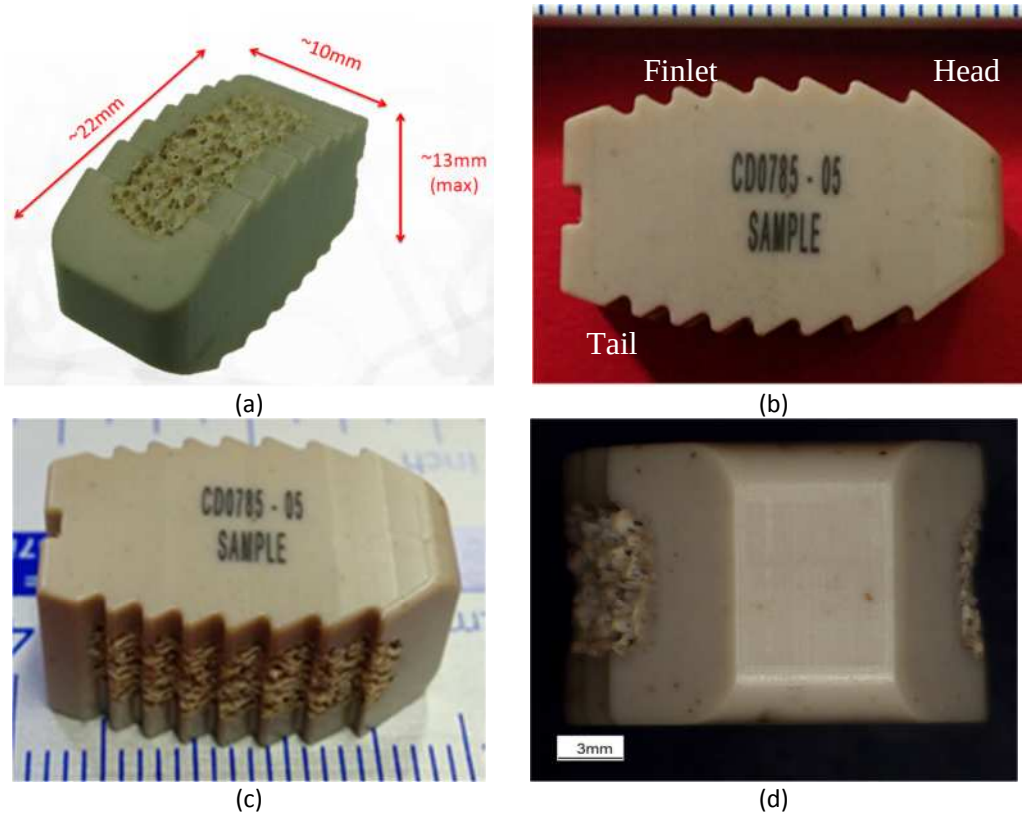

Figure 6.15: Prototype spinal cage employing porous and moulded PEEK showing (a) its dimension, (b) the lateral view, (c) the 60° angle view and (d) the head view.

The moulding technique successfully integrated the insert and moulded PEEK and the salt was able to be removed after machining to produce a hybrid part

containing both solid and porous PEEK sections. Figure 6.16a shows the porous part facing to the top and the red arrow points to adjacent sides of two inserts in the cage. Figures 6.16b-d show the outer surfaces of the insert and that molten PEEK has filled partially-cleared pores created by brief leaching.

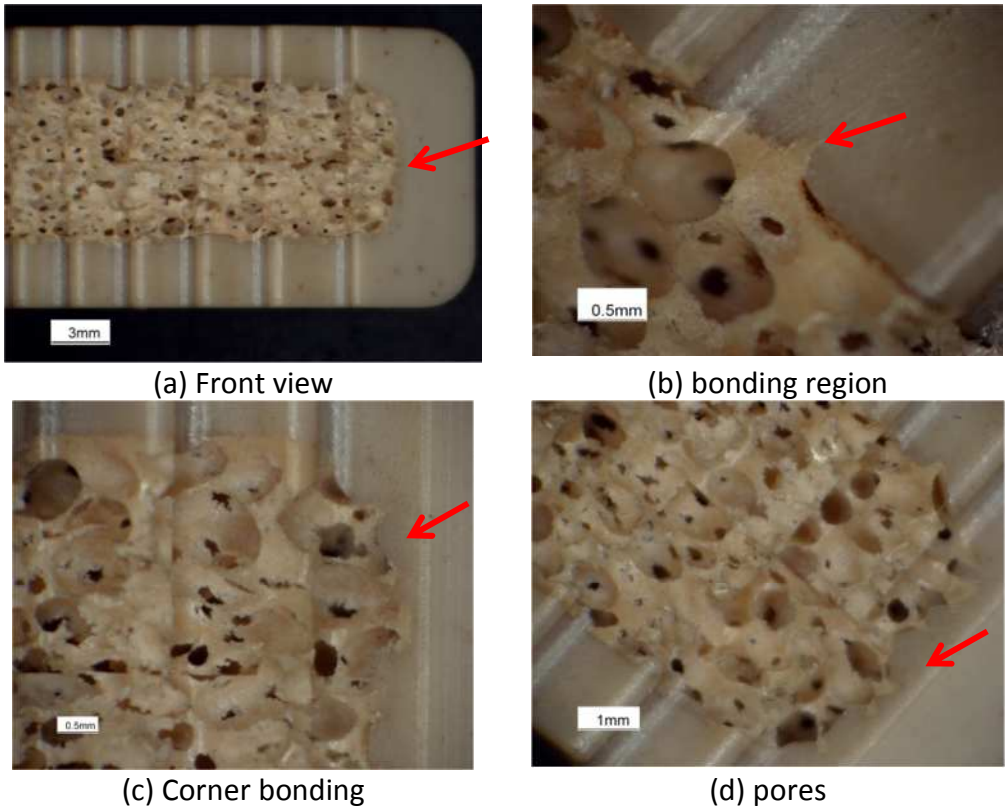

(a) Front view (b) bonding region

(c) Corner bonding (d) pores

Figure 6.16: Pores and bonding regions in the porous PEEK insert in a prototype spinal cage showing the (a) front view, (b) solid-porous PEEK bonding, (c) corner bonding and (d) the integrated porous discs in solid PEEK with the red arrows pointing border or bonding between porous and solid PEEK.

6.5 Summary

This section successfully demonstrates the capability to integrate porous and solid sections of PEEK via injection moulding. The use of partial leaching before moulding offers the possibility to lock the two components together, whilst retaining the pore structure in the original insert. Mechanical tests have

shown that porous PEEK structures are barely capable of supporting in-service loads but that they can be protected by suitable designs to ensure the applied load is borne by “pillars” of PEEK, within the porous insert.

Chapter 7: Conclusions and Future Work

This thesis reports the fabrication of porous Poly-Ether-Ether Ketone (PEEK) scaffolds using rounded sodium chloride (NaCl, salt) as a porogen. It introduces a novel fabrication technique resulting in porous PEEK scaffolds with acceptable structural characteristics that can be integrated into solid PEEK mouldings.

The objectives of the study were to:

- develop a new manufacturing technique, based on meeting the structural requirements and achieving good repeatability of the process and structure obtained
- understand the important processing factors which control the structural features and reproducibility for the processing method chosen.
- determine the potential for porous – solid PEEK integration using injection moulding with appropriate inserts and pre-treatments thereof.
- quantify the mechanical properties of porous PEEK scaffolds and integrated porous-solid PEEK parts produced by injection moulding.

Based on the findings and discussion, the conclusions of the study as follows, organised according to the objectives.

A new manufacturing technique based on meeting the structural requirements

- Porous PEEK scaffolds were fabricated via wet, dry and tapping mixing routes, producing their own unique structures based on the characteristics corresponding to the route of fabrication.
- In general, the structures contained porosity in the range between 70 to 87% (by comparing all samples), with rounded pores, dictated by the size of the salt beads used, but which were slightly elongated perpendicular to the compaction direction in the step used to consolidate the mixtures.
- Three types of PEEK were used, Vicote, LT1 and LT3, but despite their different sizes, they had little influence on the morphology of the porous structures, irrespective of the processing route used.
- The wet-mixing route coats the salt beads with PEEK powder. This led to porosities that were close to the target, uniform throughout the structure and from part-to-part. The coating, however, prevented bead-to-bead contact resulting in connectivity that was affected by dispersed, small porosity (< 150 μm) in the cell wall. This poor interconnectivity led to long salt removal times and would be unacceptable for cell migration.
- When dry-mixing it is difficult to achieve uniform mixing of the two components which have a very large size difference. Inhomogeneous mixing leads to PEEK-rich and salt-rich regions. As a result, the porosities were highly variable and deviated highly through the sample,

most likely due to the occurrence of high levels of trapped, residual salt. Pore interconnections were highly variable, owing to irregular mixing, which coupled with the high variability in porosity and high levels of residual make structures made in this way unacceptable for use in medical devices.

- The tapping route pre-establishes good and regular bead packing and bead-to-bead contact before the inter-bead spaces are filled with the fine PEEK powder. The porosity obtained is uniform and highly repeatable and pore interconnections are good, with relatively large "windows", (204 $\pm$ 41) µm, being developed between the pores, (560 $\pm$ 180) µm.
- The tapping route was the only technique one capable of producing porous structures that meet the key requirements, namely; a pore size suitable for bone in-growth; an even distribution of porosity through the structure; a high level of pore interconnectivity; a repeatable process with low deviation in porosity and a low level of residual salt (based on microCT scanning result),
- The tapping process, using LT1 PEEK, was further studied and developed as a novel route for the fabrication porous PEEK scaffolds.

Important processing factors which control the structural features

- For a fixed bead size, increasing the mass of PEEK (for bead to salt ratios of 10/1, 8/1 and 6/1) required longer tapping to produce a stable

condition and produced thicker layers of excess PEEK on top of the salt bead bed. For 1.0 – 1.4 mm diameter beads, the optimum ratio for no excess PEEK was estimated to be between 5/1 and 6/1. This optimum condition arises from the packing densities of the two components.

- For a constant mass ratio of 6/1 and different bead sizes (1.0 - 1.4 mm, 1.4 – 2.0 mm and 2.0 – 2.5 mm), reaching a steady height of the PEEK layer takes longer using small beads owing to both the smaller inter-bead spaces provided by smaller particles but also the less dense packing of large particles in a vessel of fixed size.
- The optimum mass ratio of salt beads to PEEK also differs for different sized particles (4.3/1 for the 1.4 – 2.0 mm and 4.2/1 for the 2.0 – 2.5 mm), with a more efficient filling of the larger inter-bead spaces and higher porosity for larger salt beads.
- Filling of the inter-bead spaces did not occur with a horizontal migration front. Instead, filling was observed to occur preferentially down the side walls of the vessel, following modelling predictions in the literature for segregation of different sized particles.
- The tapping process has some limitations namely; it is slow (depending on the tapping machine capability, the current machine requires 5 minutes per 1000 cycles of tapping, producing one good compacted sample of the 6:1 ratio of the salt beads to the PEEK of 5 g is restricted to 8000 taps), with the necessity to tap within a die for several thousand cycles; the porosity level is limited as it is defined by the dense random packing structure for the beads used; the filling process is not uniform from top to bottom and thus a reduced number of taps cannot be used to

increase the porosity in a “uniform” fashion; there is a limit to the minimum pore size as the PEEK powder must be considerably smaller than the beads whilst still exhibiting good flow characteristics and the window size cannot be widely varied as it is dictated by the packing of the PEEK into the spaces between the beads, a function of their sizes and not of processing.

The potential for porous – solid PEEK integration using injection moulding

- Salt / PEEK inserts manufactured by the tapping route can be integrated into injection moulded parts by supporting them within the mould cavity and over-moulding with molten PEEK. After integration, the salt is removed to produce a hybrid porous-solid PEEK part.
- Adhesion between the insert and the moulding is affected by partial leaching of the salt from the surface of the insert (see 6.1.3), to create 1 layer of pore (as a result of partial leaching prior to the moulding by leaching 1 mm sample surface about 2 minutes, see section 6.1.1), such that molten PEEK can infiltrate into these empty spaces and provide a mechanical interlock.
- Successful integration of porous PEEK structures into a generic prototype porous–solid PEEK spinal cage, shows evidence of the feasibility of this process to make hybrid medical devices.

Mechanical properties of porous PEEK scaffolds and integrated porous-solid PEEK parts produced by injection moulding.

- Porous PEEK discs, with 1.0 – 1.4 mm pores and a porosity of roughly (82.75 $\pm$ 0.17)% were compression tested and showed a Young's Modulus of (40.12 $\pm$ 2.56) MPa and a compressive yield stress of (1.61 $\pm$ 0.19 MPa. At these high porosities, the structure is barely capable of supporting typical lumbar loadings (a few MPa).
- Salt / PEEK inserts were prepared with pre-drilled holes which filled with solid PEEK during the moulding process, creating "pillars" to support the applied load and protect the porous surface. For a 22 mm diameter porous insert with 3 x 3.5 mm diameter pillars, the compressive strength increased from 1.6 to 10 MPa and the stiffness increased from 40 to 255 MPa.
- The strength and stiffness of the mouldings containing pillars were considerably contributed by the load-bearing areas of the solid PEEK pillars, enabling the appropriate design of the number and size of the pillars required to support the service load.

Future work

Due to the limitations of the study in terms of the equipment and materials available, future work can be directed to some other areas;

- The rate of production is restricted to the default tapping machine causing slow and limited production volumes due to the necessity to tap within a die and to tap for several thousand cycles. This could be addressed through a study looking at the effect of vibration frequency and amplitude on the filling rate of the PEEK powder. The effect of die diameter could also be investigated. The tapping assembly could also be modified into a matrix of cylindrical cavities to accommodate simultaneous production. In terms of the die dimensions; a lighter weight die set could be trialled in an effort to improve the rate of production (due to the limitation of the machine to only hold the load up to 900 g without affecting the tapping rate and could affect the production rate at the same time).
- The porosity level is limited and achieving good pore inter-connectivity requires the formation of a continuous network of beads in a condition of a narrow window of bead packing fraction. To enhance the bead packing fraction, the ratio of the bead size to the vessel size could be varied more widely to achieve more uniform packing.
- The filling process is not uniform from top to bottom and hence stopping the process before reaching the “steady state” is likely to produce defective samples with unfilled regions. Due to this drawback, future studies could investigate a new loading technique whereby the

salt beads and PEEK are mixed prior to tapping in an effort to reach a steady packing condition faster.

- There is a limit to the minimum pore size due to the salt bead size used and the flow rate of fine PEEK depends on the size of the inter-bead spaces. Changing the morphology of the PEEK to rounded might improve the flow rate even at lower particle sizes. Compounding the powder with an additive to increase the density might accelerate the migration too.
- The window size cannot be widely varied since it is dictated by the packing of the PEEK into the spaces between the beads as a function of the sizes of the two particles. Using a wider range of salt beads such as 0.5 – 1.4 mm or more beads with slightly flatter faces could increase the contact areas and the window size. Additionally, chemical methods to increase the window size, through the dissolution of the PEEK, could be applied**.**
- The effectiveness of bone in-growth remains to be determined as part of a wider series of future studies to look at the biological interactions with these structures.

References

1. Kurtz, S.M., ed. *PEEK biomaterial handbooks*. 2012, Elsevier.

2. Green, S. and J. Schlegel, *A polyaryletherketone biomaterial for use in medical implant applications.* Polym for the Med Ind Proc, Brussels, 2001: p. 14-15.

3. Toth, J.M., M. Wang, B.T. Estes, J.L. Scifert, H.B. Seim Iii, and A.S. Turner, *Polyetheretherketone as a biomaterial for spinal applications.* Biomaterials, 2006. **27**(3): p. 324-334.

4. Kersten, R.F.M.R., S.M. van Gaalen, A. de Gast, and F.C. Öner, *Polyetheretherketone (PEEK) cages in cervical applications: a systematic review.* The Spine Journal, 2015. 15(6): p. 1446-1460.

5. Yoo, M., W.-H. Kim, S.-J. Hyun, K.-J. Kim, T.-A. Jahng, and H.-J. Kim, *Comparison between Two Different Cervical Interbody Fusion Cages in One Level Stand-alone ACDF: Carbon Fiber Composite Frame Cage Versus Polyetheretherketone Cage.* Korean Journal of Spine, 2014. **11**(3): p. 127-135.

6. Galbusera, F., C.M. Bellini, F. Anasetti, C. Ciavarro, A. Lovi, and M. Brayda-Bruno, *Rigid and flexible spinal stabilization devices: A biomechanical comparison.* Medical Engineering & Physics, 2011. **33**(4): p. 490-496.

7. Kaech, D.L. and J.R. Jinkins, *The Intervertebral Disc Cage: Background, Theory and Specific Types.* Rivista di Neuroradiologia, 1999. **12**(1 suppl): p. 27-29.

8. Brantigan, J. and A. Steffee, *Carbon Fiber Implant to Aid Interbody Lumbar Fusion: 1-year Clinical Results in the First 26 Patients*, in *Lumbar Fusion and Stabilization*, K. Yonenobu, K. Ono, and Y. Takemitsu, Editors. 1993, Springer Japan. p. 379-395.

9. Cho, D.-Y., W.-R. Liau, W.-Y. Lee, J.-T. Liu, C.-L. Chiu, and P.-C. Sheu, *Preliminary Experience Using a Polyetheretherketone (PEEK) Cage in the Treatment of Cervical Disc Disease.* Neurosurgery, 2002. **51**(6): p. 1343-1350 10.1227/01.NEU.0000309109.71345.19.

10. Cho, D.-Y., W.-Y. Lee, and P.-C. Sheu, *Treatment of multilevel cervical fusion with cages.* Surgical Neurology, 2004. **62**(5): p. 378-385.

11. Mastronardi, L., A. Ducati, and L. Ferrante, *Anterior cervical fusion with polyetheretherketone (PEEK) cages in the treatment of degenerative disc disease. Preliminary observations in 36 consecutive cases with a minimum 12-month follow-up.* Acta Neurochir (Wien), 2006. **148**(3): p. 307-12; discussion 312.

12. Rousseau, M.A., J.Y. Lazennec, and G. Saillant, *Circumferential arthrodesis using PEEK cages at the lumbar spine.* J Spinal Disord Tech, 2007. **20**(4): p. 278-81.

13. Jiya, T., T. Smit, B.J. van Royen, and M. Mullender, *Posterior lumbar interbody fusion using non resorbable poly-ether-ether-ketone versus resorbable poly-l-lactide-co-d,l-lactide fusion devices. Clinical outcome at a minimum of 2-year follow-up.* European Spine Journal, 2011. **20**(4): p. 618-622.

14. Spruit, M., R.G. Falk, L. Beckmann, T. Steffen, and R.M. Castelein, *The in vitro stabilising effect of polyetheretherketone cages versus a titanium cage of similar design for anterior lumbar interbody fusion.* Eur Spine J, 2005. **14**(8): p. 752-8.

15. Roeder, R.K., S.M. Smith, T.L. Conrad, N.J. Yanchak, C.H. Merrill, and G.L. Converse, *Porous and bioactive PEEK implants for interbody spinal fusion.* Adv. Mater. Process, 2009. **167**(10): p. 46-48.

16. Jarman-Smith, M., M. Brady, S.M. Kurtz, N.M. Cordaro, and W.R. Walsh, *Chapter 12 - Porosity in Polyaryletheretherketone*, in *PEEK Biomaterials Handbook.* 2012, William Andrew Publishing: Oxford. p. 181-199.

17. Vaezi, M. and S.F. Yang, *A novel bioactive PEEK/HA composite with controlled 3D interconnected HA network.* International Journal of Bioprinting, 2015. **1**: p. 66-76.

18. Wang, H., S. Zhang, G. Wang, S. Yang, and Y. Zhu, *Tribological behaviors of hierarchical porous PEEK composites with mesoporous titanium oxide whisker.* Wear, 2013. **297**(1–2): p. 736-741.

19. Evans, N.T., F.B. Torstrick, C.S.D. Lee, K.M. Dupont, D.L. Safranski, W.A. Chang, A.E. Macedo, A.S.P. Lin, J.M. Boothby, D.C. Whittingslow, R.A. Carson, R.E. Guldberg, and K. Gall, *High-strength, surface-porous polyether-ether-ketone for load-bearing orthopedic implants.* Acta Biomaterialia, 2015. **13**(0): p. 159-167.

20. Tan, K.H., C.K. Chua, K.F. Leong, M.W. Naing, and C.M. Cheah, *Fabrication and characterization of three-dimensional poly(ether-ether-ketone)/-hydroxyapatite biocomposite scaffolds using laser sintering.* Proceedings of the Institution of Mechanical Engineers, Part H: Journal of Engineering in Medicine, 2005. **219**(3): p. 183-194.

21. Abu Bakar, M.S., M.H.W. Cheng, S.M. Tang, S.C. Yu, K. Liao, C.T. Tan, K.A. Khor, and P. Cheang, *Tensile properties, tension–tension fatigue and biological response of polyetheretherketone–hydroxyapatite composites for load-bearing orthopedic implants.* Biomaterials, 2003. **24**(13): p. 2245-2250.

22. Roderic, S.L., *Composite Biomaterials*, in *Biomaterials*. 2002, CRC Press. p. 79-93.

23. O'Brien, F.J., *Biomaterials & scaffolds for tissue engineering.* Materials Today, 2011. **14**(3): p. 88-95.

24. Matassi, F., L. Nistri, D. Chicon Paez, and M. Innocenti, *New biomaterials for bone regeneration.* Clinical Cases in Mineral and Bone Metabolism, 2011. **8**(1): p. 21-24.

25. M. F. Ashby, A.G.E., N. A. Fleck, L. J. Gibson, J. W. Hutchinson, and H. N. G. Wadley, *Metal Foams: A Design Guide*. 2000, Boston, Mass, USA: Butterworth Heinemann.

26. Liu, X. and P. Ma, *Polymeric Scaffolds for Bone Tissue Engineering.* Annals of Biomedical Engineering, 2004. **32**(3): p. 477-486.

27. Ma, P.X., *Scaffolds for tissue fabrication.* Materials Today, 2004. **7**(5): p. 30-40.

28. Mattiason, B., A. Kumar, and I.Y. Galaev, eds. *Macroporous polymers*. ed. p.p.a.b.b. applications. 2010, CRC press.

29. Tan, K.H., C.K. Chua, K.F. Leong, C.M. Cheah, P. Cheang, M.S. Abu Bakar, and S.W. Cha, *Scaffold development using selective laser sintering of polyetheretherketone–hydroxyapatite biocomposite blends.* Biomaterials, 2003. **24**(18): p. 3115-3123.

30. Schmidt, M., D. Pohle, and T. Rechtenwald, *Selective Laser Sintering of PEEK.* CIRP Annals - Manufacturing Technology, 2007. **56**(1): p. 205-208.

31. Wang, L., L. Weng, S. Song, Z. Zhang, S. Tian, and R. Ma, *Characterization of polyetheretherketone–hydroxyapatite nanocomposite materials.* Materials Science and Engineering: A, 2011. **528**(10–11): p. 3689-3696.

32. Landy, B.C., S.B. Vangordon, P.S. McFetridge, V.I. Sikavitsas, and M. Jarman-Smith, *Mechanical and in vitro investigation of a porous PEEK foam for medical device implants.* J Appl Biomater Funct Mater, 2013. **11**(1): p. e35-44.

33. Werner, P., R. Verdejo, F. Wöllecke, V. Altstädt, J.K.W. Sandler, and M.S.P. Shaffer, *Carbon Nanofibers Allow Foaming of Semicrystalline Poly(ether ether ketone).* Advanced Materials, 2005. **17**(23): p. 2864-2869.

34. Mikos, A.G., A.J. Thorsen, L.A. Czerwonka, Y. Bao, R. Langer, D.N. Winslow, and J.P. Vacanti, *Preparation and characterization of poly(l-lactic acid) foams.* Polymer, 1994. **35**(5): p. 1068-1077.

35. Zhang, J., L. Wu, D. Jing, and J. Ding, *A comparative study of porous scaffolds with cubic and spherical macropores.* Polymer, 2005. **46**(13): p. 4979-4985.

36. Silva, M.M.C.G., L.A. Cyster, J.J.A. Barry, X.B. Yang, R.O.C. Oreffo, D.M. Grant, C.A. Scotchford, S.M. Howdle, K.M. Shakesheff, and F.R.A.J. Rose, *The effect of anisotropic architecture on cell and tissue infiltration into tissue engineering scaffolds.* Biomaterials, 2006. **27**(35): p. 5909-5917.

37. Gross, K.A. and L.M. Rodríguez-Lorenzo, *Biodegradable composite scaffolds with an interconnected spherical network for bone tissue engineering.* Biomaterials, 2004. **25**(20): p. 4955-4962.

38. Kramschuster, A. and L.-S. Turng, *An injection molding process for manufacturing highly porous and interconnected biodegradable polymer matrices for use as tissue engineering scaffolds.* Journal of Biomedical Materials Research Part B: Applied Biomaterials, 2010. **92B**(2): p. 366-376.

39. Mi, H.-Y., X. Jing, and L.-S. Turng, *Fabrication of porous synthetic polymer scaffolds for tissue engineering.* Journal of Cellular Plastics, 2015. **51**(2): p. 165-196.

40. Jinnapat, A. and A. Kennedy, *The manufacture of spherical salt beads and their use as dissolvable templates for the production of cellular solids via a powder metallurgy route.* Jounal of Alloys and Compounds, 2010. **499**: p. 43-47.

41. Davis, J.R., ed. *Handbook of Materials for medical devices*. 2003, ASM International.

42. Kurtz, S.M. and J.N. Devine, *PEEK biomaterials in trauma, orthopedic, and spinal implants.* Biomaterials, 2007. **28**(32): p. 4845-4869.

43. Davis, W., A.K. Allouni, K. Mankad, D. Prezzi, T. Elias, J. Rankine, and I. Davagnanam, *Modern spinal instrumentation. Part 1: Normal spinal implants.* Clinical Radiology, 2013. **68**(1): p. 64-74.

44. Gunzburg, R. and M. Szpalski, *Surgical Procedures: Cages, Prostheses, and Instrumentation*, in *Spinal Imaging*, J.M. Van Goethem, L. van den Hauwe, and P. Parizel, Editors. 2007, Springer Berlin Heidelberg. p. 391-396.

45. Kurtz, S.M. and A.A. Edidin, *Spine Technology Handbook*. 2006: Elsevier Inc.

46. Porto, I.C.C.d.M., *Polymer Biocompatibility*. Polymerization. 2012.

47. Joon, B.P. and K. Young Kon, *Metallic Biomaterials*, in *Biomaterials*. 2002, CRC Press. p. 1-20.

48. Romano, J.J., N.T. Iliff, and P.N. Manson, *Use of medpor porous polyethylene*. Craniofac. Surg., 1993. **4**(3): p. 142-147.

49. Kurtz, S.M., *Chapter 13 - Applications of Polyaryletheretherketone in Spinal Implants: Fusion and Motion Preservation*, in *PEEK Biomaterials Handbook*. 2012, William Andrew Publishing: Oxford. p. 201-220.

50. Kurtz, S.M., *Chapter 1 - An Overview of PEEK Biomaterials*, in *PEEK Biomaterials Handbook*. 2012, William Andrew Publishing: Oxford. p. 1-7.

51. Fink, J.K., *Handbook of Engineering and specialty Thermoplastics*. 2010: Wiley. 383.

52. Sastri, V.R., *Plastics in medical devices*. Properties, requirements, and applications. 2010: Elsevier.

53. Attwood, T., P.C. Dawson, J.L. Freeman, L.R. Hog, J.B. Rose, and P.A. Staniland, *Synthesis and properties of polyaryletherketones.* Polymer, 1981. **22**.

54. Chanda, M. and S.K. Roy, *Industrial Polymers, Specialty Polymers, and Their Applications*. 2009: CRC Press.

55. Zhao, M., M. An, Q. Wang, X. Liu, W. Lai, X. Zhao, S. Wei, and J. Ji, *Quantitative proteomic analysis of human osteoblast-like MG-63 cells in response to bioinert implant material titanium and polyetheretherketone.* Journal of Proteomics, 2012. **75**(12): p. 3560-3573.

56. Brantigan, J.W., A.D. Steffee, and J.M. Geiger, *A carbon fiber implant to aid interbody lumbar fusion. Mechanical testing.* Spine (Phila Pa 1976), 1991. **16**(6 Suppl): p. S277-82.

57. Brantigan, J.W., P.C. McAfee, B.W. Cunningham, H. Wang, and C.M. Orbegoso, *Interbody lumbar fusion using a carbon fiber cage implant versus allograft bone. An investigational study in the Spanish goat.* Spine (Phila Pa 1976), 1994. **19**(13): p. 1436-44.

58. Cho, D.Y., W.Y. Lee, P.C. Sheu, and C.C. Chen, *Cage containing a biphasic calcium phosphate ceramic (Triosite) for the treatment of cervical spondylosis.* Surg Neurol, 2005. **63**(6): p. 497-503; discussion 503-4.

59. Toth, J.M., *Chapter 7 - Biocompatibility of Polyaryletheretherketone Polymers*, in *PEEK Biomaterials Handbook*. 2012, William Andrew Publishing: Oxford. p. 81-92.

60. Sekerci, Z., A. Ugur, R. Ergun, and M. Sanli, *Early changes in the cervical foraminal area after anterior interbody fusion with polyetheretherketone (PEEK) cage containing synthetic bone particulate: a prospective study of 20 cases.* Neurol Res, 2006. **28**(5): p. 568-71.

61. Ferguson, S.J., J.M. Visser, and A. Polikeit, *The long-term mechanical integrity of non-reinforced PEEK-OPTIMA polymer for demanding spinal applications: experimental and finite-element analysis.* Eur Spine J, 2006. **15**(2): p. 149-56.

62. Kulkarni, A.G., H.T. Hee, and H.K. Wong, *Solis cage (PEEK) for anterior cervical fusion: preliminary radiological results with emphasis on fusion and subsidence.* Spine J, 2007. **7**(2): p. 205-9.

63. Rao, P.J., M.H. Pelletier, W.R. Walsh, and R.J. Mobbs, *Spine Interbody Implants: Material Selection and Modification, Functionalization and Bioactivation of Surfaces to Improve Osseointegration.* Orthopaedic Surgery, 2014. **6**(2): p. 81-89.

64. Converse, G.L., T.L. Conrad, C.H. Merrill, and R.K. Roeder, *Hydroxyapatite whisker-reinforced polyetherketoneketone bone ingrowth scaffolds.* Acta Biomaterialia, 2010. **6**(3): p. 856-863.

65. Stevens, M.M., *Biomaterials for bone tissue engineering.* Materials Today, 2008. **11**(5): p. 18-25.

66. Kang, H., C.-Y. Lin, and S. Hollister, *Topology optimization of three dimensional tissue engineering scaffold architectures for prescribed bulk modulus and diffusivity.* Structural and Multidisciplinary Optimization, 2010. **42**(4): p. 633-644.

67. Lin, C.Y., N. Kikuchi, and S.J. Hollister, *A novel method for biomaterial scaffold internal architecture design to match bone elastic properties with desired porosity.* Journal of Biomechanics, 2004. **37**(5): p. 623-636.

68. Su, X.-b., Y.-q. Yang, P. Yu, and J.-f. Sun, *Development of porous medical implant scaffolds via laser additive manufacturing.* Transactions of Nonferrous Metals Society of China, 2012. **22, Supplement 1**(0): p. s181-s187.

69. Torres, F.G., S.N. Nazhat, S.H. Sheikh Md Fadzullah, V. Maquet, and A.R. Boccaccini, *Mechanical properties and bioactivity of porous PLGA/TiO2 nanoparticle-filled composites for tissue engineering scaffolds.* Composites Science and Technology, 2007. **67**(6): p. 1139-1147.

70. DiRienzo, A.L., C.M. Yakacki, M. Frensemeier, A.S. Schneider, D.L. Safranski, A.J. Hoyt, and C.P. Frick, *Porous poly(para-phenylene) scaffolds for load-bearing orthopedic applications.* Journal of the Mechanical Behavior of Biomedical Materials, 2014. **30**(0): p. 347-357.

71. Jaekel, D.J., D.W. MacDonald, and S.M. Kurtz, *Characterization of PEEK biomaterials using the small punch test.* Journal of the Mechanical Behavior of Biomedical Materials, 2011. **4**(7): p. 1275-1282.

72. Rae, P.J., E.N. Brown, and E.B. Orler, *The mechanical properties of poly(ether-ether-ketone) (PEEK) with emphasis on the large compressive strain response.* Polymer, 2007. **48**(2): p. 598-615.

73. Edwards, S.L. and J.A. Werkmeister, *Mechanical evaluation and cell response of woven polyetheretherketone scaffolds.* Journal of Biomedical Materials Research Part A, 2012: p. n/a-n/a.

74. Gibson, L.J. and M.F. Ashby, *Cellular Solids: Structure and Properties*. 1999: Cambridge University Press.

75. Chan, B.P. and K.W. Leong, *Scaffolding in tissue engineering: general approaches and tissue-specific considerations.* European Spine Journal, 2008. **17**(Suppl 4): p. 467-479.

76. Loh, Q.L. and C. Choong, *Three-dimensional scaffolds for tissue engineering applications: Role of porosity and pore size.* Tissue Engineering Part B: Reviews, 2013. **19**(6): p. 485-502.

77. Ramay, H.R. and M. Zhang, *Preparation of porous hydroxyapatite scaffolds by combination of the gel-casting and polymer sponge methods.* Biomaterials, 2003. **24**(19): p. 3293-3302.

78. Hollister, S.J., *Scaffold Design and Manufacturing: From Concept to Clinic.* Advanced Materials, 2009. **21**(32-33): p. 3330-3342.

79. Puppi, D., F. Chiellini, A.M. Piras, and E. Chiellini, *Polymeric materials for bone and cartilage repair.* Progress in Polymer Science, 2010. **35**(4): p. 403-440.

80. Velasco, M.A., Narv, #xe1, C.A. ez-Tovar, Garz, #xf3, and D.A. n-Alvarado, *Design, Materials, and Mechanobiology of Biodegradable Scaffolds for Bone Tissue Engineering.* BioMed Research International, 2015. **2015**: p. 21.

81. Jones, J.R., G. Poologasundarampillai, R.C. Atwood, D. Bernard, and P.D. Lee, *Non-destructive quantitative 3D analysis for the optimisation of tissue scaffolds.* Biomaterials, 2007. **28**(7): p. 1404-1413.

82. Zeltinger, J., J.K. Sherwood, D.A. Graham, R. Mueller, and L.G. Griffith, *Effect of pore size and void fraction on cellular adhesion, proliferation, and matrix deposition.* Tissue Eng, 2001. **7**(5): p. 557-72.

83. Clemow, A.J.T., A.M. Weinstein, J.J. Klawitter, J. Koeneman, and J. Anderson, *Interface mechanics of porous titanium implants.* Journal of Biomedical Materials Research, 1981. **15**(1): p. 73-82.

84. Tsuruga, E., H. Takita, H. Itoh, Y. Wakisaka, and Y. Kuboki, *Pore Size of Porous Hydroxyapatite as the Cell-Substratum Controls BMP-Induced Osteogenesis.* Journal of Biochemistry, 1997. **121**(2): p. 317-324.

85. Murphy, C.M., M.G. Haugh, and F.J. O'Brien, *The effect of mean pore size on cell attachment, proliferation and migration in collagen–glycosaminoglycan scaffolds for bone tissue engineering.* Biomaterials, 2010. **31**(3): p. 461-466.

86. Bobyn, J.D., R.M. Pilliar, H.U. Cameron, and G.C. Weatherly, *The optimum pore size for the fixation of porous-surfaced metal implants by the ingrowth of bone.* Clin Orthop Relat Res, 1980(150): p. 263-70.

87. Bobyn, J.D., G.J. Stackpool, S.A. Hacking, M. Tanzer, and J.J. Krygier, *Characteristics of bone ingrowth and interface mechanics of a new porous tantalum biomaterial.* J Bone Joint Surg Br, 1999. **81**(5): p. 907-14.

88. Cook, S.D., R.L. Barrack, K.A. Thomas, and R.J. Haddad, Jr., *Tissue growth into porous primary and revision femoral stems.* J Arthroplasty, 1991. **6 Suppl**: p. S37-46.

89. Yoon, J.J. and T.G. Park, *Degradation behaviors of biodegradable macroporous scaffolds prepared by gas foaming of effervescent salts.* Journal of Biomedical Materials Research, 2001. **55**(3): p. 401-408.

90. Laurencin, C.L. and L.S. Nair, *Nanotechnology and tissue engineering*. The scaffold. 2008: CRS Press.

91. Lee, J.-S., H.D. Cha, J.-H. Shim, J.W. Jung, J.Y. Kim, and D.-W. Cho, *Effect of pore architecture and stacking direction on mechanical properties of solid freeform fabrication-based scaffold for bone tissue engineering.* Journal of Biomedical Materials Research Part A, 2012. **100A**(7): p. 1846-1853.

92. Ryan, G., A. Pandit, and D.P. Apatsidis, *Fabrication methods of porous metals for use in orthopaedic applications.* Biomaterials, 2006. **27**(13): p. 2651-2670.

93. Conley Wake, M., A.G. Mikos, G. Sarakinos, J.P. Vacanti, and R. Langer, *Dynamics of fibrovascular tissue ingrowth in hydrogel foams.* Cell Transplantation, 1995. **4**(3): p. 275-279.

94. Conrad, T.L., D.J. Jaekel, S.M. Kurtz, and R.K. Roeder, *Effects of the mold temperature on the mechanical properties and crystallinity of hydroxyapatite whisker-reinforced polyetheretherketone scaffolds.* J Biomed Mater Res B Appl Biomater, 2013. **101**(4): p. 576-83.

95. Sinclair, S.K., G.J. Konz, J.M. Dawson, R.T. Epperson, and R.D. Bloebaum, *Host bone response to polyetheretherketone versus porous tantalum implants for cervical spinal fusion in a goat model.* Spine (Phila Pa 1976), 2012. **37**(10): p. E571-80.

96. Jones, A.C., C.H. Arns, A.P. Sheppard, D.W. Hutmacher, B.K. Milthorpe, and M.A. Knackstedt, *Assessment of bone ingrowth into*

porous biomaterials using MICRO-CT. Biomaterials, 2007. **28**(15): p. 2491-2504.

97. Jones, A.C., A. Sakellariou, A. Limaye, C.H. Arns, T.J. Senden, T. Sawkins, M.A. Knackstedt, D. Rohner, D.W. Hutmacher, A. Brandwood, and B.K. Milthorpe, *Investigation of microstructural features in regenerating bone using micro computed tomography.* Journal of Materials Science: Materials in Medicine, 2004. **15**(4): p. 529-532.

98. Bouxsein, M.L., S.K. Boyd, B.A. Christiansen, R.E. Guldberg, K.J. Jepsen, and R. Müller, *Guidelines for assessment of bone microstructure in rodents using micro–computed tomography.* Journal of Bone and Mineral Research, 2010. **25**(7): p. 1468-1486.

99. Goldstein, S.A., R. Goulet, and D. McCubbrey, *Measurement and significance of three-dimensional architecture to the mechanical integrity of trabecular bone.* Calcif Tissue Int, 1993. **53 Suppl 1**: p. S127-32; discussion S132-3.

100. Kinney, J.H. and A.J.C. Ladd, *The Relationship Between Three-Dimensional Connectivity and the Elastic Properties of Trabecular Bone.* Journal of Bone and Mineral Research, 1998. **13**(5): p. 839-845.

101. Poukalova, M., C.M. Yakacki, R.E. Guldberg, A. Lin, M. Saing, S.D. Gillogly, and K. Gall, *Pullout strength of suture anchors: effect of mechanical properties of trabecular bone.* J Biomech, 2010. **43**(6): p. 1138-45.

102. Odgaard, A., *Three-dimensional methods for quantification of cancellous bone architecture.* Bone, 1997. **20**(4): p. 315-328.

103. Kabel, J., A. Odgaard, B. van Rietbergen, and R. Huiskes, *Connectivity and the elastic properties of cancellous bone.* Bone, 1999. **24**(2): p. 115-120.

104. Jinnapat, A. and A.R. Kennedy, *The manufacture of spherical salt beads and their use as dissolvable templates for the production of cellular solids via a powder metallurgy route.* Journal of Alloys and Compounds, 2010. **499**(1): p. 43-47.

105. Turner, C.H. and D.B. Burr, *Basic biomechanical measurements of bone: A tutorial.* Bone, 1993. **14**(4): p. 595-608.

106. Thompson, I. and L.L. Hench, *6.39 - Medical Applications of Composites*, in *Comprehensive Composite Materials*, A.K. Zweben, Editor. 2000, Pergamon: Oxford. p. 727-753.

107. Galante, J., W. Rostoker, and R.D. Ray, *Physical properties of trabecular bone.* Calcified Tissue Research, 1970. **5**(1): p. 236-246.

108. Yaszemski, M.J., R.G. Payne, W.C. Hayes, R. Langer, and A.G. Mikos, *Evolution of bone transplantation: molecular, cellular and tissue strategies to engineer human bone.* Biomaterials, 1996. **17**(2): p. 175-185.

109. Thompson, I.D. and L.L. Hcnch, *Mechanical properties of bioactive glasses, glass-ceramics and composites.* Proceedings of the Institution of Mechanical Engineers, Part H: Journal of Engineering in Medicine, 1998. **212**(2): p. 127-136.

110. Ashman, R.B. and R. Jae Young, *Elastic modulus of trabecular bone material.* Journal of Biomechanics, 1988. **21**(3): p. 177-181.

111. Planell, J.A., S.M. Best, D. Lacroix, and A. Merolli, eds. *Bone repair materials*. 2009, CRC.

112. Baji, A., W. Shing-Chung, T.S. Srivatsan, G.O. Njus, and G. Mathur, *Processing Methodologies for Polycaprolactone-Hydroxyapatite Composites: A Review.* Materials & Manufacturing Processes, 2006. **21**(2): p. 211-218.

113. Dreischarf, M., S.-A. Aboulfazl, N. Arjmand, A. Rohlmann, and H. Schmidt, *Estimation of Loads on Human Lumbar Spine: A Review of In Vivo and Computational Model Studies.* Journal of Biomechanics, 2015.

114. Friedrich, K., H.J. Sue, P. Liu, and A.A. Almajid, *Scratch resistance of high performance polymers.* Tribology International, 2011. **44**(9): p. 1032-1046.

115. Garcia-Gonzalez, D., A. Rusinek, T. Jankowiak, and A. Arias, *Mechanical impact behavior of polyether–ether–ketone (PEEK).* Composite Structures, 2015. **124**: p. 88-99.

116. Chen, Y., X. Wang, X. Lu, L. Yang, H. Yang, W. Yuan, and D. Chen, *Comparison of titanium and polyetheretherketone (PEEK) cages in the surgical treatment of multilevel cervical spondylotic myelopathy: a prospective, randomized, control study with over 7-year follow-up.* European Spine Journal, 2013. **22**(7): p. 1539-1546.

117. Chou, Y.-C., D.-C. Chen, W.A. Hsieh, W.-F. Chen, P.-S. Yen, T. Harnod, T.-L. Chiou, Y.-L. Chang, C.-F. Su, S.-Z. Lin, and S.-Y. Chen, *Efficacy of anterior cervical fusion: Comparison of titanium cages, polyetheretherketone (PEEK) cages and autogenous bone grafts.* Journal of Clinical Neuroscience, 2008. **15**(11): p. 1240-1245.

118. Jockisch, K.A., S.A. Brown, T.W. Bauer, and K. Merritt, *Biological response to chopped-carbon-fiber-reinforced peek.* J Biomed Mater Res, 1992. **26**(2): p. 133-46.

119. Morrison, C., R. Macnair, C. MacDonald, A. Wykman, I. Goldie, and M.H. Grant, *In vitro biocompatibility testing of polymers for*

orthopaedic implants using cultured fibroblasts and osteoblasts. Biomaterials, 1995. **16**(13): p. 987-92.

120. Katzer, A., H. Marquardt, J. Westendorf, J.V. Wening, and G. von Foerster, *Polyetheretherketone--cytotoxicity and mutagenicity in vitro.* Biomaterials, 2002. **23**(8): p. 1749-59.

121. Girasole, G., G. Muro, A. Mintz, and J. Chertoff, *Transforaminal lumbar interbody fusion rates in patients using a novel titanium implant and demineralized cancellous allograft bone sponge.* The International Journal of Spine Surgery, 2013. **7**(1): p. e95-e100.

122. Verdejo, R., P. Werner, J. Sandler, V. Altstädt, and M.S.P. Shaffer, *Morphology and properties of injection-moulded carbon-nanofibre poly(etheretherketone) foams.* Journal of Materials Science, 2009. **44**(6): p. 1427-1434.

123. Wassgren, C., C. Brennen, and M. Hunt, *Vertical vibration of a deep bed of granular material in a container.* Journal of applied mechanics, 1996. **63**(3): p. 712-719.

124. An, X.Z., R.Y. Yang, R.P. Zou, and A.B. Yu, *Effect of vibration condition and inter-particle frictions on the packing of uniform spheres.* Powder Technology, 2008. **188**(2): p. 102-109.

125. Mueller, G.E., *Radial porosity in packed beds of spheres.* Powder Technology, 2010. **203**(3): p. 626-633.

126. An, X.-z., *Densification of the packing structure under vibrations.* International Journal of Minerals, Metallurgy, and Materials, 2013. **20**(5): p. 499-503.

127. Taguchi, Y.h., *New origin of a convective motion: Elastically induced convection in granular materials.* Physical Review Letters, 1992. **69**(9): p. 1367-1370.

128. An, X.Z., C.X. Li, R.Y. Yang, R.P. Zou, and A.B. Yu, *Experimental study of the packing of mono-sized spheres subjected to one-dimensional vibration.* Powder Technology, 2009. **196**(1): p. 50-55.

129. Debbas, S. and H. Rumpf, *On the randomness of beds packed with spheres or irregular shaped particles.* Chemical Engineering Science, 1966. **21**(6–7): p. 583-608.

130. Mueller, G.E., *Numerically packing spheres in cylinders.* Powder Technology, 2005. **159**(2): p. 105-110.

131. Zou, R.P. and A.B. Yu, *The packing of spheres in a cylindrical container: the thickness effect.* Chemical Engineering Science, 1995. **50**(9): p. 1504-1507.

132. Suzuki, M., T. Shinmura, K. Iimura, and M. Hirota, *Study of the Wall Effect on Particle Packing Structure Using X-ray Micro Computed Tomography.* Advanced Powder Technology, 2008. **19**(2): p. 183-195.

133. Yu, A.B. and J.S. Hall, *Packing of fine powders subjected to tapping.* Powder Technology, 1994. **78**(3): p. 247-256.

134. Theuerkauf, J., P. Witt, and D. Schwesig, *Analysis of particle porosity distribution in fixed beds using the discrete element method.* Powder Technology, 2006. **165**(2): p. 92-99.

135. de Klerk, A., *Voidage variation in packed beds at small column to particle diameter ratio.* AIChE Journal, 2003. **49**(8): p. 2022-2029.

136. Benenati, R.F. and C.B. Brosilow, *Void fraction distribution in beds of spheres.* AIChE Journal, 1962. **8**(3): p. 359-361.

137. Zhang, Z.P., L.F. Liu, Y.D. Yuan, and A.B. Yu, *A simulation study of the effects of dynamic variables on the packing of spheres.* Powder Technology, 2001. **116**(1): p. 23-32.

138. Remond, S., *DEM simulation of small particles clogging in the packing of large beads.* Physica A: Statistical Mechanics and its Applications, 2010. **389**(21): p. 4485-4496.

139. Jain, A., M.J. Metzger, and B.J. Glasser, *Effect of particle size distribution on segregation in vibrated systems.* Powder Technology, 2012.

140. Vanel, L., A.D. Rosato, and R.N. Dave, *Rise-Time Regimes of a Large Sphere in Vibrated Bulk Solids.* Physical Review Letters, 1997. **78**(7): p. 1255-1258.

141. Rosato, A., F. Prinz, K.J. Standburg, and R. Swendsen, *Monte Carlo simulation of particulate matter segregation.* Powder Technology, 1986. **49**(1): p. 59-69.

142. Schröter, M., S. Ulrich, J. Kreft, J.B. Swift, and H.L. Swinney, *Mechanisms in the size segregation of a binary granular mixture.* Physical Review E, 2006. **74**(1): p. 011307.

143. Ulrich, S., M. Schröter, and H.L. Swinney, *Influence of friction on granular segregation.* Physical Review E, 2007. **76**(4): p. 042301.

144. Zhang, F., L. Wang, C. Liu, P. Wu, and S. Zhan, *Patterns of convective flow in a vertically vibrated granular bed.* Physics Letters A, 2014. **378**(18–19): p. 1303-1308.

145. Jinnapat, A. and A. Kennedy, *The manufacture and characterisation of aluminium foams made by investment casting using dissolvable spherical sodium chloride bead preforms*, in *Department of*

Mechanical, Materials and Manufacturing Engineering. 2011, University of Nottingham.

146. Siddiq, A.R. and A.R. Kennedy, *Porous poly-ether ether ketone (PEEK) manufactured by a novel powder route using near-spherical salt bead porogens: Characterisation and mechanical properties.* Materials Science and Engineering: C, 2015. **47**(0): p. 180-188.

Appendices

Appendix 1: Data sheets for PEEK powder

VICOTE® 701

Polyetheretherketone
Victrex plc

UL IDES | Prospector

Product Description

VICOTE 701-707 grades are specially developed powder coatings. They are available in various average particle sizes from 10 - 50 microns. The powders are off-white in color and are available in various melt viscosities depending on the film thickness and level of melt flow required. Typical film thicknesses range from < 100 microns up to 500 microns. Film thicknesses above 1 mm are possible by building up the coating thickness by the hot flocking technique.

Like other non-coating grades of VICTREXPEEK polymer, VICOTE Coatings are thermoplastic in nature and exhibit flow above the melt temperature. When processed using the correct guidelines, the coatings will exhibit the excellent properties that VICTREX PEEK polymer is renowned for.

- High continuous use temperature of 260°C (500°F)
- Excellent wear, abrasion and cut through resistance at these high temperatures
- Excellent chemical and radiation resistance
- Low level of extractables
- Hydrolysis resistant
- Inherently flame retardant

General			
Material Status	• Commercial: Active		
Availability	• Asia Pacific	• Europe	• North America
Features	• Flame Retardant • Good Abrasion Resistance • Good Chemical Resistance	• Good Wear Resistance • High Heat Resistance • Hydrolysis Resistant	• Low Extractables • Radiation (Gamma) Resistant
Uses	• Coating Applications		
Agency Ratings	• FDA 21 CFR 175.300		
Appearance	• Natural Color		
Forms	• Powder		
Processing Method	• Coating		

Physical	Nominal Value Unit	Test Method
Density	1.32 g/cm³	ISO 1183
Thermal	**Nominal Value Unit**	**Test Method**
Glass Transition Temperature (DSC)	143 °C	DSC
Melting Temperature	343 °C	DSC
RTI Elec	260 °C	UL 746
RTI Imp	260 °C	UL 746
RTI Str	260 °C	UL 746
Additional Information	**Nominal Value Unit**	**Test Method**
Konig Hardness	3.3 min	ISO 1522

Extrusion	Nominal Value Unit
Drying Temperature	120 to 150 °C
Drying Time	< 3.0 hr

Notes

[1] Typical properties: these are not to be construed as specifications.

PEEK-OPTIMA® LT1

Polyetheretherketone
Invibio Inc.

UL IDES | Prospector

Product Description

PEEK-OPTIMA® polymer from Invibio® is a high performance biomaterial providing advanced solutions for implant manufacturers. Formulated to meet the most exacting in-vivo criteria, PEEK-OPTIMA is biocompatible, safe and stable.

Manufacturers of cardiovascular, dental, neurological and orthopaedic implants choose PEEK-OPTIMA for its:

- Excellent mechanical performance
- High wear resistance
- Ability to be repeatedly sterilized without impairing performance
- Biocompatibility
- Drug and Device Master Files lodged with the FDA

Invibio offers a 'no-change' agreement for the assured long-term supply of PEEK-OPTIMA. This guarantees its specification and production methods over an agreed period of time.

General

Material Status	• Commercial: Active		
Availability	• Europe	• North America	
Features	• Biocompatible • Ethylene Oxide Sterilizable • Good Stability • Good Sterilizability	• Good Wear Resistance • High Purity • High Strength • Hydrolysis Resistant	• Low Extractables • Low Residuals • Radiation Sterilizable • Steam Sterilizable
Uses	• Body Implants	• Dental Applications	• Medical/Healthcare Applications
Agency Ratings	• DMF Unspecified Rating • FDA Unspecified Rating • ISO 10093 -3, -11, -6, -18	• ISO 10993 Part 2 • ISO 10993 Part 4 • MAF Unspecified Rating	• USP Class VI
Appearance	• Natural Color		
Forms	• Granules		
Processing Method	• Compression Molding	• Extrusion	• Injection Molding

Physical	Nominal Value	Unit	Test Method
Density	1.30	g/cm³	ISO 1183
Molding Shrinkage - Flow (210°C)	1.2	%	
Water Absorption (23°C, 24 hr)	0.50	%	ISO 62
Mechanical	**Nominal Value**	**Unit**	**Test Method**
Tensile Stress			ISO 527-2
Yield [2]	115	MPa	
Yield	100	MPa	
Tensile Strain			ISO 527-2
Break [2]	20	%	
Break	40	%	
Flexural Modulus			ISO 178
-- [2]	4000	MPa	
--	4100	MPa	
Flexural Strength			ISO 178
--	165	MPa	
-- [2]	170	MPa	
Compressive Stress	135	MPa	ISO 604
Shear Modulus	1150	MPa	ISO 15310
Shear Strength	90.0	MPa	ASTM D732
Poisson's Ratio	0.36		ASTM D638
Impact	**Nominal Value**	**Unit**	**Test Method**
Notched Izod Impact Strength			ISO 180
-- [2]	4.7	kJ/m²	
--	7.5	kJ/m²	
Unnotched Izod Impact Strength [2]	No Break		ISO 180
Hardness	**Nominal Value**	**Unit**	**Test Method**
Rockwell Hardness (M-Scale)	99		ASTM D785

Revision History
Document Created: 06 September 2012
Added to Prospector: August 2009
Last Updated: 11/08/2009

PEEK-OPTIMA® LT1

06 September 2012

Polyetheretherketone
Invibio Inc.

Thermal	Nominal Value Unit	Test Method
Melting Temperature	340 °C	
CLTE - Flow		ASTM D696
-- [3]	0.000047 cm/cm/°C	
-- [4]	0.00011 cm/cm/°C	
RTI Elec	260 °C	UL 746
RTI Imp	260 °C	UL 746
RTI Str	260 °C	UL 746
Fill Analysis	**Nominal Value Unit**	**Test Method**
Melt Viscosity [5]	0.000440 MPa	Internal Method

Notes

[1] Typical properties: these are not to be construed as specifications.
[2] Rod
[3] Below Tg
[4] Above Tg
[5] Capillary Rheometer

PEEK-OPTIMA® LT3

Polyetheretherketone
Invibio Inc.

UL IDES | Prospector

Product Description

PEEK-OPTIMA® polymer from Invibio® is a high performance biomaterial providing advanced solutions for implant manufacturers. Formulated to meet the most exacting in-vivo criteria, PEEK-OPTIMA is biocompatible, safe and stable.

Manufacturers of cardiovascular, dental, neurological and orthopaedic implants choose PEEK-OPTIMA for its:

- Excellent mechanical performance
- High wear resistance
- Ability to be repeatedly sterilized without impairing performance
- Biocompatibility
- Drug and Device Master Files lodged with the FDA

Invibio offers a 'no-change' agreement for the assured long-term supply of PEEK-OPTIMA. This guarantees its specification and production methods over an agreed period of time.

General			
Material Status	• Commercial: Active		
Availability	• Europe	• North America	
Features	• Biocompatible • Ethylene Oxide Sterilizable • Good Stability • Good Sterilizability	• Good Wear Resistance • High Purity • High Strength • Hydrolysis Resistant	• Low Extractables • Low Residuals • Radiation Sterilizable • Steam Sterilizable
Uses	• Body Implants	• Dental Applications	• Medical/Healthcare Applications
Agency Ratings	• DMF Unspecified Rating • FDA Unspecified Rating • ISO 10093 -3, -11, -6, -18	• ISO 10993 Part 2 • ISO 10993 Part 4 • MAF Unspecified Rating	• USP Class VI
Appearance	• Natural Color		
Forms	• Granules		
Processing Method	• Compression Molding	• Extrusion	• Injection Molding

Physical	Nominal Value Unit	Test Method
Density	1.30 g/cm³	ISO 1183
Molding Shrinkage - Flow (210°C)	1.3 %	
Water Absorption (23°C, 24 hr)	0.50 %	ISO 62
Mechanical	**Nominal Value Unit**	**Test Method**
Tensile Stress		ISO 527-2
Yield [2]	115 MPa	
Yield	108 MPa	
Tensile Strain		ISO 527-2
Break [2]	20 %	
Break	25 %	
Flexural Modulus		ISO 178
-- [2]	4000 MPa	
--	4200 MPa	
Flexural Strength [2]	170 MPa	ISO 178
Compressive Stress	135 MPa	ISO 604
Shear Modulus	1000 MPa	ISO 15310
Shear Strength	88.0 MPa	ASTM D732
Poisson's Ratio	0.36	ASTM D638
Impact	**Nominal Value Unit**	**Test Method**
Notched Izod Impact Strength		ISO 180
-- [2]	4.7 kJ/m²	
--	4.5 kJ/m²	
Unnotched Izod Impact Strength [2]	No Break	ISO 180
Hardness	**Nominal Value Unit**	**Test Method**
Rockwell Hardness (M-Scale)	99	ASTM D785
Thermal	**Nominal Value Unit**	**Test Method**
Melting Temperature	340 °C	

Revision History
Document Created: 06 September 2012
Added to Prospector: August 2009
Last Updated: 11/08/2009

PEEK-OPTIMA® LT3
Polyetheretherketone
Invibio Inc.

06 September 2012

Thermal	Nominal Value Unit	Test Method
CLTE - Flow		ASTM D696
_[3]	0.000047 cm/cm/°C	
_[4]	0.00011 cm/cm/°C	
RTI Elec	260 °C	UL 746
RTI Imp	260 °C	UL 746
RTI Str	260 °C	UL 746
Fill Analysis	**Nominal Value Unit**	**Test Method**
Melt Viscosity[5]	0.000160 MPa	Internal Method

Notes

[1] Typical properties: these are not to be construed as specifications.

[2] Rod

[3] Below Tg

[4] Above Tg

[5] Capillary Rheometer

Appendix 2: Data sheets of Boron Nitride Aerosol

HENZE
BORON NITRIDE PRODUCTS

Product Information

HeBoCoat® 401E Boron Nitride Aerosol

Product Description

HeBoCoat® 401E is a boron nitride aerosol coating. Due to the ethanol base a good wetting of the substrate surface and quick drying is achieved. Inorganic binders provide a good adhesion up to high temperatures especially on metallic, ceramic and glass surfaces. By the use of fine boron nitride powder particles good releasing and lubricating coatings are obtained, even at high temperatures. Boron nitride is stable up to 900 °C in air and up to 2000 °C under inert gas atmosphere.

Typical Applications

- Release agent for sintering, welding, soldering and brazing, anti spatter
- Release agent and lubricant in glass processing
- Protection of graphite in siliconizing processes, release coating

Instructions for Use

- Shake well before use
- For good results only clean, dry, dust and oil free surfaces may be coated
- Spray distance approx. 20 cm
- The coating is dry when no smell of solvent is perceptible

Packing Units

- 500 ml/can, 12 cans in a box

Storage and Safety

For further information please read carefully the safety data sheet.

Appendix 3: Mastersizer 2000 particle analysis

MASTERSIZER 2000

Result Analysis Report

Sample Name: Vicote Averaged Result	**SOP Name:** Sodium bicarbonate	**Measured:** 18 February 2014 13:37:16	
Sample Source & type:	**Measured by:** bbzmc2	**Analysed:** 18 February 2014 13:37:18	
Sample bulk lot ref: 1	**Result Source:** Averaged		
Particle Name: Sodium bicarbonate	**Accessory Name:** Scirocco 2000	**Analysis model:** General purpose (fine)	**Sensitivity:** Normal
Particle RI: 1.500	**Absorption:** 0.1	**Size range:** 0.020 to 2000.000 um	**Obscuration:** 1.01 %
Dispersant Name:	**Dispersant RI:** 1.000	**Weighted Residual:** 0.373 %	**Result Emulation:** Off
Concentration: 0.0003 %Vol	**Span :** 1.196	**Uniformity:** 0.375	**Result units:** Volume
Specific Surface Area: 0.696 m²/g	**Surface Weighted Mean D[3,2]:** 8.624 um	**Vol. Weighted Mean D[4,3]:** 12.186 um	

d(0.1): 6.092 um **d(0.5):** 11.402 um **d(0.9):** 19.728 um

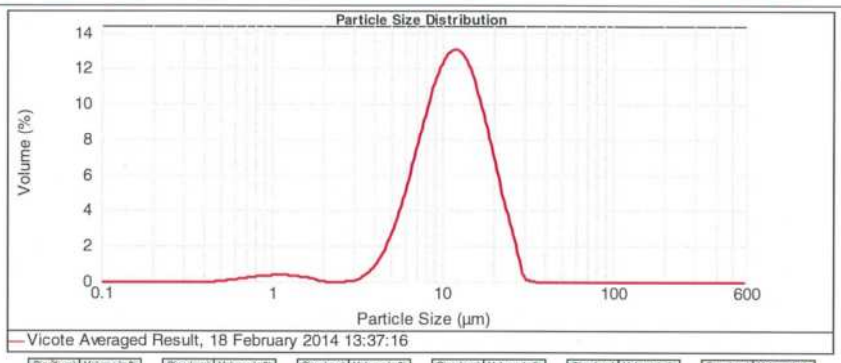

Size (µm)	Volume In %	Size (µm)	Volume In %	Size (µm)	Volume In %	Size (µm)	Volume In %	Size (µm)	Volume In %	Size (µm)	Volume In %
0.010	0.00	0.105	0.00	1.096	0.33	11.482	11.79	120.226	0.00	1258.925	0.00
0.011	0.00	0.120	0.00	1.259	0.30	13.183	11.09	138.038	0.00	1445.440	0.00
0.013	0.00	0.138	0.00	1.445	0.23	15.136	9.56	158.489	0.00	1659.587	0.00
0.015	0.00	0.158	0.00	1.660	0.13	17.378	7.48	181.970	0.00	1905.461	0.00
0.017	0.00	0.182	0.00	1.905	0.00	19.953	5.21	208.930	0.00	2187.762	0.00
0.020	0.00	0.209	0.00	2.188	0.00	22.909	3.19	239.883	0.00	2511.886	0.00
0.023	0.00	0.240	0.00	2.512	0.00	26.303	1.02	275.423	0.00	2884.032	0.00
0.026	0.00	0.275	0.00	2.884	0.07	30.200	0.06	316.228	0.00	3311.311	0.00
0.030	0.00	0.316	0.00	3.311	0.33	34.674	0.00	363.078	0.00	3801.894	0.00
0.035	0.00	0.363	0.00	3.802	0.86	39.811	0.00	416.869	0.00	4365.158	0.00
0.040	0.00	0.417	0.00	4.365	1.76	45.709	0.00	478.630	0.00	5011.872	0.00
0.046	0.00	0.479	0.00	5.012	3.08	52.481	0.00	549.541	0.00	5754.399	0.00
0.052	0.00	0.550	0.03	5.754	4.80	60.256	0.00	630.957	0.00	6606.934	0.00
0.060	0.00	0.631	0.11	6.607	6.76	69.183	0.00	724.436	0.00	7585.776	0.00
0.069	0.00	0.724	0.16	7.586	8.77	79.433	0.00	831.764	0.00	8709.636	0.00
0.079	0.00	0.832	0.24	8.710	10.46	91.201	0.00	954.993	0.00	10000.000	
0.091	0.00	0.955	0.29	10.000	11.56	104.713	0.00	1096.478	0.00		
0.105	0.00	1.096	0.33	11.482		120.226	0.00	1258.925	0.00		

Operator notes: *Average of 3 measurements from SB20*

Malvern Instruments Ltd.
Malvern, UK
Tel := +[44] (0) 1684-892456 Fax +[44] (0) 1684-892789

Mastersizer 2000 Ver. 5.40
Serial Number : MAL1014135

File name: SB20
Record Number: 64
19 Feb 2014 12:40:50

MASTERSIZER 2000

Result Analysis Report

Sample Name: LT1 Averaged Result	**SOP Name:** Sodium bicarbonate	**Measured:** 18 February 2014 13:48:42	
Sample Source & type:	**Measured by:** bbzmc2	**Analysed:** 18 February 2014 13:48:43	
Sample bulk lot ref: 1	**Result Source:** Averaged		
Particle Name: Sodium bicarbonate	**Accessory Name:** Scirocco 2000	**Analysis model:** General purpose (fine)	**Sensitivity:** Normal
Particle RI: 1.500	**Absorption:** 0.1	**Size range:** 0.020 to 2000.000 um	**Obscuration:** 0.53 %
Dispersant Name:	**Dispersant RI:** 1.000	**Weighted Residual:** 0.441 %	**Result Emulation:** Off
Concentration: 0.0006 %Vol	**Span :** 1.630	**Uniformity:** 0.509	**Result units:** Volume
Specific Surface Area: 0.159 m²/g	**Surface Weighted Mean D[3,2]:** 37.666 um	**Vol. Weighted Mean D[4,3]:** 61.197 um	

d(0.1): 21.349 um **d(0.5):** 54.228 um **d(0.9):** 109.758 um

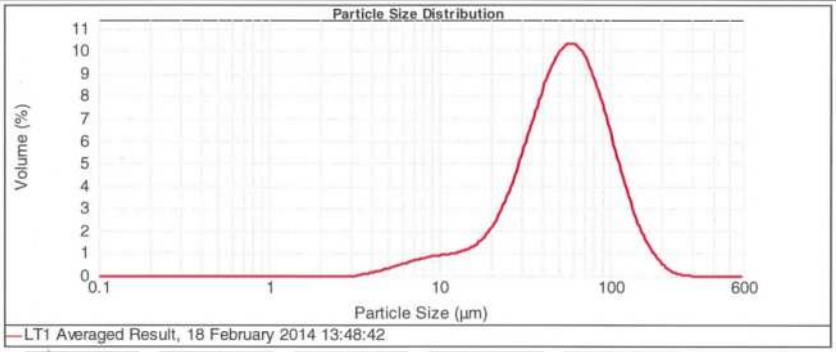

Size (µm)	Volume In %	Size (µm)	Volume In %	Size (µm)	Volume In %	Size (µm)	Volume In %	Size (µm)	Volume In %	Size (µm)	Volume In %
0.010	0.00	0.105	0.00	1.096	0.00	11.482	0.91	120.226	3.14	1258.925	0.00
0.011	0.00	0.120	0.00	1.259	0.00	13.183	1.02	138.038	2.00	1445.440	0.00
0.013	0.00	0.138	0.00	1.445	0.00	15.136	1.23	158.489	1.17	1659.587	0.00
0.015	0.00	0.158	0.00	1.660	0.00	17.378	1.62	181.970	0.60	1905.461	0.00
0.017	0.00	0.182	0.00	1.905	0.00	19.953	2.24	208.930	0.21	2187.762	0.00
0.020	0.00	0.209	0.00	2.188	0.00	22.909	3.12	239.883	0.07	2511.886	0.00
0.023	0.00	0.240	0.00	2.512	0.00	26.303	4.23	275.423	0.00	2884.032	0.00
0.026	0.00	0.275	0.00	2.884	0.00	30.200	5.51	316.228	0.00	3311.311	0.00
0.030	0.00	0.316	0.00	3.311	0.05	34.674	6.82	363.078	0.00	3801.894	0.00
0.035	0.00	0.363	0.00	3.802	0.13	39.811	8.01	416.869	0.00	4365.158	0.00
0.040	0.00	0.417	0.00	4.365	0.24	45.709	8.89	478.630	0.00	5011.872	0.00
0.046	0.00	0.479	0.00	5.012	0.35	52.481	9.32	549.541	0.00	5754.399	0.00
0.052	0.00	0.550	0.00	5.754	0.48	60.256	9.20	630.957	0.00	6606.934	0.00
0.060	0.00	0.631	0.00	6.607	0.61	69.183	8.54	724.436	0.00	7585.776	0.00
0.069	0.00	0.724	0.00	7.586	0.71	79.433	7.41	831.764	0.00	8709.636	0.00
0.079	0.00	0.832	0.00	8.710	0.79	91.201	6.01	954.993	0.00	10000.000	
0.091	0.00	0.955	0.00	10.000	0.85	104.713	4.52	1096.478	0.00		
0.105	0.00	1.096		11.482		120.226		1258.925	0.00		

Operator notes: *Average of 3 measurements from SB20*

Malvern Instruments Ltd.
Malvern, UK
Tel := +[44] (0) 1684-892456 Fax +[44] (0) 1684-892789

Mastersizer 2000 Ver. 5.40
Serial Number : MAL1014135

File name: SB20
Record Number: 65
19 Feb 2014 12:41:00

MASTERSIZER 2000

Result Analysis Report

Sample Name: LT3 Averaged Result	**SOP Name:** Sodium bicarbonate	**Measured:** 18 February 2014 13:59:04	
Sample Source & type:	**Measured by:** bbzmc2	**Analysed:** 18 February 2014 13:59:05	
Sample bulk lot ref: 1	**Result Source:** Averaged		
Particle Name: Sodium bicarbonate	**Accessory Name:** Scirocco 2000	**Analysis model:** General purpose (fine)	**Sensitivity:** Normal
Particle RI: 1.500	**Absorption:** 0.1	**Size range:** 0.020 to 2000.000 um	**Obscuration:** 0.64 %
Dispersant Name:	**Dispersant RI:** 1.000	**Weighted Residual:** 0.346 %	**Result Emulation:** Off
Concentration: 0.0006 %Vol	**Span :** 1.576	**Uniformity:** 0.48	**Result units:** Volume
Specific Surface Area: 0.202 m²/g	**Surface Weighted Mean D[3,2]:** 29.702 um	**Vol. Weighted Mean D[4,3]:** 46.004 um	

d(0.1): 15.418 um **d(0.5):** 42.137 um **d(0.9):** 81.839 um

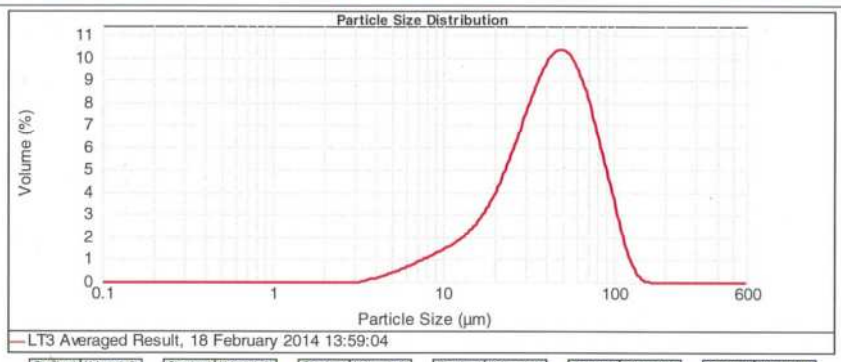

Size(µm)	Volume In %	Size (µm)	Volume In %	Size (µm)	Volume In %	Size (µm)	Volume In %	Size (µm)	Volume In %	Size (µm)	Volume In %
0.010	0.00	0.105	0.00	1.096	0.00	11.482	1.69	120.226	0.62	1258.925	0.00
0.011	0.00	0.120	0.00	1.259	0.00	13.183	2.04	138.038	0.09	1445.440	0.00
0.013	0.00	0.138	0.00	1.445	0.00	15.136	2.51	158.489	0.00	1659.587	0.00
0.015	0.00	0.158	0.00	1.660	0.00	17.378	3.16	181.970	0.00	1905.461	0.00
0.017	0.00	0.182	0.00	1.905	0.00	19.953	4.00	208.930	0.00	2187.762	0.00
0.020	0.00	0.209	0.00	2.188	0.00	22.909	5.03	239.883	0.00	2511.886	0.00
0.023	0.00	0.240	0.00	2.512	0.00	26.303	6.18	275.423	0.00	2884.032	0.00
0.026	0.00	0.275	0.00	2.884	0.00	30.200	7.36	316.228	0.00	3311.311	0.00
0.030	0.00	0.316	0.00	3.311	0.06	34.674	8.39	363.078	0.00	3801.894	0.00
0.035	0.00	0.363	0.00	3.802	0.16	39.811	9.11	416.869	0.00	4365.158	0.00
0.040	0.00	0.417	0.00	4.365	0.29	45.709	9.36	478.630	0.00	5011.872	0.00
0.046	0.00	0.479	0.00	5.012	0.44	52.481	9.03	549.541	0.00	5754.399	0.00
0.052	0.00	0.550	0.00	5.754	0.61	60.256	8.14	630.957	0.00	6606.934	0.00
0.060	0.00	0.631	0.00	6.607	0.80	69.183	6.79	724.436	0.00	7585.776	0.00
0.069	0.00	0.724	0.00	7.586	1.00	79.433	5.15	831.764	0.00	8709.636	0.00
0.079	0.00	0.832	0.00	8.710	1.20	91.201	3.52	954.993	0.00	10000.000	
0.091	0.00	0.955	0.00	10.000	1.42	104.713	1.86	1096.478	0.00		
0.105		1.096		11.482		120.226		1258.925			

Operator notes: *Average of 3 measurements from SB20*

Malvern Instruments Ltd.
Malvern, UK
Tel := +[44] (0) 1684-892456 Fax +[44] (0) 1684-892789

Mastersizer 2000 Ver. 5.40
Serial Number : MAL1014135

File name: SB20
Record Number: 66
19 Feb 2014 12:41:12